Hamilton–Jacobi theory for connecting equilibrium magnetic fields across a toroidal surface supporting a plasma pressure discontinuity

A thesis submitted for the degree of
Doctor of Philosophy
of the Australian National University

Mathew McGann

7 July 2013

Statement of original work

The work contained in this thesis is my own original research. Any material taken from other references is explicitly acknowledged as such.

Mathew McGann
7 July 2013

Acknowledgements

I would like to thank Robert Dewar for his supervision throughout this thesis, his supervisory style has had a deep effect on how I work and think. I owe a debt of graditude to Stuard Hudson for his work and his help, and to his family for their hospitality. Thanks also to other members of the physics deparment who had input into this thesis, Matthew Hole, Graham Dennis and Greg Von Nessi, as well as Boyd Blackwell and Henry Gardner. I am also in the debt of Robert MacKay and Ralf Kaiser who hosted me and discussed my work with me when I was overseas. Finally to Richard Dendy, for our discussions and his advice during my travels.

Just as important were my physics graduate peers, inlcuding Steve Lade, Lei Chang, Michael Dudalev, Yves Barmaz, David Barmaz and Rachel Poldy – especially for our writing sessions at the Gods. My discussions with Cameron Cairns were helpful in reminding me of why I enjoy physics, especially when interests started to shift.

I made many friends in the many years of my PhD, all of them had an effect on me. In my early impressionable days of thesis, I'd like to thank: John De la Cruz, Romi, Ambar and Tanya for being very... impressionable. I have made lifelong friends in Madalina, Div, Will, Kunnal, Rish, Maryam, Nino, Amir, Pam, Sepi, Ashkan, Behzad, Brendan, Peter, Stephan, the other Maryam and of course Iman. I thank all of you for your friendship over the last few years. ANUedge was kind enough to employ me for the last stretch, and I've enjoyed every minute. Thank you to Tom and Rohini, and to Matt and Sarah for their non-departmental thesis advice.

To my friends who pre-date this work, George, Jamie, Todd, Kev, Shaun, Brett and Ignatius, you all provided much needed distractions and fun. Many thanks to my friends who pre-date even those guys, Brendan, Ruben, Shaun and Josh for trying their best to stop me becoming too lame against overwhelming pressure from the city of Canberra's cultural influence, only time will tell if they succeeded.

I also need to thank my family, my parents and brother who have supported me every step of the way. Thank you to Jen's family for their support too. Finally, a heartfelt thank you to Jen. You supported me the entire time, it's time to submit this and give you the attention you deserve. [insert clever meta-joke in an attempt to give a unique character to the acknowledgements here].

Mathew McGann
7 July 2013

Abstract

This thesis investigates the force balance condition that appears on internal flux surfaces within the Multiple Region RelaXed MagnetoHydroDynamic (MRXMHD) formulation of a toroidal fusion plasma equilibrium. This condition acts as a boundary condition between two constant pressure annular regions, separated by a toroidal current sheet. A pressure discontinuity must be allowed on these boundaries in order to have a non-trivial pressure profile, however the force balance condition strongly constrains the allowable continuations of the magnetic field (field configurations) across the surface.

The MRXMHD formulation and the computer code `SPEC` (which uses MRXMHD to solve for the entire equilibrium field) use these pressure-loaded flux surfaces as analytic and computational boundaries for the plasma respectively. Therefore understanding the conditions under which magnetic fields can be connected across these flux surfaces is important, as the determination of a global solution will depend on continuation being possible across all internal boundaries. This thesis investigates the conditions for continuation using methods from Hamiltonian mechanics. It is an exploratory investigation that identifies some necessary factors determining existence, but falls short of providing sufficient conditions under which continuation is possible.

The force balance condition is formulated as a Hamilton-Jacobi equation on the surface whose solutions (provided they lay on an invariant torus) correspond to the magnetic field on one side of the interface when provided with the pressure (analagous to Hamiltonian energy) and the rotational transform (analagous to the winding number of the Hamiltonian trajectory). The Hamilton-Jacobi equation is then written as an inverse problem, which provides a generalised interpretation in which two solutions are selected, one for each side of the interface. The pressure jump and rotational transform discontinutity across the surface is then identically the difference in Hamiltonian energies and winding numbers respectivey of the two selected solutions. Another derivation of the pressure jump condition based on the vanishing of the divergence of the total stress tensor in the neighbourhood of a toroidal surface of discontinuity is also provided.

The pressure jump Hamiltonian problem is in general very complicated and so quite opaque to the effect of the perturbative variables. To determine some general features, a simplification of the Hamiltonian is derived that is a first order approximation in three perturbative variables. This proves to be a helpful toy problem for the investigation of Hamiltonian systems with more than one source of chaos, and is

similar in nature to the double pendulum Hamiltonian. This simplified version also does succeed in shedding light on the nature of the pressure jump Hamiltonian.

An appeal to the Birkhoff theorem resolves the current disagreement on whether Hamiltonian trajectories map homeomorphically to actual magnetic field lines. A corollary of this reconciliation implies that the winding number of the Hamiltonian solution is conserved under the mapping as the rotational transform of the resulting field line. As a result the KAM theorem can be applied to describe the *persistence* of field configurations, but not the conditions for continuation. The latter must be done computationally by solving for orbits and determining if they result in an ergodic covering of an invariant surface *a-posteriori* using Greene's residue.

A program was written in FORTRAN, named `PJH`, that solves for trajectories of the pressure jump Hamiltonian and determines the regularity of the solution orbits using Greene's residue. To determine the effect of deformations to the surface and the effects of increasing the pressure discontinuty, robustness plots are invented and produced. These plots are contour plots of the residue as a function of a parametrisation of the deformation and the energy. These plots show that in general increases in deformations and increases in pressure discontinuities do destroy a selected orbit. There is also evidence of pressure (energy) *bands* in which solutions are allowed.

Robustness plots are provided for three cases: the simplified Hamiltonian, simulations of `SPEC` interfaces and flux surfaces extracted from the plasma volume from a `SPEC` equilibrium. The latter two inform the prescription and management of flux interfaces in `SPEC`. Continuation across rotational transform discontunities is also investigated. In some cases energy healing is observed in which increasing energy can disallow a continuation, then allow it again at a higher energy. The implications of the results to MRXMHD and `SPEC` are then articulated.

Contents

List of Figures

List of Tables

Chapter 1

Introduction

1.1 Background research

1.1.1 Determining the equilibrium field of a fusion plasma

The most developed type of fusion reactor is a magnetic confinement device that exploits the electrical properties of a plasma to channel the plasma into a toroidal shape using a set of magnetic coils to generate the required magnetic field. While experiments have shown that confinement is (at least for a short time) possible, the interaction between the field generated by the coils and the field generated by the plasma inside results in a field the general structure of which has not been completely determined to this day. The resultant field is known as the equilibrium field $\boldsymbol{B}$ and the determination of this field is an open problem in fusion physics.[Gra67]

The first attempt of relevance to this thesis to determine the magnetic structure was introduced by Kruskal and Kulsrud in 1958, who developed a variational principle where one minimises the potential energy of the plasma in the plasma volume.[KK58] In 1958 Grad and Rubin considered the plasma as a perfectly conducting fluid in the presence of a magnetic field and determined that the quantity $P + B^2/2$ must be continous even if $\boldsymbol{B}$ or P, the pressure, is discontinuous, though this can only occur across toroidal surfaces within the toroidal volume named *flux surfaces*.[GR58]

The next major step came from Taylor in 1974 in the form of *Taylor relaxation* where one minimises the magnetic energy under constraints of constant helicity throughout the plasma volume.[Tay74] Taylor developed this relaxation principle to explain the self-organised behaviour in reversed field pinch fusion reactors. Helicity can be thought of as a measure of how 'twisted' the field lines are in the toroidal volume, so under relaxation with conserved Helicity, two or more field lines that are twisted must remain twisted, suggesting a very complex structure for the magnetic field at equilibrium. Under Taylor relaxation, the equilibrium field can be shown to be of a Beltrami form

$$\boldsymbol{\nabla} \times \boldsymbol{B} = \mu \boldsymbol{B} \,, \tag{1.1}$$

where μ is constant throughout the volume.

From the application of Taylor relaxation to toroidal plasmas emerged the *sharp boundary* model[BFL+86],[KU04], which considered the plasma as a constant pressure, force-free field within an outermost flux surface referred to as an *interface* surrounded by a vacuum region. In this formulation the quantity $P + B^2/2$ must be the same on each side of the outer interface because across this interface the pressure of the plasma drops from P to zero discontinuously. This outermost sharp boundary discontinuity is an idealisation of the edge of the plasma and the investigations of Berk *et al*[BFL+86] and Kaiser and Salat[KS94] provided insights into the stability of this important area of the plasma. More information regarding these investigations can be seen in Section 1.1.2.

An extension to the sharp boundary model was introduced in 1996 by Bruno and Lawrence. In it the outermost interface of the plasma is, like the examples above, assumed to be a sharp boundary. However, as tokamaks and stellarators are much less turbulent than reverse field pinches, it was arugued that Taylor relaxation can occur *locally*, meaning one can divide the plasma volume into regions of relaxation, separated by flux surfaces which act as ideal MHD (MagnetoHydroDynamic) barriers, refered to as *internal interfaces*. When Taylor relaxation is applied between each interface, a generalised version of the sharp boundary condition appears for every flux surface used as an interface within the volume. Bruno and Lawrence proved that such a construction of a plasma as a union of toroidal annular 'shells' of Taylor relaxed plasmas was possible, and found that the quantity $P + B^2/2$ must be the same on each side of the interface.[BL96]

Taking this construction to the next step was the formulation of MRXMHD (Multiple Region RelaXed MHD). MRXMHD formalises the idea of concentric taylor relaxed regions into a single principle.[HDHM12] The formulation results in the same internal structure: force-free, Beltrami field regions of constant pressure containing chaotic regions separated by flux surfaces that each hold a pressure discontinuity. On either side of the flux surface, the quantity $P + B^2/2$ is equal, this quantity will be referred to as the *force balance quantity*. Adding internal interfaces with pressure discontinuities (or *pressure jumps*) across them removes the requirement that P be continuous within the plasma volume, allowing the Taylor relaxation to occur in a constant pressure region. This ensures the formulation is consistent with the formation of chaotic magnetic structures in the volumes.

Within MRXMHD, the internal flux surfaces are essential for understanding the nature of the equilibrium field as they separate chaotic regions and act as boundary conditions for calculations of the equilibrium field in each volume. Thus one finds need for an investigation into the nature of these internal flux surfaces.

1.1.2 Investigations into the nature of flux surfaces with pressure discontinuities

Within the sharp boundary model, various works investigated the outer boundary and the pressure discontinuity condition that must hold on it. As it was important to understand the nature of the outermost interface that formed the boundary conditions for the Taylor relaxation in the plasma volume, so too is it important to understand the multitude of pressure-jump-bearing internal interfaces that act as boundary conditions for the calculation of the Beltrami field between them.

In 1986, Berk *et al* formulated the force balance condition as a Hamilton-Jacobi equation, and went on to investigate the suitability of using Hamiltonian existence criteria (for example, the KAM theory) to infer the existence of equilibria with sharp boundaries.[BFL+86] By assuming the pressure jump interface $\mathcal{S}$ to be located on a magnetic surface that is somehow known to be an invariant torus of a non-integrable vacuum magnetic field, and taking the pressure jump to be the perturbation parameter, they were then able to invoke the KAM theorem without having to assume the system to be close to axisymmetric. However, this was under the restrictive assumption that the field outside $\mathcal{S}$ was, to within a constant factor, the unperturbed vacuum field.

Later, Kaiser and Salat proved the existence of flux surfaces using only geometrical arguments (i.e. without using a Hamiltonian form), but the approach again used restrictive assumptions on the magnetic field, namely that it vanishes on the outside of the interface $\mathcal{S}$.[KS94]

As their approach did not use a Hamiltonian formulation, Kaiser and Salat considered the problem of whether the flux surface exists to be a question of whether one can find a simple analytic covering of geodesics on the surface (in contrast to Berk *et al* who asked whether it is possible to find a solution to the Hamilton–Jacobi equation). With a Hamiltonian formulation Berk *et al* appealed to the KAM theory to insist that flux surfaces will persist under changes in the system,[BFL+86] but Kaiser and Salat reject this appeal as incomplete, with concerns that the Hamiltonian solutions do not map back homeomorphically to geodesics on the surface.[KS94] To make up for the loss of Hamiltonian existence criteria to investigate the sharp boundary, Kaiser and Salat provide instead what they call a 'big bump' criterion. This criterion uses only geometrical arguments, but can only provide a negative statement of existence from local arguments.

With the introduction of boundaries internal to the plasma, the previous research on the outer boundary must be generalised from a plasma/vacuum interface to a plasma/plasma interface. This thesis extends the Hamiltonian formulation introduced by Berk to describe the outer interface of the sharp boundary model to derive a

new Hamiltonian to describe the inner interfaces of the MRXMHD formulation. The resulting *pressure jump Hamiltonian* is based on the force balance condition as derived within MRXMHD.

The thesis reconciles Kaiser and Salat's concern over the applicability of the Hamiltonian formulation as a method of inferring existence results of field lines by appealing to the Birkhoff theorem. The pressure jump Hamiltonian proves to be too complicated for analytical treatment and so a first order simplification is derived for analytical and numerical treatment. The unsimplified version is also solved numerically to determine both if the simplification is representative of the problem, and to shed some insight into the nature of both the internal interfaces and the flux surfaces that appear in between the interfaces. This is done with specific emphasis on how these findings help the construction of a code to calculate the equilibrium field based on MRXMHD.

1.1.3 Computer codes for the calculation of plasma equilibria

With the theoretical variational principles in Section 1.1.1, computer programs named *equilibrium codes* started to be developed to calculate the magnetic field structure within the plasma volume. The most used 3D equilibrium code at the time of publication is `VMEC` (Variational Moments Equilibrium Code), which solves the energy minimisation formulation of Kruskal and Kulsrud using a moments representation of the magnetic field where the coordinates are expanded in a Fourier series.[HW83] In the minimisation Hirshman *et al* treat the coordinate system as the independent variables; to this end they assume the coordinates in their coordinate system are flux coordinates. This assumption necessarily generates an equilibrium field in which flux surfaces are assumed to exist at every point in the plasma and results in a continuous pressure profile.

However, according to Taylor relaxation, the field in a plasma volume is Beltrami and does not require that flux surfaces exist everywhere. Chaotic structures akin to chaotic islands have been observed within the plasma and practical attempts to reduce edge localised modes intentionally break the outer flux surfaces to maintain stability.[ET12] There has also been work to explain thermal transport within the plasma using chaotic structures called cantori.[Hud08][Hud09] Such internal field structures are inconsistent with continually nested flux surfaces, and so `VMEC` lacks the ablity to discern the chaotic nature of the equilibrium field.

To remedy this a new generation of code written by Dr Stuart Hudson has been developed, now referred to as the Stepped Pressure Equilibrium Code (`SPEC`). The code requires only a finite set of flux surfaces to exist within the volume, allowing chaotic structures to be discerned in the plasma volume. A coordinate system is interpolated between the flux surfaces, and a modified Taylor relaxation is executed

which allows the chaotic nature of the field to be resolved.[HDHM12]

SPEC requires a set of flux surfaces to be defined as interfaces during the computation of the equilibrium field. Which flux surfaces should be used and what effect this selection has on the equilibrium calculation are as yet unanswered questions. These algorithmic questions are the computational analogues of the questions into the nature of these flux surfaces that emerged in the last section. So, in investigation of the nature of the internal flux surfaces, this thesis also reports on the implications for SPEC.

1.2 Thesis outline and publications

1.2.1 Outline

Chapter two explains the MRXMHD formulation and derives the structure of the equilibrium according to its principles. From this we identify the force balance condition that allows a pressure discontunity across interfaces. This pressure jump condition is then formulated as a Hamilton–Jacobi equation, a generalisation of the work done by Berk *et al.* Kaiser and Salat's concern about the application of the Hamilton–Jacobi treatment mentioned in Section 1.1.2 is then solved, providing a consistent explanation to prove that inferences from the Hamiltonian system are acceptable. Finally the discontinuity condition is positioned as an inverse problem from which a more general understanding of the problem results.

Chapter three outlines how solutions to the pressure jump Hamiltonian equations are calculated and selected as valid continuations. The Hamiltonian equations are solved using a program written by the author named PJH, this code is described and the capabilities and limitations of the code are discussed. The code is also capable of using Greene's residue to numerically investigate whether the continuation is possible. This calculation is also described, along with the number theory required to calculate the residue. Still in Chapter three, the three cases of interest are defined. The first is a simplified first-order approximation to the pressure jump Hamiltonian that is more easily solved and more simply probed for the effect of perturbative parameters (including the magnitude of the pressure jump). The second case is a simulation of SPEC interfaces to inform SPEC. The third case is of a flux surface that has been extracted from a plasma volume. This final case is provided as a less artificial investigation of the pressure discontinuity condition.

Chapter four investigates the phase space of the Hamiltonian for the three cases defined in the previous chapter. The phase space of the simplified system illuminates the complex phase spaces of the latter two cases. This investigation explains the destructive effect of deformations, the prescribed field and the pressure jump on the

Hamiltonian trajectories.

Chapter five attempts to understand the nature of pressure-loaded flux surfaces by differentiating between *resilience*, (how likely a flux surface is to withstand further perturbations), and the concept of *robustness*, (how likely the flux surface is to withstand all possible perturbations). Robustness is conveyed through the invention of a robustness diagram, which shows what magnitude of pressure jump the flux surface can withstand as a function of some parametrisation of the deformation of the surface geometry. This allows the conditions of continuation to be qualitatively compared across the three cases.

Following this in Chapter six the thesis returns to the original motivation of the thesis and identifies the results of the numerical investigations in Chapters four and five that are relevant to MRXMHD and the code `SPEC`. Suggestions are then made to improve both the MRXMHD formulation and `SPEC` itself. Modifications to the `PJH` code are then discussed, and future work is suggested.

1.2.2 Work and publications

The work toward this thesis produced a `VMEC` introductory manual "VMEC Introduction" which is available online on the H–1 Wiki. General work toward the MRXMHD formulation lead to papers looking at MRXMHD from an entropy point of view.[DHM+08] This thesis lead directly to the publication of the pressure jump Hamiltonian formulation and the proof of its applicability in 2010.[MHDv10] The formulation of MRXMHD has gradually evolved over the lifetime of this thesis, which led to more publications.[HDHM12]

Important results from Chapter four and five are currently being developed into a paper.

Chapter 2

MRXMHD and the formulation of the pressure jump Hamiltonian

This chapter will first describe how fusion works and how one can research using first principles. Then the simplification is described that moves us to an approach to fusion where the device is envisaged as a collection of toroidal surfaces, composed of twisted magnetic field lines; and between these surfaces chaotic structures can exist (MRXMHD). Then concentrating on a single flux surface, a force-balance condition is derived and investigated. Upon investigation it is realised that the force-balance condition can be formulated as a Hamiltonian dynamical problem. The Hamiltonian treatment is then investigated.

2.1 Magnetohydrodynamics in fusion theory

2.1.1 Magnetic confinement fusion

The purpose of fusion power research is to utilise the energy that is released when light nuclei fuse to create a larger nucleus for the purposes of electrical power generation. There are many possible reactions, but the most feasible is the reaction between hydrogen isotopes, deuterium ($D = {}^2H$) and tritium ($T = {}^3H$).

A deuterium–tritium reaction involves fusing together the hydrogen isotope deuterium (whose nucleus contains a proton and a neutron) with the hydrogen isotope tritium (whose nucleus contains one proton and two neutrons) which results in the following reaction:

$$\mathrm{D} + \mathrm{T} \longrightarrow \mathrm{H}e + \mathrm{n}\ . \tag{2.1}$$

The deuterium–tritium reaction creates the fused product helium, and a stray neutron. The helium is typically an unwanted "ash" byproduct in the reaction and is removed after thermalisation to extract its energy, the neutron however quickly escapes and collides with the 'blanket' i.e. walls that surround the device designed

especially to absorb neutrons. These collisions, combined with other heat escaping the plasma, heat the blanket. The blanket is in thermal contact with the water which it converts to steam, which turns turbines to generate electrical energy. The mechanism by which electrical energy is extracted is in principle no different to any other fuel based power source. It is a heat engine.

It is difficult to get nuclei to fuse because of the strong electrostatic forces that cause them to repel each other. There are many methods to try to fuse atoms. One method, referred to as 'inertial confinement fusion' fires lasers from all angles toward a pellet of fuel in order to compress the pellet and force the atoms inside to fuse. Alternatively, one can facilitate D and T nuclei to collide and rely on their momentum to fuse the nuclei. Currently, the most advanced method is to heat the atoms to a very high temperature, embuing them with so much energy that they are more likely to collide and fuse.

At such high temperatures molecules break down into atoms, and the atoms themselves break into their component parts: electrons and ions (atomic nuclei). This leaves a mixture of electrons and ions floating in space, and so at this temperature gas has turned into a *plasma*. A plasma is considered a new state of matter because once the electrons have been stripped, the mixture has new properties. The most important properties of a plasma are that it can conduct electricity, can be affected by magnetic fields and exhibits collective behaviour because each particle can produce a field that affects every other particle in the plasma. It is a very complicated system indeed.

These properties make the system very difficult to model and predict, but also provide a unique opportunity to confine the mixture. As the particles can be manipulated by magnetic fields, one can use magnetic fields to locally contain the plasma while the particles inside fuse.

2.1.2 Principles of magnetic confinement

The most challenging aspect of creating break-even fusion is the confinement of the plasma. At such high temperatures (ITER, the large machine currently being built in France, is projected to reach temperatures in excess of $1.5 \times 10^7\, K$) the surroundings are in comparison extremely cold, and if the plasma comes in contact with the surroundings it quickly cools, the fusion reactions become less frequent and the fusion can cease. This means we require a method in which the plasma makes no physical contact with its surroundings.

As the fusion reactants are now in a plasma state, they can be manipulated by magnetic fields as each charged particle in the plasma (ion or electron) is affected by the Lorentz force. By using an appropriate configuration of magnetic coils one can

channel the plasma into a cylindrical shape. To confine the plasma at the ends, the line of loop magnets is bent to create a toroidal shape, thus the field now resembles a torus and the plasma follows this field generating a *toroidal plasma*.

There are various ways to heat the plasma. The most common is by sending radio-frequency electromagnetic waves tuned to the natural resonance frequency of the particles. This energises the particles and helps keep the temperature high. The eventual goal is to establish a steady state in which the fusion power produced is greater than the power required to keep the plasma in a steady state.

2.1.3 Magnetohydrodynamics and confinement

Assuming ideal MHD, the Lorentz force per unit volume is

$$\boldsymbol{F} = \boldsymbol{j} \times \boldsymbol{B} \,, \tag{2.2}$$

where $\boldsymbol{F}$ is the force, $\boldsymbol{B}$ is the magnetic field, and $\boldsymbol{j}$ is the *current density* $\boldsymbol{j} = \boldsymbol{\nabla} \times \boldsymbol{B}$. For confinement to be effective, one needs the force to act against the natural tendency to of the plasma to flow along the pressure gradients $\boldsymbol{\nabla} P$. Thus the basic equation determining confinement is that

$$\boldsymbol{\nabla} P = \boldsymbol{j} \times \boldsymbol{B} \,. \tag{2.3}$$

It is necessary to define the two main directions that will commonly be used. The *toroidal* direction is the direction pointing around the torus "the long way round", whereas the *poloidal* direction is the direction pointing "the short way round". Often it may be necessary to refer to the *radial* direction, which generally points out of the toroid.

With these directions we can define different cross sections. A *toroidal cross section* is the shape caused by the intersection of a plane defined by a constant value of toroidal angle. A *poloidal cross section* is similarly defined, but is typically less helpful, and thus less used in the literature.

Figure 2.1 illustrates these directions and cross sections.

2.1.4 Tokamaks and stellarators

All toroidal geometries can be divided into two types. A torus that has the same toroidal cross section throughout the entire toroidal angle is referred to as *axisymmetric*, all other shapes deviate from axisymmetry and are therefore *nonaxisymmetric*.

A *tokamak* is the name given to an ideally axisymmetric toroidal fusion device while *stellarators* are nonaxisymmetric.

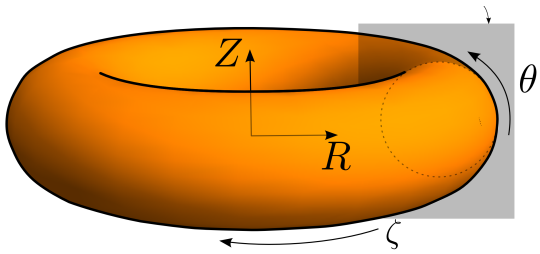

(a) A stylised illustration of a tokamak. Note the shape is axisymmetric.

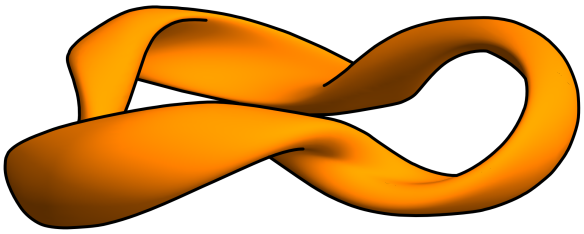

(b) A stylised illustration of a stellarator. The shape is not axisymmetric. While this complicates construction of the device, the more complicated confining magnetic field allows the plasma to be confined without inducing currents in the plasma.

Figure 2.1: A stylised representation of the difference between a tokamak and a stellarator.

Tokamaks are currently the most technically advanced type of fusion device. Despite the current focus on tokamaks, stellarator research is still an active area of research and each method benefits from the research done on the other. The division of labour has however changed the nature of research into each type. Research into tokamaks is increasingly experimental, with a larger emphasis on engineering and materials.

While being more complex, larger and often more expensive to build, stellarators have the benefit that only the external magnetic field is in principle required to contain it. In contrast, tokamaks require the introduction of large toroidal currents into the plasma to generate internal poloidal magnetic fields that maintain the axisymmetric shape.

The axisymmetric shape makes tokamaks simpler to model, but in general, tokamaks are never truly axisymmetric anyway. By virtue of the magnetic field being generated by a finite number of coils, there will always be nonaxisymmetry as the magnetic field strength will "dip" in between coils, causing a ripple throughout the plasma that destroys true axisymmetry and make the field dependent on the third (ζ) dimension. Further, advanced tokamaks intentionally *introduce* such 3D fields, for example the use of resonant magnetic perturbation coils used to suppress edge localised modes.[Eva13] Stellerator theory is natively three-dimensional, and so has

renewed importance in understanding 3D effects.

2.1.5 The equilibrium field

The magnetic field is set up by a collection of current carrying coils. A direct calculation using the Biot-Savart rule can determine the magnetic field generated by these coils, which give the *vacuum field*. However, when one adds plasma to the field, the ions and electrons of the plasma will interact with the magnetic field generating their own fields in the process. This complex interaction results in an *equilibrium field*. The equilibrium field is a good representation of the plasma system because the particles tend to follow the magnetic field lines.

This thesis assumes ideal MHD, i.e. that the Larmor radius is sufficiently smaller than our length scales of interest and that resistivity is small enough so that diffusion is slower than our timescales of interest. Within this domain of applicability, the plasma is in static equilibrium, and $\boldsymbol{B}$ is the equilibrium field. This field is found by solving Equation (2.3), when the Lorentz force density balances the pressure gradient within the plasma, repeated here:

$$\boldsymbol{\nabla} p = \boldsymbol{j} \times \boldsymbol{B} \, . \tag{2.4}$$

The best way to solve Equation (2.4) and calculate the general equilibrium 3D field is still an open problem in fusion, but the problem has a solution in ideal tokamaks and this idealised solution exhibits structure relevant to the general problem. In the case of a perfect tokamak, the plasma toroid is filled (foliated) with a nested set of helical magnetic field lines. Each field line lies on an infinitely thin toroidal surface, the union of this infinity of surfaces fills the toroidal volume.

For such a field line, there are two configurations, either the field line will meet up with itself and repeat or it will never meet up with itself and will wrap around the torus forever. The field lines that wrap around the torus forever will cover the surface completely. As magnetic field lines cannot cross, these field lines act as a barrier to field lines internal to the surface, and therefore will conserve the flux within. For this reason, this structure is known as a *flux surface* and is extremely important for confinement. The middlemost structure within the union of flux surfaces is a closed loop referred to as the *magnetic axis*.

Embedding the field lines in a toroidal geometry means the field lines can have effectively an infinite length in a finite volume. For example, a helically winding field line may wrap around an infinite number of times without meeting up with itself but remaining on a surface. Thinking of a field line $\boldsymbol{B}$ as the locus of the position of a

particle $\boldsymbol{r}$[1]

$$\frac{d\boldsymbol{r}}{dt} = \boldsymbol{B} \ , \tag{2.5}$$

the very long field lines correspond to very long timescales of particle trajectories. Physical problems on long timescales can produce unique behaviours often ignored when treating small time scales, like sensitivity to initial conditions, or *chaos*. Indeed there is strong theoretical and experimental evidence for the appearance of chaos in the volume of a toroidal fusion plasma.[HN10][EMB+06]

For the full 3D problem, rather than trying to solve the force balance condition Equation (2.4) and identifying the flux surfaces in the plasma, the method of Multiple RelaXed MHD (MRXMHD) *prescribes* a finite set of flux surfaces that one can expect to exist as an initial guess at the strucure of the field. The plasma volume has then been divided up into 1) flux surfaces and 2) the volume between the flux surfaces where the magnetic field is calculated based on Taylor relaxation. As the guessed initial geometry of the prescribed surfaces is not expected to be that of the true equilibrium flux surfaces, an additional step in the construction of the equilibrium is required and that is to adjust the surfaces to get a globally consistent solution consistent with the appearance of chaotic field lines in the plasma volume.[HHD07]

2.2 MRXMHD

2.2.1 Prescribing flux surfaces

For the purposes of MRXMHD, toroidal flux surfaces need only be nested and must not touch each other. Mathematically, a flux surface is usually best described using a Fourier series. One prescribes N toroidal surfaces each labelled as $\mathcal{S}_l = R_l(\theta,\zeta)\hat{R} + Z_l(\theta,\zeta)\hat{Z}$ with the form

$$R_l(\theta,\zeta) = \sum_{n=-N}^{N}\sum_{m=0}^{M} R_{l;mn}\cos\left(m\theta - n\zeta\right) \ , \tag{2.6}$$

$$Z_l(\theta,\zeta) = \sum_{n=-N}^{N}\sum_{m=0}^{M} Z_{l;mn}\sin\left(m\theta - n\zeta\right) \ . \tag{2.7}$$

where θ and ζ are a poloidal and toroidal angle respectively This representation we refer to as RZ form, and simplifies to 2D Cartesian coordinates $[R(\theta;\zeta = \text{const})$

[1]This can be an especially helpful way to think about the field lines, not just becuase there are mathematical benefits to thinking this way, but also because to a first approximation, the ions and electrons *do* follow the field lines, and $\boldsymbol{r}(t)$ can be thought of the equation of motion of a particle.

and $Z(\theta;\zeta = \text{const})]$ when the torus is viewed from a toroidal cross section, as in Figure 2.1. The Fourier coefficients are introduced so that all the information of the surface is contained within the Fourier components R_{mn} and Z_{mn}, and so that computationally the surface will be smooth for a finite number of components. This description is very common in fusion research, see Appendix A.3 for more detailed description of this representation of a flux surface.

When the flux surfaces are prescribed in this way, they are assumed to exist for the purposes of MRXMHD. When this is done they are refered to as *interfaces*.

But what of the magnets that generate the field? We ignore these in this thesis because one can always reverse engineer a set of coils, however complicated, to create the 3D structure implied by the flux surfaces prescribed.

2.2.2 Building the plasma from flux surfaces interfaces

With a set of flux surfaces prescribed, the question remains of what the field is like within the volumes between the surfaces. This can be done using the method first described by Hudson, Hole and Dewar in 2006 which has since become known as MRXMHD (Multiple-Region RelaXed MagnetoHydroDynamics).[HHD06]

Consider a set of concentric tori $\mathcal{S}_l$ that one wishes to prescribe as flux surfaces within the plasma volume, bounded by the outermost flux surface $\mathcal{S}_N$. Under conventional Taylor relaxation one must minimise the plasma energy under the constraint of conserved helicity and mass. To do this one can introduce the Lagrangian multipliers μ_l and ν_l and extremise the functional:[HHD07]

$$\mathcal{F} = \sum_l \left(U_l - \mu_l H_l/2 - \nu_l M_l/2\right) \tag{2.8}$$

in each of the volumes V_l between the surfaces $\mathcal{S}_l$ and $\mathcal{S}_{l+1}$. Here U_l is the plasma energy, H_l is the helicity and M_l is the mass[2] within each volume. Explicitly they are

$$U_l = \int_{V_l} \left(\frac{P_l}{\alpha - 1} + \frac{B_l^2}{2\mu_0}\right) dV \tag{2.9}$$

$$H_l = \int_{V_l} \boldsymbol{A}_l \cdot \boldsymbol{B}_l \, dV \tag{2.10}$$

$$M_l = \int_{V_l} P_l^{1/\alpha} \, dV \ , \tag{2.11}$$

where P_l is the pressure in each volume, $\boldsymbol{A}$ is the vector potential ($\boldsymbol{\nabla} \times \boldsymbol{A} = \boldsymbol{B}$), μ_0 is the permeability of free space (omitted from now on), and α is the ratio of specific heats.

[2] Strictly M involves both mass and entropy.[DHM+08]

Where MRXMHD differs from conventional Taylor relaxation is that now there are *multiple* volumes in which to extremise the functional, and there are potentialll an infinity of additional variables to describe the geometry of the flux surfaces. The functional is extremised by allowing variations in the pressure δP_l, the magnetic field $\delta \boldsymbol{A}_l$ *and* the geometry of the interfaces $\boldsymbol{\eta}$. When this is done, one finds that

$$\delta F_l = \int_{V_l} (\boldsymbol{\nabla} \times \boldsymbol{B}_l - \mu_l \boldsymbol{B}_l) \cdot \delta \boldsymbol{A} \, dV \tag{2.12a}$$

$$+ \int_{V_l} \left(\frac{1}{\alpha - 1} - \nu_l \frac{P_l^{1/\alpha}}{\alpha P_l} \right) \delta P_l \, dV \tag{2.12b}$$

$$+ \int_{S_l} \left(\frac{P_l}{\alpha - 1} - \nu_l P_l^{1/\alpha} - \frac{B^2}{2} \right) (\boldsymbol{n} \cdot \boldsymbol{\eta}) dS \quad = 0 \, , \quad \forall \delta P, \delta \boldsymbol{A}, \text{ and } \delta \eta \tag{2.12c}$$

Thus according to Equation (2.12a), at relaxation the magnetic field is Beltrami in each volume, i.e. the field satisfies

$$\boldsymbol{\nabla} \times \boldsymbol{B} = \mu_l \boldsymbol{B} \, , \tag{2.13}$$

in each volume. Equation (2.12b) states that the pressure in each volume is constant. The surface term [Equation (2.12c)] implies that the quantity $(P + B^2/2)$ must be the same on one side of the surface as the other, thus allowing a pressure discontinuity by allowing an associated discontinuity in the magnetic field. As the pressure has been assumed constant in each volume, this discontinuity condition allows a non-trivial pressure profile $P(s)$ (where s is the radial coordinate) only by having a stepped pressure profile.

A code is being developed by Dr Stuart Hudson named `SPEC` (Stepped-Pressure Equilibrium Code) that can calculate the 3D structure of the magnetic field from a collection of prescribed flux surfaces and appropriate boundary conditions.

2.2.3 The pressure jump condition

The pressure discontinuities arising from the MRXMHD formulation is the focus of this thesis, as the nature of these infinitely thin, pressure–discontinuity sustaining surfaces is not apparent. They are more general than the previous "sharp boundaries" mentioned in Section 1.1.2 as these surfaces allow a Beltrami field on both sides of the surface, and do not require the pressure to be zero on one side. Thus the sharp boundary model can be seen as a special case of a flux surface that forms the interface to a vacuum field, i.e. the last closed surface on the outside of the plasma. Understanding the nature of these flux surfaces is important to the workings of an equilibrium code like `SPEC`.

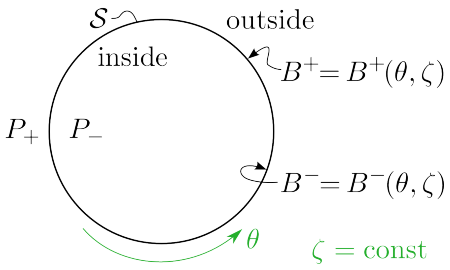

Figure 2.2: A toroidal cut showing the cross section of the plasma and the various definitions. The cross section is a circle for simplicity, but the theory will work for a surface $\mathcal{S}$ of any shape.

A more precise statement of the pressure jump condition is: when there is a discontinuity in the pressure across a surface $\mathcal{S}$, the following must apply on $\mathcal{S}$,

$$P_\pm = \text{const} \tag{2.14a}$$

$$\boldsymbol{B}^\pm \cdot \boldsymbol{n} = 0 \tag{2.14b}$$

$$(\boldsymbol{\nabla} \times \boldsymbol{B}^\pm) \cdot \boldsymbol{n} = 0 \tag{2.14c}$$

$$\left[\!\left[\frac{1}{2} B^2 + P \right]\!\right] = 0 \,. \tag{2.14d}$$

In Equations (2.14), $\boldsymbol{n}$ is the normal to the surface, and the notation $[\![x]\!]$ refers to the difference between x on one side of the surface and x on the other side. $x^\pm$ or $x_\pm$ refer to a quantity s on one side of the interface, a minus sign refers to the *inner side* (that faces the magnetic axis) whereas a plus sign refers to the outer side. Equations (2.14a - 2.14c) must hold on both sides of the surface [note a different constant pressure on either side in the case of Equation (2.14a) is allowed]. We refer to Equations (2.14) collectively as the *pressure jump conditions*.

While this derivation was reached through the MRXMHD formulation of a fusion plasma, it is possible to derive the same pressure jump disconinuity condition from first principles by considering the general plasma stress tensor when taking into account only kinetic and electromagnetic stress. This is done in Appendix A.5.

The field on the inner side (side closest to the magnetic axis) of $\mathcal{S}$ is given by $\boldsymbol{B}^-$, and the field on the outer side is given by $\boldsymbol{B}^+$, as shown in Figure 2.2. Equation (2.14d) then becomes

$$\frac{1}{2} B^{+2} - \frac{1}{2} B^{-2} = P_- - P_+ \,. \tag{2.15}$$

When Equation (2.15) is written in terms of the covariant components of the

magnetic fields, one finds that

$$\Delta P = \sum_{i,j\in\{\theta,\zeta\}} \frac{1}{2} g^{ij} B_i^+ B_j^+ - \frac{1}{2} g^{ij} B_i^- B_j^- \ , \tag{2.16}$$

where $\Delta P = P_- - P_+$ and $g^{ij} = g^{ij}(\theta,\zeta)$ are the contravariant metric coefficients defined on the 2-dimensional Riemannian manifold $\mathcal{S}$, related to the covariant coefficients by inverting the 2×2 matrix $[g_{ij}]$,[BL96]

$$g^{\theta\theta} = g_{\zeta\zeta}/\sqrt{g} \ , \qquad g^{\theta\zeta} = -g_{\theta\zeta}/\sqrt{g} \ , \qquad g^{\zeta\zeta} = g_{\theta\theta}/\sqrt{g} \ , \tag{2.17}$$

where $\sqrt{g} = g_{\theta\theta}g_{\zeta\zeta} - g_{\theta\zeta}^2$ is the determinant. We shall also need the 2-dimensional contravariant components of the surface magnetic field, defined by

$$B^\theta = g^{\theta\theta} B_\theta + g^{\theta\zeta} B_\zeta \tag{2.18a}$$

$$B^\zeta = g^{\theta\zeta} B_\theta + g^{\zeta\zeta} B_\zeta \ . \tag{2.18b}$$

For more information on the covariant and contravariant representations of vectors, and for more information about the metric see Appendix A.1

The major advantage of MRXMHD and `SPEC` is the ability to resolve volumes of chaos and islands in the Beltrami fields. Such structures are known to be very important in the stability and confinement of fusion plasmas, but no other existing equilibrium code is fully consistent with field line chaos, either ignoring it or treating it in an ad-hoc way. For instance in the famous VMEC code, where requiring the pressure to be a continuous function results in the plasma being composed of a complete nested set of flux surfaces, a situation that one would expect only in an ideal tokamak.

Recent results show that only a small number of interfaces are required to get agreement with experimental data.[HDHM12] However there is in principle no upper limit on the number of surfaces one can prescribe, so one can approach a continuous pressure profile by portioning smaller and smaller pressure jumps among more and more flux surfaces.[HHD06]

2.3 Hamiltonian formulation of the pressure jump condition

2.3.1 Setting up the problem

As stated in Section 2.2.3, one can construct the pressure jump condition on a surface $\mathcal{S}$ with two sides: $+$ for the outer side and $-$ for the inner side.

Stating the pressure jump condition under these definitions led to Equation (2.15), which is repeated here:

$$\frac{1}{2}B^{+2} - \frac{1}{2}B^{-2} = P_- - P_+ \,. \tag{2.19}$$

We will now show that Equation (2.19) is analogous to a Hamiltonian system, which can be realised when one writes the magnetic field in covariant or contravariant notation. To be precise, the equation becomes a Hamilton-Jacobi equation. The reason for doing this is that under a Hamiltonian formulation, one may apply the tools developed for Hamiltonian mechanics to investigate the existence of given solutions. Physically, this amounts to determining existence properties of the interfaces prescribed in MRXMHD.

2.3.2 Hamiltonian treatment

The keys to the Hamiltonian treatment are Equations (2.14b) and (2.14c), together they imply that on $\mathcal{S}$,

$$\partial_\theta B^\pm_\zeta - \partial_\zeta B^\pm_\theta = 0 \,. \tag{2.20}$$

Equation (2.20) is implicitly satisfied if the field components can be written as

$$B^\pm_\theta = \partial_\theta f^\pm \,, \qquad\qquad B^\pm_\zeta = \partial_\zeta f^\pm \,, \tag{2.21}$$

where the two scalar functions $f^\pm(\theta,\zeta)$ are referred to as *surface potentials*. The surface potentials f^- and f^+ define fully the fields on the inner and outer sides of $\mathcal{S}$ (B^- and B^+ respectively).

By using f rather than $\boldsymbol{B}$, Equations (2.14b) and (2.14c) are implicitly satisfied and the pressure jump conditions reduce to the single condition

$$\Delta P = \sum_{i,j\in\{\theta,\zeta\}} \frac{1}{2}g^{ij}\partial_\theta f^+ \partial_\zeta f^+ - \frac{1}{2}g^{ij}\partial_\theta f^- \partial_\zeta f^- \,. \tag{2.22}$$

Given a surface (which defines R and Z which in turn defines g^{ij}) and a field on one side of the surface (which defines, say f^-) the goal is to find the potential on the other side of the surface (f^+) (See Figure 2.3). If f^+ can be found that has continuous second partial derivatives [$f^+ \in C^2(P^+)$], the magnetic field will satisfy force balance and lie on the surface, satisfying Equations (2.14).

The problem is symmetric, one can either, given f^- find f^+ (work inside-out), or given f^+ find f^- (work outside-in). Thus the unknown surface field potential is referred to simply as f. Then the pressure jump condition becomes a problem of

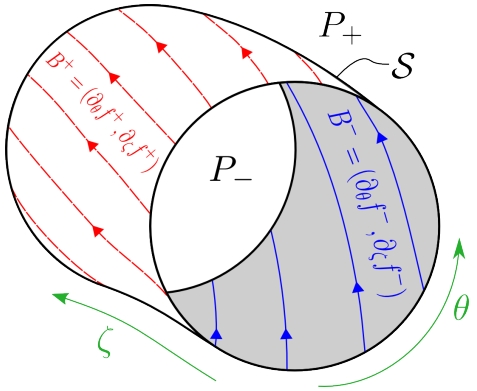

Figure 2.3: A depiction of a toroidal segment of the surface $\mathcal{S}$ to demonstrate the quantities required for the Hamiltonian.

calculating f from the equation

$$H(\theta, \zeta, \partial_\theta f, \partial_\zeta f) = \Delta P \ . \tag{2.23}$$

where

$$H(\theta, \zeta, p_\theta, p_\zeta) = \frac{1}{2} g^{ij} p_i p_j + V(\theta, \zeta) \ , \tag{2.24}$$

where there is an implicit sum of $i, j \ \in \{\theta, \zeta\}$, and

$$V(\theta, \zeta) = -\frac{1}{2} g^{ij} \partial_i f^- \partial_j f^- \ , \tag{2.25}$$

and where f^- has been arbitrarily chosen as the given potential: the *prescribed field* on what we refer to as the *prescribed side*.

Equation (2.23) is a partial differential equation for f. More specifically, Equation (2.23) is a time independent Hamilton-Jacobi equation with $\partial_i f = p_i$. The Hamiltonian in Equation (2.24) we refer to as the *pressure jump Hamiltonian*.

As a Hamiltonian system, ΔP is identified with the energy and f is a type two generating function (Hamilton's characteristic function) considered to generate the canonical pairs (θ, p_θ) and (ζ, p_ζ) through

$$p_\theta = \partial_\theta f = B_\theta \ , \qquad\qquad p_\zeta = \partial_\zeta f = B_\zeta \ . \tag{2.26}$$

If f exists, then the Hamiltonian orbit lies on an invariant torus in phase space. Such an orbit we refer to as *regular*, all other orbits are *irregular*. Conversely, if an invariant torus exists then the Hamilton-Jacobi equation can be integrated to find f (See Section 3.2.4 for details).

2.3.3 Solution and rotational transform

The solution of the pressure jump Hamilton-Jacobi equation is in general not unique. It may be that many Hamiltonian trajectories are regular, and so may correspond to possible field line solutions to the pressure jump condition. To differentiate between orbits one can calculate the *rotational transform*, defined as

$$\lim_{\Delta\zeta\to\infty} \frac{\Delta\theta}{\Delta\zeta} = \iota \ . \tag{2.27}$$

Given the non-intersection of phase-space characteristics for a well-defined Hamiltonian system [Arn89] and the fact that the phase-space characteristics are confined to a topological torus, it is understood that the rotational transform embodies a topological invariant of the phase-space characteristic itself. In Section 2.3.6, the existence of a map between phase-space characteristics and the magnetic field lines in configuration space that preserves characteristic topology will be shown. Since this map preserves characteristic topology, it also preserves the rotational transform. Thus the rotational transform ι of the field line in configuration space is the same as the corresponding quantity in phase space (known as the *winding number* w):

$$\iota = w \ . \tag{2.28}$$

So it is often necessary to label solutions according to their rotational transform. The physical solution ${}^{\iota}(B_\theta(\theta,\zeta), B_\zeta(\theta,\zeta))$ to the pressure jump condition (referred to as a *field line configuration*) can be identified with a solution to the pressure jump Hamilton-Jacobi equation, namely ${}^{w(=\iota)}(p_\theta(\theta,\zeta), p_\zeta(\theta,\zeta))$, refered to as a *Hamiltonian trajectory* and the two solutions are related via

$${}^{\iota}p_\theta = {}^{\iota}B_\theta, \quad {}^{\iota}p_\zeta = {}^{\iota}B_\zeta \ . \tag{2.29}$$

That is not to say that the field line configuration is the same as the Hamiltonian trajectory, as they exist in different spaces. The field line configuration exists on a torus in $\mathbb{R}^3$, while the Hamiltonian trajectory exists in a four dimensional *phase space*.

The solution to this autonomous Hamiltonian system can be found by solving the

corresponding characteristic equations,[Gar64]

$$\dot{\theta} = \frac{\partial H}{\partial p_\theta} \,, \tag{2.30a}$$

$$\dot{p_\theta} = -\frac{\partial H}{\partial \theta} \,, \tag{2.30b}$$

$$\dot{\zeta} = \frac{\partial H}{\partial p_\zeta} \,, \tag{2.30c}$$

$$\dot{p_\zeta} = -\frac{\partial H}{\partial \zeta} \,. \tag{2.30d}$$

This Hamiltonian system has two degrees of freedom, but there is a conserved property of the Hamiltonian, namely the pressure jump (the energy). Associated with this is the ignorability of the timelike coordinate, which can be used to reduce the two degrees of freedom system to a $1\frac{1}{2}$ degree of freedom system.

2.3.4 Reduction to a 1 1/2 DOF system

To simplify computation of Hamiltonian orbits, we condense these equations by dividing Equations (2.30) by Equation (2.30c) to trivialize the third of Hamilton's equations and make the toroidal coordinate the "time" variable. The division requires that $\dot{\zeta} \neq 0$, the implications of this being addressed in Section 2.3.5.

The reduced equations provide equations of motion with a more physically relevant form. The first describes the path of the Hamiltonian trajectory through configuration space:

$$\frac{d\theta}{d\zeta} = \frac{g^{\theta\theta}p_\theta + g^{\theta\zeta}p_\zeta}{g^{\theta\zeta}p_\theta + g^{\zeta\zeta}p_\zeta} = \frac{B^\theta}{B^\zeta} \,. \tag{2.31}$$

where Equations (2.18) have been utilized. Equation (2.31) is the equation of a field line. A solution to this characteristic equation of the pressure jump Hamiltonian may correspond to a field lines on the magnetic field on $\mathcal{S}$, the details when the equivalence is possible is covered in Section 3.2.5.

The second equation of motion is

$$\frac{dp_i}{d\zeta} = \frac{1}{2}\frac{\partial_i g^{ij} p_i p_j + 2\partial_i V}{g^{\theta\zeta}p_\theta + g^{\zeta\zeta}p_\zeta} \,, \qquad (p_i = B_i) \,, \tag{2.32}$$

for $i \in \{\theta, \zeta\}$. Equation (2.32) shows that the canonical momentum gives the covariant components of the magnetic field along a Hamiltonian trajectory for solutions with the required rotational transform.

The final equation of motion, Equation (2.30d), can be solved implicitly by the first two using the fact that the energy of this Hamiltonian system is conserved i.e.

the pressure jump is constant along the flux surface by Equation (2.14a). This means p_ζ can be written as a function $p_\zeta = p_\zeta(\theta, p_\theta, \zeta; \Delta P)$. When this is substituted into Equations (2.30a) and (2.30b), the entire system can be solved within two differential equations. However, inversion of the Hamiltonian brings about an arbitrary sign, which for simplicity, we choose to be positive, discussing the choice further in Section 2.3.5.

The system is now condensed into the differential system

$$\frac{d\theta}{d\zeta} = u(\theta, \zeta, p_\theta; \Delta P) \tag{2.33a}$$

$$\frac{dp_\theta}{d\zeta} = v(\theta, \zeta, p_\theta; \Delta P) \tag{2.33b}$$

One method of identifying the existence of f is to calculate the Hamiltonian trajectories. If a solution to this $1\frac{1}{2}$ degree of freedom system can be found that lies on an invariant torus in $(\theta, p_\theta, \zeta)$ space with the correct winding number, the trajectory, when projected onto the 3D geometric torus, gives the field lines that lie on that surface.

Treating the problem as Hamiltonian, one is able to utilise tools that have been developed for determination of integrability in Hamiltonian systems to investigate whether a solution (f) can be found that satisfies force balance. However, before one can utilise tools from the Hamiltonian approach, there are two concerns that need to be addressed. Firstly there is an ambiguous choice of sign in the Hamiltonian formulation, and secondly it had not been certain until now that solutions from the Hamlitonian formulation map bijectively and uniquely back to a physically relevant field line.

2.3.5 Ambiguity of sign

The pressure jump Hamiltonian is a constraint on the *square* of the magnetic field, so it is expected that there are *two* magnetic fields that would satisfy force balance on any given side. This arbitrariness is made explicit when one inverts the Hamiltonian to find $p_\zeta = p_\zeta(\theta, p_\theta, \zeta; \Delta P)$ in an effort to reduce the phase space. When completing the square one has the expression

$$g^{\theta\zeta} p_\theta + g^{\zeta\zeta} p_\zeta = \pm C \ , \tag{2.34}$$

where $C = \left[g^{\zeta\zeta}\left(2\Delta P - 2V(\theta,\zeta) - g^{\theta\theta}p_\theta^2\right) + (g^{\theta\zeta}p_\theta)^2\right]^{1/2}$. The left hand side of Equation (2.34) is the result of Equation (2.30c), i.e.

$$\frac{d\zeta}{dt} = B^\zeta = \pm C \ , \tag{2.35}$$

showing that the two solutions correspond to magnetic fields with opposite toroidal direction.

The information on the toroidal direction of the given field is similarly lost within the pressure jump Hamiltonian so the choice of sign must be made to reflect the initial conditions. It is expected that physical configurations would require a field to be in the same toroidal direction on either side of an infinitely thin flux surface, otherwise there would be a very strong current sheet, susceptible to a tearing instability.[PDJ90]

The choice of sign has also been shown to be equivalent to choosing the sign of the rate of change of toroidal flux [BL96].

When reducing the phase space of the Hamiltonian system, Hamilton's equations were divided by $\dot{\zeta}$, thus the condition in which $\dot{\zeta} = 0$ was necessarily lost. A field line that does not extend toroidally corresponds to a field configuration of infinite rotational transform – a situation we ignore as it will not ergodically cover the surface, and thus will never act as a flux surface.

2.3.6 Reconciling phase space and configuration space

Kaiser and Salat [KS94] solved the less general pressure jump discontinuity problem purely in configuration space, that is, a solution to force balance on the surface was sought that corresponded directly to geodesics covering a 3D torus. Such an approach is limited to situations where the field within the plasma volume is zero. However, Kaiser and Salat felt obliged to use this geodesic method because of concerns regarding the physical significance of Hamiltonian trajectories in phase space.

Kaiser and Salat's gravamen against the Hamiltonian formulation can be stated as the following: Suppose a solution to the pressure jump Hamiltonian system is found. This will correspond to a Hamiltonian orbit that lies in a four dimensional phase space. The actual field line however exists on the two dimensional torus embedded in Euclidean 3-space, i.e. configuration space. We must project a four dimensional phase space trajectory to the two dimensional configuration space – is it not possible that the projected trajectory intersects itself after the projection?

Assuming the magnetic field is nowhere zero, such intersections would make it impossible to interpret the projection as a physical field line.

However, it will now be proved that such crossings cannot occur, via a direct application of the Birkhoff theorem to Equations (2.33). It will thus be demonstrated

that the existence of an invariant torus in phase space sufficient to imply that a corresponding field line (identified by having ι equal to the w of the extant Hamiltonian trajectory that lies on an invariant surface) is guaranteed to exist and is consistent with Equations (2.14).

The system is a $1\frac{1}{2}$ degree of freedom Hamiltonian whose trajectories define a 2D area preserving map by integrating Equations (2.33). The mappings of interest, those generated by a trajectory that lies on an invariant surface, are also twist maps as the metric is positive definite $[\det(\partial_{p_i}\partial_{p_j}H) > 0]$. [Gol01][Mac93]

Consider the phase space variables (q, p) in a 2 dimensional area preserving twist map, the Birkhoff Theorem states that, for a rotational invariant circle, [Mei92]

$$p = Y(q) \ , \tag{2.36}$$

where Y is a Lipschitz function on $\mathbb{R}^2$, i.e. Y satisfies

$$\sup_{x,y\in\mathbb{R}^2} \frac{|Y(x) - Y(y)|}{|x - y|} < C \ , \tag{2.37}$$

for some bounded constant C. In this case we can write the phase space mapping generated by the Hamiltonian as

$$(q', p') = T(q, Y(q)) \ . \tag{2.38}$$

Let us consider the operator π that is the projection of the phase space trajectory onto configuration space,

$$\pi(q, p) = q, \tag{2.39}$$

then

$$q' = \pi(T[q, Y(q)]) = \alpha(q) \ . \tag{2.40}$$

Thus, as T is a homeomorphism and Y Lipschitz, α is also a homeomorphism [Mei92]. The injective nature of a homeomorphism implies there will be no crossings under the mapping π.

Strictly, this is only true for a two dimensional system because the Birkhoff theorem applies only for a 2D phase space. Some limited higher dimensional results have been found.[MMS89]

This means a homeomorphic mapping like Equation (2.36) can be generated to define completely the evolution of the system, and the above proof applies. Thus, when mapping the Hamiltonian trajectories to the 2D torus in configuration space no

crossings are possible.

2.4 Pressure jump Hamiltonian and the inverse formulation

2.4.1 The Hamiltonian and important Hamiltonian equivalents

The Hamiltonian formulation of the force balance condition is then the time independent Hamilton-Jacobi equation (repeated here):

$$H(\theta, \zeta, \partial_\theta f, \partial_\zeta f) = \Delta P \ , \tag{2.41}$$

with Hamiltonian

$$H(\theta, \zeta, p_\theta, p_\zeta) = \frac{1}{2} g^{ij} p_i p_j + V(\theta, \zeta) \ . \tag{2.42}$$

There are a collection of abstract quantities in Hamiltonian dynamics that are important in obtaining results from the above formulation. They are listed here along with their physical equivalents, in order to provide some physical context. Table 2.1 summarises these Hamiltonian quantities and their physical equivalents for quick reference.

Energy

The general form for a Hamilton-Jacobi equation is

$$H(q_i, p_i) = E \ , \tag{2.43}$$

upon direct comparison with Equation (2.23), one can see that the Hamiltonian energy is equal to the pressure jump. Importantly, as the pressure jump is defined to be constant over the surface, so the energy is over the Hamiltonian trajectory.

Canonical coordinates

Canonical coordinates conserve the form of Hamiltonian's equations. Thus one is free to change between canonical coordinates without affecting Hamilton's equations. In the pressure jump Hamiltonian, the formalisation was based on the coordinates $q_i \in \{\theta, \zeta\}$. The realisation of the Hamilton-Jacobi equation form in Equation (2.23) allows us to identify directly the momenta $p_i = \partial_i f = B_i$ as the momenta canonical to q_i.

Action angle coordinates

In integrable systems acanonical tranformation can be made to *action-angle coordinates* in which the Hamiltonian trajectory is trivial, i.e. for the action angle coordinate pair (I, Θ), I (the momentum) is constant so that $\Theta = \omega_\Theta t + \Theta_0$. The configuration variable Θ is now trivial in that it is a straight line in the coordinates (I, Θ).

It might help to see it this way, a common method of solving a Hamiltonian problem is to transform to coordinates in which the motion is simpler. For instance one can use polar coordinates to easily solve a pendulum, whereas Cartesian coordinates would be best for a rolling ball on a plane. In a general physical system, motion would be much more complicated than in any of these two situations, but it should still always be possible to find a transformation to a set of coordinates in which the motion is simpler. Further, it is possible to find a set of coordinates in which the motion is not only simpler, but completely trivial, i.e. a straight line. The coordinates in which the motion is a straight line are action angle coordinates. Indeed, if a transformation to action angle coordinates is not possible, then the motion is *irregular* (see Section 3.2.4 for more details)

In the first situation one had complicated motion [finely detailed trajectory $p_\theta(\theta, \zeta)$] in a simple coordinate system [say, angular coordinates $\theta(\zeta)$]; after finding action angle coordinates one now has a very simple motion (a straight line $I = \text{const}$, $\Theta = \omega\zeta + \Theta_0$) in a complicated coordinate system to construct, (Θ, ζ). In finding the action angle coordinates one has translated the complicated motion from the trajectory to the transformation to action angle coordinates. The translation is made through what is called the *conjugacy*, X

$$\theta = X\Theta \; . \tag{2.44}$$

Physically, action angle coordinates are equivalent to straight field line coordinates. To see this one must recall that the canonical momentum of a trajectory is equal to the covariant component of the magnetic field [Equation (2.26)], i.e.

$$p_\theta = B_\theta \; , \qquad\qquad p_\zeta = B_\zeta \; . \tag{2.45}$$

In the $1\frac{1}{2}$ degree of freedom system (where ζ is considered the 'time') $p_\theta = B_\theta$. Straight field line coordinates are defined as those in which the magnetic field is straight, i.e.

$$B_\theta(\theta, \zeta) = I(\text{a constant}) \Rightarrow p_\theta(\theta, \zeta) = I \; . \tag{2.46}$$

To calculate them one can utilise the transformation used for action angle coordi-

Physical Quantities and their Hamiltonian Equivalents

ΔP	Pressure jump	E	Energy
f	Surface potential	S	Action / Hamilton's characteristic function
(θ, ζ)	Curvilinear coordinates	$\boldsymbol{q}$	Generalized coordinates
(B_θ, B_ζ)	Covariant components of magnetic field	$\boldsymbol{p}$	Generalized momenta
(Θ, Φ)	Straight field line coordinates	$\boldsymbol{Q}$	action angle coordinates
ι	Rotational transform	w	Winding number (angular frequency)

Table 2.1: A table summarizing the physical interpretations of Hamiltonian quantities in the problem.

nates

$$\Theta = X^{-1}\theta \, . \tag{2.47}$$

Hamiltonian trajectories

The *Hamiltonian trajectories*, also known as *orbits* are the solutions to the Hamiltonian system given by $[\boldsymbol{q}(t), \boldsymbol{p}(t)] = [\theta(t), \zeta(t), p_\theta(t), p_\zeta(t)]$. As shown in Section 2.3.6 these each homeomorphically correspond to the magnetic field lines. What is most important about the field lines is the way in which the field line wraps around the flux surface i.e. the field line configuration, identified by the rotational transform ι.

Figure 2.4 shows the relationship between trajectories and field lines, and the relationship between SFLC and action angle coordinates.

Winding number

In action angle coordinates the motion of each of the coordinates is of the form $\Theta = \omega_\zeta$. In this ω represents the angular frequency of the coordinate.

The winding number is unique for each regular orbit and so is an identifier for the trajectories, analagous to the rotational transform of a field line configuration. Indeed, as was shown in Section 2.3.3, the winding number is a topological invariant equal to the rotational transform.

Invariant tori

The *invariant tori* of a Hamiltonian system are the closed tori drawn out by the Hamiltonian trajectories when $p_\theta(\theta, \zeta)$ and $p_\zeta(\theta, \zeta)$ can be written as continuous,

single valued, periodic functions. These are analagous to the flux surfaces drawn out by the magnetic field lines, however they are not coincident as the two tori exist in different spaces (in phase space the invariant torus is described by $p_\theta(\theta,\zeta)$, $p_\zeta(\theta,\zeta)$, whereas the flux suface itself is described by defining $\mathcal{S}$).

Potential energy function

The *potential energy function* in the pressure jump Hamiltonian is a complicated term involving the metric and the prescribed field f^-:

$$V(\theta,\zeta) = -\frac{1}{2}g^{ij}\partial_i f^- \partial_j f^- \ . \tag{2.48}$$

Generating function

All canonical transformations can be written in terms of one of four generating functions (F_1, F_2, F_3, F_4). In general, a Hamilton-Jacobi equation with H independent of time can be written as

$$H(q_i, \partial_i F_2) = E \ , \tag{2.49}$$

in this case F_2 is a generating function given the special name Hamilton's characteristic function . Upon comparison with Equation (2.23), one can see that the surface potential f is equal to Hamilton's characteristic function . The existence of f then determines the existence of an invariant torus (See Section 3.2.4 for more details).

The system was reduced to a $1\frac{1}{2}$ degree of freedom system by utilising the constancy of the energy. Although p_ζ is no longer a canonical coordinate, one can still calculate f in this situation, as p_ζ is implicitly solved in the integration of the equations of motion.

2.4.2 The inverse formulation and the two-sided principle

A more general derivation for the pressure jump Hamiltonian can be achieved by considering the pressure jump condition between two fields $\boldsymbol{B}_0$ at pressure P_0 and $\boldsymbol{B}$ at pressure P. This time there is no specification on which field is on the "inside" or "outside" because it is not strictly necessary to do so and in not doing so one can avoid thinking of the problem as a continuation problem from inside to outside. In fact $\boldsymbol{B}_0$ and P_0 do not even need to be actual physical fields, just reference fields to define the Hamiltonian.

The pressure discontinuity condition is:

$$\frac{1}{2}B_0^2 + P_0 = \frac{1}{2}B^2 + P \ . \tag{2.50}$$

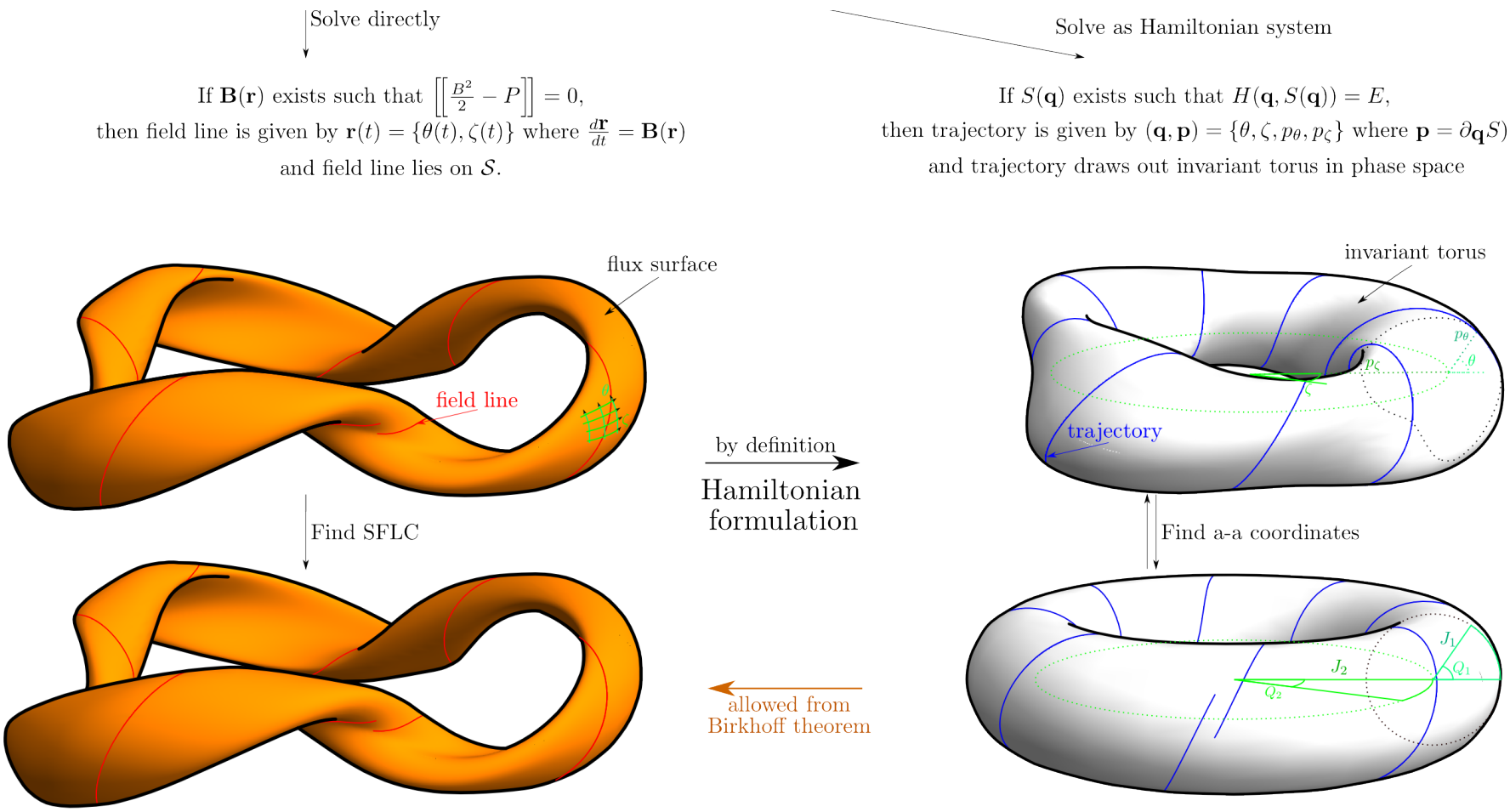

Figure 2.4: This image is a visualisation of configuration space and phase space. The left images shows a solution to the pressure jump condition (red) on a defined surface reminiscent of a fusion device (orange). Solving the pressure jump Hamiltonian system provides the functions $p_\theta(\theta, \zeta)$, $p_\zeta(\theta, \zeta)$. When p_θ and p_ζ are plotted in phase space (top right), these trajectories (blue) may ergodically cover an invariant torus (white). Provided an invariant torus is traced out, one can make a transformation to coordinates in which the momenta are constant (bottom right). The Birkhoff theorem allows one to map a phase space tracjectory back to an actual field line. Mapping the p_θ, p_ζ back to configuration space (top right to top left), will result in a field line of the same rotational transform. Mapping the action-angle solution to configuration space (bottom left to bottom right) will provide the same field line, but in coordinates in which the field lines are straight.

The scalar functions $B^2(\theta,\zeta)$ and $B_0^2(\theta,\zeta)$ can be separated into their (constant) surface average ($< . >$) and their fluctuation ($\tilde{.}$), which averages to zero:

$$B^2 =< B^2 > +\widetilde{B^2} \,, \tag{2.51a}$$

$$B_0^2 =< B_0^2 > +\widetilde{B_0^2} \,. \tag{2.51b}$$

Taking the surface average of the pressure jump condition results in the relation

$$\frac{1}{2} < B_0^2 > +P_0 = \frac{1}{2} < B^2 > +P \,, \tag{2.52}$$

which states the surface average of the square of the field to calculate $\frac{1}{2}<B^2>$ is equal to the surface average of the square of the provided field, shifted by the change in pressure. With reference to Equations (2.51), Equation (2.52) implies that

$$\widetilde{B_0^2} = \widetilde{B^2} \equiv -2\widetilde{V}(\theta,\zeta) \,. \tag{2.53}$$

Thus the squares of the two fields have the same variation.

Going back to the pressure jump condition,

$$\frac{1}{2}B_0^2 + P_0 = \frac{1}{2}B^2 + P \,, \tag{2.54}$$

$$\frac{1}{2} < B_0^2 > -\widetilde{V}(\theta,\zeta) + P_0 = \frac{1}{2}B^2(\theta,\zeta) + P \,, \tag{2.55}$$

$$\frac{1}{2} < B_0^2 > +P_0 - P = \frac{1}{2}B^2(\theta,\zeta) + \widetilde{V}(\theta,\zeta) \,. \tag{2.56}$$

The surface average and the fluctuation completely define B^2, but calculating $\boldsymbol{B}$ requires more information. Using the constraint that $\boldsymbol{B}$ is tangential to the surface, one can calculate it from a surface potential f using Equation (2.21) and substituing $\boldsymbol{B}$ into Equation (2.58). The result is

$$\frac{1}{2} < B_0^2 > +P_0 - P = \frac{1}{2}g^{ij}\partial_i f \partial_j f + \widetilde{V}(\theta,\zeta) \,, \tag{2.57}$$

Define

$$H' = \frac{1}{2}g^{ij}\partial_i f \partial_j f + \widetilde{V}(\theta,\zeta) \,. \tag{2.58}$$

Then one has a time independent Hamilton-Jacobi equation

$$H' = H'(q,\partial_q f) = E' = \frac{1}{2} < B_0^2 > +P_0 - P = \frac{1}{2} < B^2 > \;. \tag{2.59}$$

Equation (2.57) must be solved for the scalar function $f(\theta,\zeta)$, which can be con-

structed by following only those characteristics of H that ergodically cover an invariant torus. There are many trajectories that may cover an invariant torus, therefore there is one more datum that must be prescribed to fully define the pressure jump Hamiltonian problem, and that is the winding number of the trajectory, which corresponds to the rotational transform of the resulting field.

The previous derivation was made with the goal of continuing the field across an interface, that derivation sought to answer the question: For a given surface (g), given a field on one side f and a pressure jump ($P^+ - P^-$), what is the field on the other side of desired rotational transform? The derivation in this section seeks to answer the question: Given the fluctuation of the field ($\tilde{B}^2 = \tilde{V}$) and the average value of the field ($< B^2 >$), what are the possible fields and rotational transforms that could appear on either side?

The two Hamiltonians are related via

$$H = \Delta P = H' - \frac{1}{2} < B_0^2 > \ . \tag{2.60}$$

By this definition, if one uses the inverse formulation, one absorbs the constant part of the reference field into the energy. When one is instead prescribing a field by defining f on one side and continuing the field across the surface, the surface average may not easily be separated and so is included in the potential

$$V(\theta, \zeta) = \widetilde{V}(\theta, \zeta) - \frac{1}{2} < B_0^2 > \ . \tag{2.61}$$

The two sided principle

The inverse formulation is more general and removes the need to talk of "prescribed sides". And so one is free to consider two solutions, then later place them on either side of the interface. For example, for a given $\tilde{V}(\theta, \zeta)$ find one solution $\boldsymbol{B}_1$ such that $< B_1^2 >= E_1 - P_1$ and the rotational transform is ι_1, and find a second solution $\boldsymbol{B}_2$ such that $< B_2^2 >= E_2 - P_2$ and the rotational transform is ι_2. If both f_1 and f_2 are valid solutions and may be considered to be on either side of the surface. One can then ask what the pressure jump is in hindsight by calculating

$$< B_1^2 > - < B_2^2 >= E_1 - P_1 - (E_2 - P_2) \ , \tag{2.62}$$

so that

$$E_1 - E_2 = P_1 - P_2 \ , \tag{2.63}$$

and

$$\Delta E = \Delta P \, . \tag{2.64}$$

The interpretation of the energy

The pressure jump Hamiltonian defines the energy as

$$E = \Delta P \, . \tag{2.65}$$

In the inverse formulation above, Equation (2.52) states that

$$E = \Delta P = \frac{1}{2} < B^2 > - \frac{1}{2} < B_0^2 > \ . \tag{2.66}$$

In the presure jump Hamiltonian, $1/2 < B_0^2 >$ is implicit in $V(\theta, \zeta)$ whereas in the inverse formulation, this constant term is aborbed into the energy $E' = \Delta P + 1/2 < B_0^2 >$.

When solving the Hamiltonian system, defining E defines the magnitude of the pressure jump which is equal to the difference in surface averages of the square of the unknown field and the reference field. The surface average of the square of the unknown field cannot be less than zero, so there is a minimum energy

$$E_{min} = -\frac{1}{2} < B_0^2 > \, , \tag{2.67}$$

at which

$$< B^2 >= 0 \Rightarrow \boldsymbol{B} = 0 \, . \tag{2.68}$$

i.e. at this energy the only solution is the trivial field.

While E_{min} is the lowest energy for which a solution can be found, the lowest energy for which a solution f can be defined across the entire surface will generally be at an energy larger than E_{min}. This point can be found using the tools developed in the next chapter. In the inverse formulation the minimum energy is found at $E'_{min} = 0$.

2.4.3 Similar Hamiltonian system: the double pendulum

The pressure jump Hamiltonian is quite abstract and can be difficult to visualise. It may help to keep in mind a similar Hamiltonian system, the double pendulum. Consider a mass m_1 at the end of a soid, weightless rod of length l_1 whose other end is attached to a fixed point. The second pendulum consists of a similarly solid,

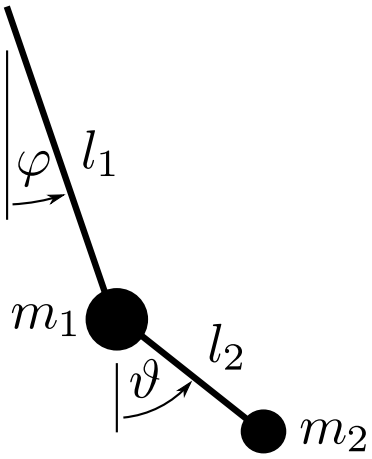

Figure 2.5: The double pendulum is a simpler Hamiltonian system to the pressure jump Hamiltonian with two angular variables (ϑ, φ).

weightless rod of length l_2 with a mass of m_2 at its end. The motion of each mass is parametrised by the angle of each pendulum to its vertical resting position, the first mass has angle φ and the second, ϑ. This situation in pictured in Figure 2.5.

Considering the kinetic energy of the two masses and the potential energy due to the gravitational force on each mass, the Hamiltonian H_{DP} for the double pendulum can be written as, [RS84]

$$H_{DP} = \frac{l_1^2(m_1+m_2)p_\vartheta^2 - 2m_2 l_1 l_2 \cos(\varphi-\vartheta)\, p_\varphi p_\vartheta + l_2^2 m_2 p_\varphi^2}{2l_1^2 l_2^2 m_2[m_1 + m_2\sin(\varphi-\vartheta)]} - m_2 g l_2 \cos\vartheta - (m_1+m_2) g l_1 \cos\varphi\,. \quad (2.69)$$

The double pendulum Hamiltonian is similar to the pressure jump Hamiltonian because they both have two angular variables and a position dependent metric. Later in this thesis, the double pendulum will be brought up to highlight similarities and to aid in the visualisation of pressure jump Hamiltonian trajectories.

2.4.4 Distinguishing between the pressure jump Hamiltonian and the magnetic field line Hamiltonian

It important to make clear that when Hamiltonian chaos is discussed in the fusion context, it is usually in reference to the chaotic structures that appear in the volumes of the fusion plasma (e.g. magnetic islands). This is usually referred to as field line chaos, and these chaotic structures are important for confinement for the device as a whole.

When investigating the field line chaos *within a plasma volume*, one refers to non-integrable solutions to the *field line Hamiltonian system*. The pressure jump Hamilto-

nian in contrast is only defined *on a single flux surface*, and the trajectories correspond to different field line configurations. For more information see Appendix A.4.

Chapter 3

Pressure jump Hamiltonian solution and existence of solutions

To appreciate the advantage that a Hamiltonian treatment can provide, the existence theory behind Hamiltonian mechanics must be covered. This chapter first explains how the Hamiltonian system is solved for the trajectories. It then explores the phase space of these trajectories with some examples to understand the effects of changing the variables in the system. The chapter then covers Greene's residue and how this can be used to determine the regularity of individual trajectories, and hence to develop a test for the existence of field line configurations of the pressure jump Hamiltonian.

3.1 Defining the problem specification

To fully define the Hamiltonian problem to be solved:

$$H(\theta, \zeta, p_\theta, p_\zeta) = \Delta P \ , \tag{3.1}$$

$$H(\theta, \zeta, p_\theta, p_\zeta) = \frac{1}{2} g^{ij} p_i p_j - \frac{1}{2} g^{ij} \partial_i f^- \partial_j f^- \ . \tag{3.2}$$

one must provide the following

Pressure jump A scalar that is equivalent to the Hamiltonian energy

Initial conditions of trajectory Two values, θ_0 and $p_{\theta 0}$, together these uniquely determine the rotational transform of the solution.

Surface geometry The metric terms are defined by the geometry of the surface $\mathcal{S}$.

Prescribed field The potential is defined by the scalar function $f^-(\theta, \zeta)$

Together these are referred to as the *problem specification*.

The first two on the list are trivial, however the final two are scalar functions with no restriction other than they are two fold periodic to match the topology of the problem.

3.1.1 Defining the surface geometry

As detailed in Appendix A.3, a toroidal surface may be completely defined by the functions $R(\theta,\zeta)$ and $Z(\theta,\zeta)$. To match the topology of the torus, the general form of these functions is

$$R = \sum_{n=-N}^{N}\sum_{m=0}^{M} R_{mn}\cos\left(m\theta - n\zeta\right) \ , \tag{3.3}$$

$$Z = \sum_{n=-N}^{N}\sum_{m=0}^{M} Z_{mn}\sin\left(m\theta - n\zeta\right) \ . \tag{3.4}$$

This Fourier decomposition provides a method of prescibing geometries by prescribing coefficients R_{mn} and Z_{mn}. An axisymmetric torus (major radius R_0, minor radius r_0) is defined using the terms.

$$\mathcal{S} = \left[\begin{array}{cccc} m & n & R_{mn} & Z_{mn} \\ \hline 0 & 0 & R_0 & 0 \\ 1 & 0 & r_0 & r_0 \end{array}\right] \ . \tag{3.5}$$

The geometry can be perturbed away from axisymmetry by introducing more R_{mn} and Z_{mn} terms, each of which introduce a "ripple" in the surface with a frequency of m in the poloidal direction and n in the toroidal direction. Any torus may be prescribed with enough Fourier components, and this construction also ensures the torus remains smooth as long as the Fourier series converges pointwise.

3.1.2 Defining the prescribed field

Like the geometry, the prescribed scalar potential function f^- must be defined and there are no restrictions as to what it can be, other than having the same periodicity as the torus. The most general form for f^- consistent with stellarator geometry is (Section 2.4.1)[Hud04]

$$f^- = I^-\theta + G^-\zeta + \hat{f}^-_{mn}\sin\left(m\theta - n\zeta\right) \ . \tag{3.6}$$

Where I^- and G^- are constants.

In the case that all the $\hat{f}^-_{mn}$ are zero, f^- represents a prescribed field in straight field line coordinates. Adding $\hat{f}^-_{mn}$ terms results in a "wiggle" in the field lines with a frequency on m in the poloidal direction and n in the toroidal direction.

Again like the geometry, a choice of I^-, G^- and the $\hat{f}^-_{mn}$s will uniquely prescribe

a field, but as shown in Appendix A.2.5 a coordinate change can always be made so that the prescribed field is in straight field line coordinates.

3.2 Computational solution of pressure jump Hamiltonian system

The $1\frac{1}{2}$ degree of freedom problem derived in Section 2.3 was solved for the trajectory $[\theta(\zeta), p_\theta(\zeta)]$. A code named `PJH` was written in FORTRAN to solve for the trajectories. As such it is able to generate Poincaré diagrams, plot the invariant tori and also plot the resulting field configurations. The code's other abilities will be introduced throughout the thesis.

To restate the pressure jump Hamiltonian problem more explicitly, `PJH` solves the equations of motion:

$$\dot{\theta} = \frac{g^{\theta\theta}p_\theta + g^{\theta\zeta}p_\zeta}{g^{\theta\zeta}p_\theta + g^{\zeta\zeta}p_\zeta}\,, \quad \text{and} \tag{3.7}$$

$$\dot{p_\theta} = \frac{1}{2}\frac{\partial_\theta g^{\theta\theta}p_\theta^2 + 2\partial_\theta g^{\theta\zeta}p_\theta p_\zeta + \partial_\theta g^{\zeta\zeta}p_\zeta^2 + 2\partial_\theta V}{g^{\theta\zeta}p_\theta + g^{\zeta\zeta}p_\zeta}\,, \tag{3.8}$$

where a dot denotes a derivative with respect to the "time" ζ ($\dot{x} = \frac{dx}{d\zeta}$), and where

$$p_\zeta = \frac{-2g^{\theta\zeta}p_\theta + \sqrt{g^{\zeta\zeta}\left(2\Delta P - 2V(\theta,\zeta) - g^{\theta\theta}p_\theta^2\right) + \left(g^{\theta\zeta}p_\theta\right)^2}}{g^{\zeta\zeta}}\,. \tag{3.9}$$

The term $V(\theta,\zeta)$ contains the information of the prescribed field and is explicitly

$$V(\theta,\zeta) = -\frac{1}{2}g^{\theta\theta}(\partial_\theta f^-)^2 - g^{\theta\zeta}\partial_\theta f^-\partial_\zeta f^- - \frac{1}{2}g^{\zeta\zeta}(\partial_\zeta f^-)^2\,. \tag{3.10}$$

The contravariant metric coefficients g^{ij} are calculated from the covariant metric coefficients g_{ij} (See Appendix A.1 for more information about covariant and contravariant representations)

$$g^{\theta\theta} = g_{\theta\theta}/G, \quad g^{\theta\zeta} = -g_{\theta\zeta}/G, \quad g^{\zeta\zeta} = g_{\zeta\zeta}/G\,, \tag{3.11}$$

$$G = g_{\theta,\theta}g_{\zeta,\zeta} - g_{\theta,\zeta}^2\,. \tag{3.12}$$

These covariant metric components are themselves calculated from the surface geometry via the unit vectors $\mathbf{e}_i$

$$g_{\theta\theta} = \mathbf{e}_\theta\cdot\mathbf{e}_\theta, \quad g_{\theta\zeta} = \mathbf{e}_\theta\cdot\mathbf{e}_\zeta, \quad g_{\zeta\zeta} = \mathbf{e}_\zeta\cdot\mathbf{e}_\zeta\,. \tag{3.13}$$

The unit vectors are most easily understood in term of the Cartesian coordinates (See Appendix A.2 for more information on the transformation between coordinates)

$$\mathbf{e}_\theta = \frac{\partial(x,y,z)}{\partial\theta} \ , \quad \mathbf{e}_\zeta = \frac{\partial(x,y,z)}{\partial\zeta} \ , \tag{3.14}$$

and the form of the functions $x(\theta,\zeta)$, $y(\theta,\zeta)$, and $z(\theta,\zeta)$ are provided in terms of the functions $R(\theta,\zeta)$ and $Z(\theta,\zeta)$

$$x = R(\theta,\zeta)\cos(\zeta) \tag{3.15}$$
$$y = R(\theta,\zeta)\sin(\zeta) \tag{3.16}$$
$$z = Z(\theta,\zeta)\sin(\theta) \ . \tag{3.17}$$

Finally, $R(\theta,\zeta)$ and $Z(\theta,\zeta)$ are defined via the surface components R_{mn}, Z_{mn} (See Appendix A.3 for details of this decomposition)

$$R = \sum_{n=-N}^{N}\sum_{m=0}^{M} R_{mn}\cos\left(m\theta - n\zeta\right) \ , \tag{3.18}$$
$$Z = \sum_{n=-N}^{N}\sum_{m=0}^{M} Z_{mn}\sin\left(m\theta - n\zeta\right) \ . \tag{3.19}$$

The system is solved using a shooting method after setting $\theta(0) = 0$. As the metric is positive definite, we are assured that integrating the equations of motion from different values of $p_\theta(0)$ will follow a trajectory of different winding number, and that the winding number increases with increasing p_θ.[Gol01]

To solve the Hamiltonian system the NAG routine `D02CJF` was utilised. `D02CJF` used a variable-order, variable-step Adams method to solve the partial differential equations Equation (2.31) and Equation (2.32). The main reason for using this subroutine was its ease-of-use and high precision over long integration ranges. It also has the ability to output phase information while the trajectory was followed, allowing easy output of Poincaré diagrams and other phase information. For more information on the implications of this choice, see Section 3.2.1 and for information of other alternative methods of solution, see Section 6.3.1.

To calculate the Hamiltonian trajectories, the `PJH` program requires the following information supplied as a `PJH` input file:

Geometry of flux surface The flux surface $\mathcal{S}$ must be supplied in RZ form (R_{mn} and Z_{mn} – see Appendix A.3 for more details),

Prescribed field The prescribed field f^- must be specified in f_{mn} form (See next section).

All other aspects of the problem specification are defined by options when the code is called. For a description of the `PJH` input file, and more information about the options of the program see Appendix A.7.

We benchmarked the code and validated it by comparing the results to two other programs. A code to calculate the pressure jump Hamiltonian was written independently by Stuart Hudson. The code was not finished and was incorrect, but the code was completed enough so that the independently written `PJH` program could be compared resulting in two correct agreeing versions. As both programs were written with different code, the agreement of their results implied that coding errors were very unlikely.

We also compared `PJH` to results collected from `SPEC`. At the time of writing `SPEC` was capable of calculating the field in two regions with a pressure discontinuity between them. `SPEC` solves the physical situation with a formulation that is related to, but different from `PJH`. The continued field configuration provided by `PJH` agreed with the field discontinuity that appeared in `SPEC`. That the results of `SPEC` agreed with the results of `PJH` was additional strong evidence that the formulation and the subsequent solution by the code was sound within the MRXMHD framework.

3.2.1 Accuracy

Integration tolerance when following field lines

The accuracy of `PJH` when following field lines is determined by the tolerance of the integration, ν_l. We will introduce more accuracy parameters later in the thesis when more of the code's capabilities are described. The accuracy of the field line tracing though is paramount and so was always set at the minimum tolerance that `D02CJF` would allow. This was typically $\nu_l = 10^{15}$. Such a low tolerance is possible because, while the trajectories are chaotic, they remain very smooth along their entire length.

The truncation of Fourier series

Both the shape of the surface g^{ij}, and the form of the surface potential f^- are considered as Fourier series. The number of Fourier terms to include in their description needs to be kept in check. There is a tradeoff between maximising the accuracy of the functions by increasing the number of Fourier terms and the speed of the calculation. The sine and cosine basis of the Fourier series ensures the surfaces and the prescribed field are smooth even when the Fourier compenents are truncated at m_{max} and n_{max}. However, truncations are sacrifices in accuracy.

This issue is most important when calculating input files from `SPEC`. More details

of this can be found in Section 3.4.3 when SPEC is used as input.

Problems at high rotational transform

Some problems became evident when following Hamiltonian trajectories. As trajectories were followed for a certain 'time' (toroidal distance), the length of the high winding number orbits tended to be longer, because they undergo poloidal rotations more frequently per toroidal transit than orbits with a low winding number. Calculation of such orbits was also more time consuming because the 1 1/2 degree of freedom formulation uses ζ as the time coordinate, and the intergration needed to take smaller steps. Thus the error increased for higher p_θ orbits.

This issue of high-winding-number accuracy was dealt with by limiting investigations to low winding numbers, mainly because in later sections it becomes necessary to follow very long field lines. The sacrifice of keeping to a regime of low w was not too limiting as field lines in fusion reactors have rotational transforms in this regime. Other methods of solving the Hamiltonian problem, including variational methods or symplectic integration were attempted, but deemed at least equally unsuitable for the reasons outlined in Section 6.3.1.

3.2.2 The phase space of the pressure jump Hamiltonian

The Hamiltonian trajectory $[\theta(\zeta), p_\theta(\zeta)]$ draws out a path in phase space. A helpful way to investigate the behaviour of Hamiltonian trajectories is to observe the trajectories' intersections with a plane of constant coordinate. This is refered to as a *Poincaré diagram*

For the pressure jump Hamiltonian system, a plane of constant ζ is used for Poincaré diagrams because the field lines of interest in fusion tend to have low rotational transform (so there are many toroidal transits per poloidal transit).

As the radius of an invariant torus is given by the Hamiltonian momentum, trajectories of different winding number will appear at different positions on the vertical axis on the Poincaré diagram. In configuration (real) space, all corresponding field lines will lie on the same 3D torus (the prescribed one) but each corresponding field line configuration will have a different rotational transform corresponding to the winding number of the trajectory.

3.2.3 The structure of phase space

Figure 3.1 contains Poincaré sections of the phase space of the pressure jump Hamiltonian under a deformation

$$\mathcal{D} = \left[\begin{array}{cccc} m & n & R_{mn} & Z_{mn} \\ \hline 0 & 1 & \delta & -\delta \\ 2 & 1 & \delta & \delta \end{array}\right]. \tag{3.20}$$

This deformation is selected because it can produce sufficient chaos for the purposes of exploring phase space structures. At the end of this chapter in Section 3.4, three standard cases for investigation will be defined.

In particular, Figure 3.1(a) shows the unperturbed Hamiltonian ($\delta = 0$) and Figure 3.1(b) shows the Hamiltonian perturbed in order to illustrate chaotic structures that appear in the pressure jump Hamiltonian. Below is a description of each structure and what it means for the physical system this represents.

The *irrational orbits* appear as curves crossing the Poincaré section, but in actual fact they are a union of an infinity of intersections of the trajectory with the Poincaré plane so that one can write $p_\theta(\theta)$ as a continuous function on said curve. This occurs when the winding number of this trajectory is an irrational number $w = w_{irr}$. In this case the trajectory continues to wrap around the orbit making w_{irr} poloidal traversals every single toroidal transit. The trajectory continues to wrap around but never intersect itself; it is said to *ergodically cover* the invariant torus. Physically, this corresponds to a field line that similarly ergodically covers the prescribed surface with a rotational transform of w_{irr}, which ensures $\mathcal{S}$ is a flux surface.

Any irrational invariant surfaces that have survived any nonzero pertubation are refered to as *KAM surfaces*. They are named after the KAM theorem which described their persistance under perturbations to the Hamiltonian.[Bro04]

A *rational orbit* appears as a finite number of dots that lie on a curve in Figure 3.1. This trajectory has a rational winding number $w = p/q$ where $p, q \in \mathbb{N}$. Thus for q toroidal transits the trajectory will undergo p poloidal transits and intersect the Poincaré diagram p times before then intersecting on top of the points already plotted. This means the trajectory is an invariant curve, but not an invariant torus as physically the field line will not cover the flux surface ergodically. However, it is theoretically possible to consider some kind of rational flux surface formed as the union of an infinity of rational field lines placed "side by side" on the surface. These are discussed further in Section 3.2.5.

Irrational trajectories in the neighbourhood of a rational will tend to, as the system

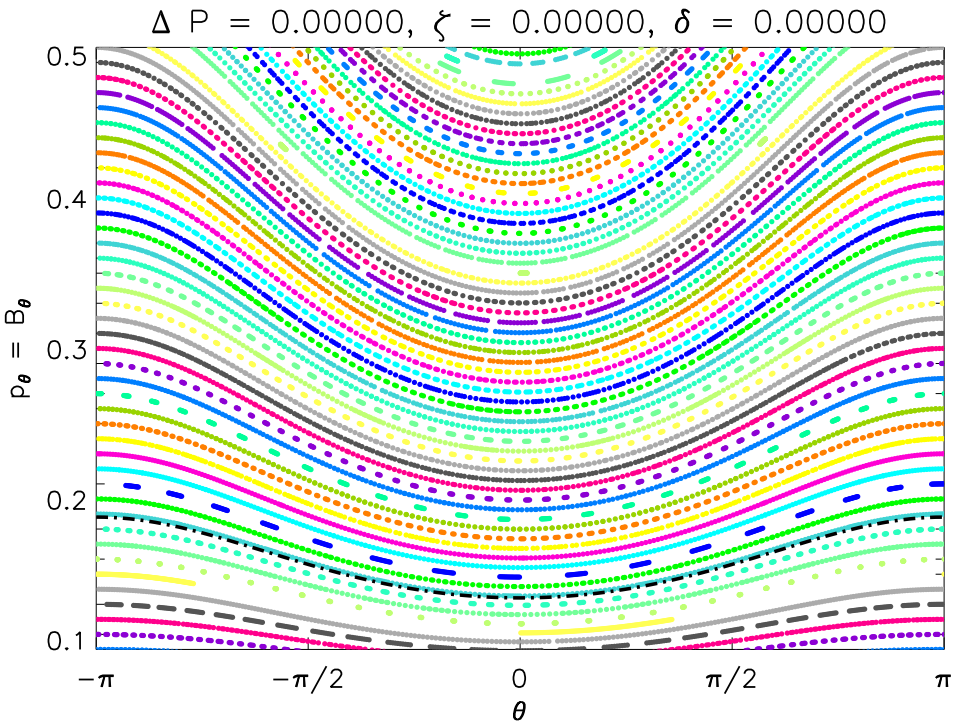

(a) A Poincaré section of the pressure jump Hamiltonian with no perturbation (system is completely integrable).

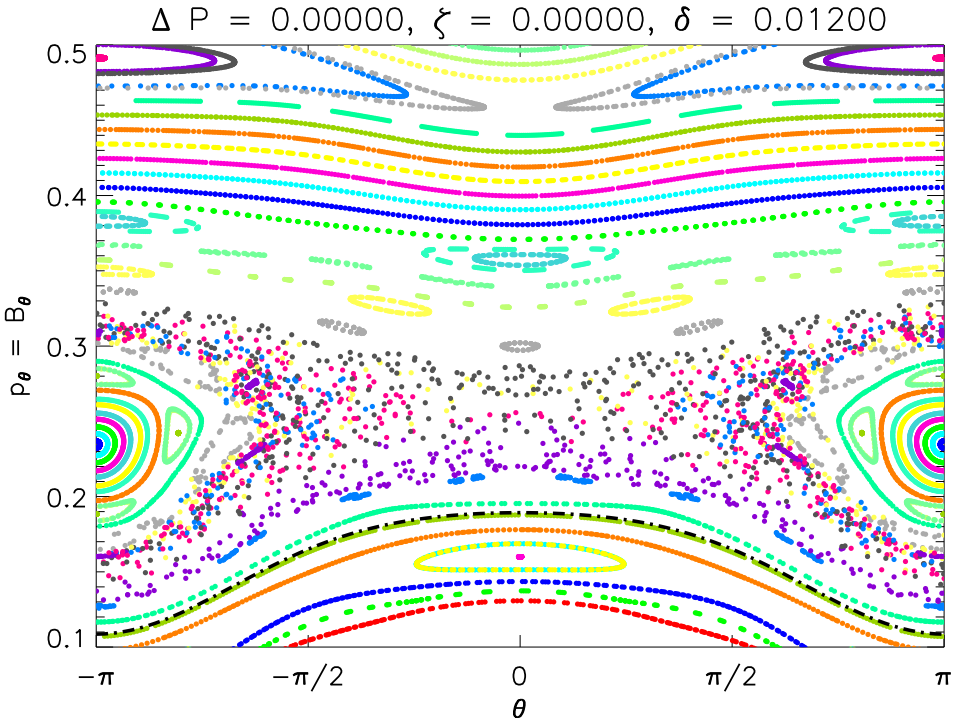

(b) A Poincaré section of the pressure jump Hamiltonian with some perturbation (system is no longer completely integrable).

Figure 3.1: (colour online) Two typical Poincaré diagrams enabling some visualisation of the phase space of the Hamiltonian system. Different colours correspond to different orbits. The dot-dash curve is a representation of the prescribed field $\partial_\theta f^-$.

is perturbed, deviate from their invariant torus and no longer draw out an invariant torus (and so a winding number cannot be defined). In this case their intersection with a Poincaré plane is a set of closed curves called *islands*. As this trajectory has deviated from its once invariant torus, it upsets the nearby rational and irrational orbits and turns them into islands too. In this case there is physically no solution for a field line to satisfy force balance with a well defined rotational transform.

The Poincaré points in between island groups can be stochastic, and the trajectories in this area are *chaotic*. The size of the islands and the size of the chaotic regions generally increases with increasing perturbation leaving only a finite measure of irrational orbits that are valid solutions.[Mac92] For more information on how to determine whether a trajectory is valid as a solution to the pressure jump Hamiltonian system, see the next section.

As an island or chaotic region increases in size, it may approach an irrational orbit that has so far survived the purturbations. At a high enough perturbation, the orbit will become *critical* and turn into a *cantorus*.[Hud04] The irrational trajectory ceases to completely draw out an invariant torus, but instead leaves gaps through which nearby trajectories may "leak". When the irrational orbit turns into a cantorus, the function $p_\theta(\theta)$ becomes discontinuous with holes corresponding to the *cantor set*.[Niv56]

The phase space of the Hamiltonian (as it is seen using a Poincaré section) contains all the above structures *on all scales*. As one can always find rationals between any two irrationals, so one can always find an island in between two irrational orbits. An island may increase to a stage where it overlaps another island, creating a region of strong chaos. The entire infinity of rational orbits still exist, but they may be surrounded by islands or by chaos and they may be stable or unstable.

3.2.4 Implications of chaotic trajectories

As the Hamiltonian is non-integrable, it is important to understand how chaotic trajectories should be interpreted in the original pressure discontinuity problem. A chaotic trajectory corresponds to one in which the generating function of the Hamiltonian cannot be found. As shown below, this corresponds to the case where f cannot be calculated on the continued side.

Typically, in a general Hamiltonian system, the goal is to find a Hamiltonian trajectory $(\boldsymbol{q}, \boldsymbol{p})$ for a given Hamiltonian $H(\boldsymbol{q}, \boldsymbol{p})$. To solve this one may simply attempt to solve Hamilton's equations, but it is often better to transform to another coordinate system first. A different coordinate system can evince symmetries and smplifications that may not be immediately apparent.

As Hamilton's equations can be derived from the Lagrangian variational priciple

($\delta \int L\, dt = 0$), it is important that this principle still holds in the new coordinate system. This only allows a certain set of transformations to new coordinate systems to be possible for a given Hamiltonian. Such coordinates are canonical coordinates. We know by definition that,[LL92]

$$\partial \left[\int_{t_1}^{t_2} p_i \dot{q}_i - H(\boldsymbol{q}, \boldsymbol{p})\, dt \right] = 0 \,, \tag{3.21}$$

but for the transformation $(\boldsymbol{q}, \boldsymbol{p}) \to (\bar{\boldsymbol{q}}, \bar{\boldsymbol{p}})$, to be canonical we insist that

$$\partial \left[\int_{t_1}^{t_2} \bar{p}_i \dot{\bar{q}}_i - K(\bar{\boldsymbol{q}}, \bar{\boldsymbol{p}})\, dt \right] = 0 \,. \tag{3.22}$$

As both variational principles vary the entire quadrature, the integrands may differ by a complete differential $\frac{dF}{dt}$

$$p_i \dot{q}_i - H(\boldsymbol{q}, \boldsymbol{p}) = \bar{p}_i \dot{\bar{q}}_i - K(\bar{\boldsymbol{q}}, \bar{\boldsymbol{p}}) + \frac{dF}{dt} \,. \tag{3.23}$$

F may be a function of any combination of the old or new coordinates.[LL92] For instance, if $F = F_2(\boldsymbol{q}, \bar{\boldsymbol{p}}, t)$, then one can expand the differential in Equation (3.23) and collect like terms to find

$$p_i = \frac{\partial F_2}{\partial q_i} \,, \tag{3.24a}$$

$$\bar{q}_i = \frac{\partial F_2}{\partial \bar{p}_i} \,, \tag{3.24b}$$

$$K(\bar{\boldsymbol{q}}, \bar{\boldsymbol{p}}) = H(\boldsymbol{q}, \boldsymbol{p}) + \frac{\partial F_2}{\partial t} \,. \tag{3.24c}$$

From Equations (3.24) one can see how a function F_2 contains all the information necessary to transform from one canonical coordinate system to another. For this reason F_2 is refered to as a generating function, as one can generate a new set of canonical coordinates using F_2.

However, the ability to do this transformation relies on $F_2(\boldsymbol{q}, \bar{\boldsymbol{p}}, t)$ existing. If the trajectory is chaotic, $p_i(q)$ is not continuous and therefore cannot be differentiated for Equation (3.24a). Indeed, if $p_i(q)$ is not continuous, one no longer has an invariant surface. Also, once F_2 cannot be defined, action angle coordinates cannot be defined. Conversely, if F_2 does exist the trajectory will draw out an invariant torus and that solution is *integrable*.

It was found in Section 2.4.1 that the generating function F_2 is, in the pressure jump Hamiltonian system, the surface potential f, and in Section 2.4.1 that action angle coordinates are analagous to straight field line coordinates. The destruction of a field line configuration occurs when the transformation to straight field line coordi-

nates is impossible.

SFLC coordinates are often defined throughout the volume when the field $\boldsymbol{B}$ is integrable and invariant tori exist at every point in the plasma volume. In general the pressure jump Hamiltonian is non-integrable, and such coordinates are only defined on the invariant tori [See Appendix A.2.5].

3.2.5 Selecting a trajectory as a solution to the pressure jump condition

Just because a Hamiltonian trajectory has been followed in phase space and lies on an invariant torus, does not mean it corresponds to a valid solution to the pressure jump condition in real space. As mentioned in the previous section, the necessary condition for a solution to the pressure jump criterion is the existence of the scalar function $f(\theta, \zeta)$ over the entire flux surface that is single valued and periodic.

The physical equivalent of this requirement is that the following three conditions be satisfied:

1. Only one field configuration may exist (as defined in Section 2.3.3),

2. The field configuration must be irrational, *and*

3. The field line must lie on the flux surface.

Point 1 stems from the fact that there is only one solution for f. When one trajectory is of interest, it is fair to refer to this as a field line configuration. However, while we can talk of a 'set' of trajectories, or a 'class' of orbits (e.g. the set of KAM surfaces), one could not say that they are all solutions to the pressure jump condition. All trajectories are solutions to the pressure jump Hamiltonian's equations of motion, but only one orbit is the solution to the pressure jump *condition*. To clarify this subtle difference, solutions to the Hamiltonian systems that have not satisfied the above three rules will be refered to as *potential* or *candidate* field line configurations.

The requirement that the solution f be defined across the entire prescribed surface suggests the rotational transform of the field line configuration must be irrational as only an irrational trajectory covers the entire surface. However it is, in principle, possible to find a solution f that corresponds to a rational field line. One could perhaps envisage an infinity of rational field lines side by side which in union cover the surface. Only irrational flux surfaces are considered in this thesis, though the nature and role of rational flux surfaces within the MRXMHD framework is still an open question. For instance, `SPEC` allows one to set an interface to have a rational rotational transform, and it is still possible to calculate a field line equilibrium. For

an equilibrium with a prescribed rational interface, the islands and chaos that would be caused by the presence of said rational are suppressed.

However, while they are unsuitable as physical solutions, rational trajectories are the only types that can be investigated in a reliable way because of their finite length. Sometimes characteristics of irrational solutions can be inferred by the behaviour of nearby rational ones, for example Greene's residue, which is introduced in the next section.

While the above points disregard trajectories because of their nature in phase space, there are physical arguments that may further restrict the choice of trajectories as physical solutions. The dot-dash curve in Figure 3.1 represents the trajectory of the prescribed field $p_\theta^- = \partial_\theta f^-$. The dot-dash curve matches the contours of the trajectories and in particular, there exists an orbit that is the same as the prescribed field. This trajectory corresponds to a solution that has the same rotational transform as the prescribed field, i.e. a field that is continuous through the flux surface. Selecting any other trajectory as the solution results in a discontinuity in the rotational transform of the field. One is free to allow solutions with a jump in rotational transform within MRXMHD but there has been evidence that a flux surface with a rotational transform jump across it can be unstable in some situations.[MHD09]

3.3 Irrationality, Greene's residue and the transition to chaos

This thesis is mainly concerned with Hamiltonian trajectories of the pressure jump Hamiltonian and the associated field configurations that can be said to satisfy force balance. This section outlines a method for determining whether the trajectory of the Hamiltonian system with a given winding number is regular or not (i.e. whether it lies on an invariant torus). The winding number of a given Hamiltonian trajectory has been shown to be a strong predictor of the regularity of the orbit.[Gre79] For consision, a trajectory with a rational winding number will be referred to as a rational trajectory (or rational orbit), a trajectory with an irrational winding number will be referred to as an irrational trajectory (or irrational orbit).

3.3.1 Greene's residue

Greene's residue is a quantity that can be determined for a rational Hamiltonian trajectory and amounts to a measure of the linear stability of the rational orbit. Its uses expand past determining the stability of rationals, however, for example here it is used to determine whether a given irrational trajectory is regular or not.

Greene's Rrsidue is best explained when the Hamiltonian is expressed as a mapping. To write the trajectory as a mapping one considers the equations of motion to map one phase location to some other under Hamilton's equations. For instance the change in position of one Poincaré point (θ, p_θ) at, say $\zeta = 0$, to any other Poincaré point (θ', p'_θ) at $\zeta = \zeta$ can be written as

$$\begin{pmatrix} \theta' \\ p' \end{pmatrix} = M' \begin{pmatrix} \theta \\ p \end{pmatrix} . \tag{3.25}$$

The goal is to calculate the tangent map, which can be found by considering the nearby phase location

$$\begin{pmatrix} \theta' + \delta\theta' \\ p' + \delta p' \end{pmatrix} = M_\zeta \begin{pmatrix} \theta + \delta\theta \\ p + \delta p \end{pmatrix} . \tag{3.26}$$

Linearising the divergence of the two resultant points gives the tangent map T_ζ

$$\begin{pmatrix} \delta\theta' \\ \delta p' \end{pmatrix} = \begin{pmatrix} \partial_\theta\theta' & \partial_p\theta' \\ \partial_\theta p' & \partial_p p' \end{pmatrix} \begin{pmatrix} \delta\theta \\ \delta p \end{pmatrix} = T_\zeta \begin{pmatrix} \delta\theta \\ \delta p \end{pmatrix} . \tag{3.27}$$

The tangent map must be calculated along the entire length of the trajectory so rationals with $w = p/q = \tau_N$ are selected whose phase location repeats after q toroidal transits.

$$\begin{pmatrix} \theta_N \\ p_N \end{pmatrix} = {}^{p/q}M_q \begin{pmatrix} \theta \\ p \end{pmatrix} . \tag{3.28}$$

With the values of the tangent map, one can then calculate the *residue* r, given by

$$r_q(p/q) = \frac{2 - \mathrm{Tr}\left({}^{\tau_N}T_q\right)}{4} . \tag{3.29}$$

The residue can be calculated for any rational orbit. One is restricted to rationals simply because it is not possible to follow the entire irrational trajectory because it is infinitely long. A rational trajectory $w = m/n$ can be followed around toroidally n times, then the trajectory repeats, allowing the residue of the rational trajectory to be calculated after a finite number of transits.

3.3.2 Determining Greene's residue for an irrational orbit

Regular irrational orbits are of interest because they correspond physically to flux surfaces consistent with pressure balance. However they are infinitely long and so

cannot be investigated without approximation of the irrational value. The existence of Hamiltonian trajectories is highly dependant on their winding number, and previous work has shown the dependence to be a fractal, a "devil's staircase". This fractal dependence means an approximation to an irrational via a truncation of the decimal value (for instance to investigate 3.141592 instead of π) may not provide any insight into the existence of a single rational to infer the existence of a nearby irrational trajectory.

However, Greene showed that it is possible to infer the existence of an irrational orbit by considering the residues of a sequence of rational orbits that are near to the irrational of interest and whose winding numbers converge to that irrational.

Investigations are restricted to *noble* irrationals, as it has been conjectured with evidence in simpler systems that the last regular trajectory to become irregular is always a noble.[Mac86] Noble irrationals also satisfy the diophantine condition, and so this conjecture of regularity is consistent with what is suggested from the KAM theorem. For more information see Appendix A.6.

This highlights a difference in the investigation in this thesis as compared to previous computational work in the field of Hamiltonian dynamics. Previously, determinations of regularity using Hamiltonian tools were restricted to simple Hamiltonian systems such as the standard map,[Gre79],[GMVF81] the Henon-Heiles system[Gre80], and the double pendulum[PR94]. These systems are easily computable (keeping in mind the computational power of the computer in the 1980s and 1990s) and the systems have a one-parameter perturbation that allows a simpler and cleaner transition from regularity. As a result they provide clearer understanding of the effects that cause irregularity. These simplified approaches are also the obvious way to find some examples of universal behaviour, and determine general rules for which orbits are more likely to exist. In contrast the pressure jump Hamiltonian contains an infinity of variables capable of producing chaotic effects (owing to the complicated geometry of fusion devices). Thus, this thesis must instead limit itself to investigating individual rotational transforms for certain system specifications that hint at more general behaviour.

Calculating the tangent map

The components of the tangent map cannot be explicitly calculated because the Hamiltonian is not integrable, but if one differentiates the tangent map,

$$\frac{dT_\zeta}{d\zeta} = \begin{pmatrix} \frac{d}{d\zeta}\partial_\theta\theta' & \frac{d}{d\zeta}\partial_p\theta' \\ \frac{d}{d\zeta}\partial_\theta p' & \frac{d}{d\zeta}\partial_p p' \end{pmatrix} = \begin{pmatrix} \partial_\theta\frac{d}{d\zeta}\theta' & \partial_p\frac{d}{d\zeta}\theta' \\ \partial_\theta\frac{d}{d\zeta}p' & \partial_p\frac{d}{d\zeta}p' \end{pmatrix}, \tag{3.30}$$

and expand it to

$$\frac{dT_\zeta}{d\zeta} = \begin{pmatrix} \partial_\theta\dot{\theta}'\partial_\theta\theta' + \partial_p\dot{\theta}'\partial_\theta p' & \partial_\theta\dot{\theta}'\partial_p\theta' + \partial_p\dot{\theta}'\partial_p p' \\ \partial_\theta\dot{p}'\partial_\theta\theta' + \partial_p\dot{p}'\partial_\theta p' & \partial_\theta\dot{p}'\partial_p\theta' + \partial_p\dot{p}'\partial_p p' \end{pmatrix}, \tag{3.31}$$

it can then be condensed into the differential equation

$$\frac{dT_\zeta}{d\zeta} = \begin{pmatrix} \partial_\theta\dot{\theta}' & \partial_p\dot{\theta}' \\ \partial_\theta\dot{p}' & \partial_p\dot{p}' \end{pmatrix} T_\zeta. \tag{3.32}$$

The elements of the matrix in Equation (3.32) here can be integrated along the field line, because they are derivatives of the equations of motion. Thus there is a system of four differential equations to solve along the Hamiltonian trajectory, one each for the elements of the matrix $T_{i,j}$ in addition to the phase trajectory itself. To calculate the tangent map, one needs to integrate the four Equations (3.32) while integrating the trajectory. So then the trajectory information is stored in the six-dimensional array $[\theta_i, p_{\theta i}, T_{11}, T_{12}, T_{21}, T_{22}]$.

Selecting which trajectories to investigate

Now that the residue can be calculated for a rational orbit, one must select a set of rationals to investigate, from which one can infer the residue of that irrational. Greene asserts, with computational evidence, that one can infer the residue of an irrational surface from the limit of the residues of a sequence of nearby rationals, that converge to the irrational[Gre79]. Specifically, the assertion is that if one can set up a sequence of rational numbers $\tau_N = \frac{p_N}{q_N}$ that converge to the irrational number w_{irr}, then

$$r(w_{irr}) = \lim_{N\to\infty} r(\tau_N)\ , \tag{3.33}$$

provided the sequence is the sequence of rationals

$$\tau_N = [a_0, a_1, \ldots, a_N]\ , \tag{3.34}$$

whose continued fraction representation (Appendix A.6.3) is truncated at the (N)th partial quotient. This sequence of rationals can also be generated by following the *noble path* between two rationals in the Farey tree representation detailed in Appendix A.6.4. The irrational being approached in this fashion is always a unique noble between an interval p_1/q_1 and p_2/q_2, and so in this thesis it is referred to as $\gamma_{[p_1,q_1,p_2,q_2]}$. The convergents within the interval are written as $\tau_N^{[p_1q_1p_2q_2]}$. This notation is described in more detail in Appendix A.6.6.

As mentioned, Greene introduced the above as assertions, with numerical evidence

for the standard map, in 1979, with expectations that the idea could be generalised to other maps and to other irrationals.[Gre79] Since then, some progress has been made, the most by his student Robert MacKay in 1992[Mac92]. Still the residue as a criterion of stochastic transition has not been rigourously proved, but there is strong numerical evidence in the literature. All results found in this thesis were consistent with Greene's conjectures.

Finding a trajectory with a given winding number

Now that the rationals to investigate are known, the trajectories corresponding to these rationals need to be found in phase space. This amounts to searching for the initial conditions that produce a trajectory of the desired rational winding number.

We assume stellarator symmetry[DH98] so that a trajectory of any winding number can be found with a search along the $\theta = 0$ ray so that $w = w(p_\theta)$.[Hud04] As $w(p_\theta)$ is not known, the correct field line is found iteratively. The goal is to find a certain rational winding number, say $w = p/q$. By keeping the starting point at $\theta = 0$, and integrating the equations of motion until $\zeta = 2\pi q$, the winding number can be written as

$$w(p_\theta) = \frac{\theta(\zeta)|_{2\pi q}}{2\pi} \ , \tag{3.35}$$

(here $\theta \in \mathbb{R}$, not periodic in 2π). To find p_θ, one must find the root of

$$w(p_\theta) - \iota = 0 \ . \tag{3.36}$$

`PJH` does this using the NAG Routine `C05NBF`. This routine was used because it is a reliable code for root finding for nonlinear equations as it guarantees global convergence for starting points far from the solution and a fast rate of convergence for reasonable conditions. However the subroutine had difficulties in highly chaotic configurations. The techniques for dealing with these limitations are discussed below. As Equation (3.35) has no explicit form, one cannot supply the derivitives, `C05NBF` does not need derivitives and instead approximates the Jacobian using forward differences.

The routine iterates on p_θ until

$$\theta(\zeta) = 2\pi m \ . \tag{3.37}$$

This process does not require the tangent map so one can save time by only integrating the phase information. The starting point $p_\theta = I$ was used as it is guaranteed to lie on the irrational for zero pressure ($\partial_\theta f^-(0,0) = I$).

At low deformation and for small pressure jumps, we found that the routine was

quite reliable in finding the given winding number because the irrational trajectory lay within a region of regular irrational orbits and at each step of the iteration the winding number was well defined. The task became more difficult when significant areas of phase space were chaotic because the rational orbits are hidden amongst trajectories with badly defined rotational transforms.

The iteration was improved by relying on the fact that the trajectory corresponding to the winding number of interest will move continuously with an increase in the purturbation (as long as it remains stable), trajectories with the same winding number tend to have a similar initial momentum. Thus a trajectory can be followed if the pressure jump is increased slowly enough (with the previously found initial condition becoming a good guess for the unknown momentum).

To this effect we wrote an addtion algorithm; if the routine was having trouble finding the intial p_θ value, the code will set the pressure to zero (where chaos is at a minimum) and start finding the root. The code then gradually increased the pressure, ensuring p_θ could be found at each step. This algorithm worked very well, especially with variable step changes. The algorithm ceases to work when the step in the pressure required to still track the trajectory of interest within the chaos becomes less than machine precision, but practically the limit was well above this as the time taken increased exponentionally with decreasing step size. However for the configurations of interest in this thesis, this algorithm was able to track the trajectories of interest to a pressure high enough to observe the desired results.

Once the initial conditions for the desired rational rotational transform have been found, the integration can start again, this time integrating the tangent map as well. Once the trajectory is calculated for the entire $\zeta = 2\pi n$, one can calculate the residue of that orbit using Equation (3.29).

3.3.3 Why not use the KAM theory?

Investigations into the regularity of Hamiltonian systems invariably refer to the *KAM theory*.[Bro04] The KAM theory considers the perturbed Hamiltonian

$$H_K = H_0 + \epsilon H_\epsilon \,, \tag{3.38}$$

which is a linear combination of the Hamiltonian function H_0 and the perturbation ϵH_ϵ. Consider that a trajectory with winding number w_{irr} exists in the Hamiltonian system H_0. The KAM theorem may be summarised as the statement that, so long as w_{irr} is sufficiently irrational, i.e. satisfies the Diophantine condition

$$|qw - p| > \frac{C_D}{q\epsilon} \tag{3.39}$$

where $C_D > 0$ and $\epsilon \geq 1$, then the trajectory with this winding number is likely to persist (i.e. *still* exist) under sufficiently small and smooth perturbations of the phase space. What is important to note is that the theorem is *perturbative*.

Previous treatments of the problem have suggested using the KAM theory to prove the persistence of flux surfaces under small perturbations in the Hamiltonian. The first paper to use a Hamilton–Jacobi formulation in this context and the first to investigate the suitability of using the KAM theory to infer the existence of field lines in this problem was by Berk *et al* [BFL+86]. By assuming the pressure jump interface $\mathcal{S}$ to be located on a magnetic surface that is somehow known to be an invariant torus of a non-integrable vacuum magnetic field (this would be their H_0), and taking the pressure jump to be the perturbation parameter, they were then able to invoke the KAM theorem to state persistence arguments.

The critical difference was that Berk *et al* were able to assume an extant invariant torus of the unperturbed Hamiltonian H_0, so that persistence conclusions could be drawn for sufficiently smooth and small ϵ. In MRXMHD, one does not have the luxury of knowing *a-priori* if a flux surface should exist for use as an interface, this is equivalent to knowing if a trajectory w_{irr} exists for the pressure jump Hamiltonian H in the first place. So considering whether the trajectory w_{irr} exists for the Hamiltonian $H + \epsilon H_\epsilon$ is not possible.

Thus this thesis cannot utilise the KAM theorem. Instead the less rigorous Grene's residue is used. Despite its only partial mathematical justification, [Mac92], Greene's residue has proved very helpful in investigations of this kind in the past [Hud04, PR94, SK81].

3.3.4 Computational calculation of the tangent map

`PJH` can also integrate the tangent map and calculate the resulting residue. It does this by solving the equations

$$\partial_\theta \dot{\theta} = \frac{1}{\dot{\zeta}} \left(\partial_\theta g^{\theta\theta} p_\theta + \partial_\theta g^{\theta\zeta} p_\zeta + g^{\theta\zeta} \partial_\theta p_\zeta - \dot{\theta} \partial_\theta \dot{\zeta} \right) , \tag{3.40a}$$

$$\partial_p \dot{\theta} = \frac{1}{\dot{\zeta}} \left(g^{\theta\theta} + g^{\theta\zeta} \partial_{p_\theta} p_\zeta - \dot{\theta} \partial_{p_\theta} \dot{\zeta} \right) , \tag{3.40b}$$

$$\partial_\theta \dot{p} = -\frac{1}{\dot{\zeta}} \left(\frac{1}{2} \partial_\theta^2 g^{\theta\theta} p_\theta^2 + \partial_\theta^2 g^{\theta\zeta} p_\theta p_\zeta + \partial_\theta g^{\theta\zeta} p_\theta \partial_\theta p_\zeta + \frac{1}{2} \partial_\theta^2 g^{\zeta\zeta} p_\zeta^2 + \partial_\theta g^{\zeta\zeta} p_\zeta \partial_\theta p_\zeta + \partial_\theta^2 V + \dot{p_\theta} \partial_\theta \dot{\zeta} \right) , \tag{3.40c}$$

$$\partial_p \dot{p} = -\frac{1}{\dot{\zeta}} \left(\partial_\theta g^{\theta\theta} p_\theta + \partial_\theta g^{\theta\zeta} p_\zeta + \partial_\theta g^{\theta\zeta} p_\theta \partial_{p_\theta} p_\zeta + \partial_\theta g^{\zeta\zeta} p_\zeta \partial_{p_\theta} p_\zeta + \dot{p_\theta} \partial_{p_\theta} \dot{\zeta} \right) , \tag{3.40d}$$

along with the equations of motion Equations (2.33). The above equations depend on the derivitives of many quantities that must themselves be differentiated.

Each equation in Equations (3.40) is more complicated than the original equations of motion, and these four equations must be integrated at the same time as the equations of motion [Equations (3.7)]. This is very time consuming and a limitation on the code. For a discussion of the possible improvements that could yet be made to the code, see Section 6.3.

3.3.5 Residue curves

Now that residues can be calculated for periodic orbits, this section demonstrates how these residues are used to determine whether a Hamiltonian trajectory is regular or not.

As explained, one cannot access the residue of an irrational surface directly so one must determine the residues for nearby rational convergents to the irrational. The limit of the residues of the convergents approaches the residue of the irrational. To visualise this process, one can use a *residue curve*, that plots the residue as a function of the convergent rationals

Consider Figure 3.2, it contains Poincaré diagrams of the configuration in Section 3.2.3, but this time an irrational has been searched for and located. In the Poincaré diagram the position of the irrational is illustrated by plotting a high order rational marked by crosses. The irrational is indistinguishable from the plotted rational at the scale of the plot.

Figure 3.2 also contains residue curves of the irrational alongside the corresponding Poincaré diagrams. The irrational of interest is

$$w = \gamma_{[0111]} = 0.618033988... \,, \tag{3.41}$$

the same as the prescribed rotational transform (See Appendix A.6 for further explanation of the notation).

Figures 3.2(a), 3.2(c) and 3.2(e) are Poincaré diagrams of the pressure jump Hamiltonian at three different pressures. In Figure 3.2(a) the residues of the convergent rationals converge to zero, from this it can be inferred that the residue of the irrational is also zero, and so the trajectory with winding number w_{irr} does lie on an invariant torus (and further there exists a field configuration consistent with force balance on the physical flux surface).

Figure 3.2(f) shows the residues approaching infinity. From this is inferred that the irrational phase trajectory does not lie on an invariant torus and that no corresponding field line configuration exists. In the corresponding Poincaré diagram(Figure 3.2(e)), one can see that the points of the plotted rational trajectory are no longer equally laid

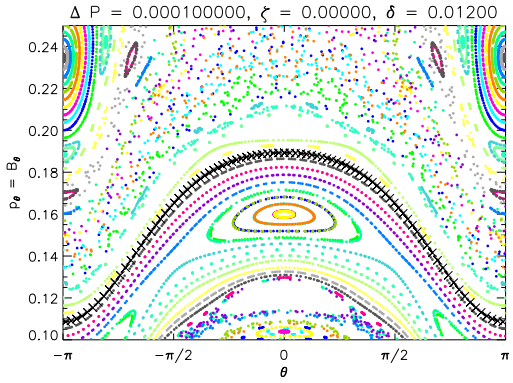

(a) Poincaré diagram of the pressure jump Hamiltonian ($E = 0.0001000$).

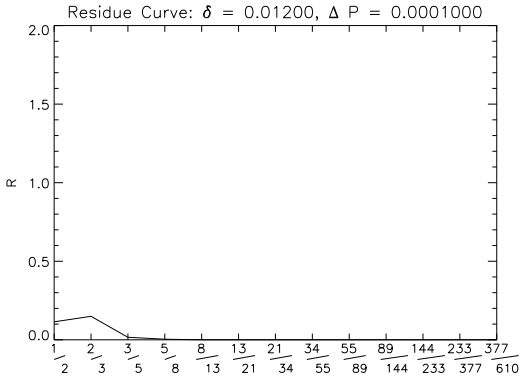

(b) Residue curve for the trajectory $\gamma_{[0111]}$ ($E = 0.0001000$).

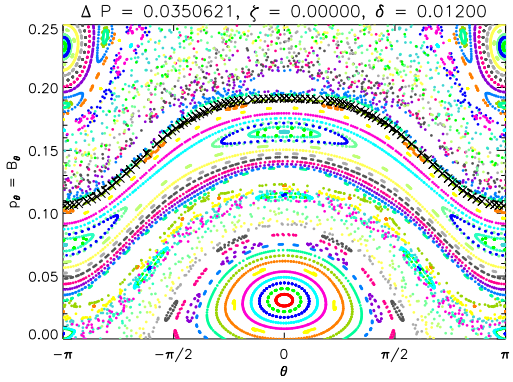

(c) Poincaré diagram of the pressure jump Hamiltonian ($E = 0.0350621$).

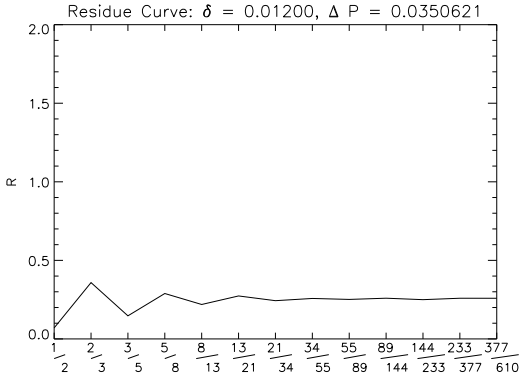

(d) A residue curve for the trajectory $\gamma_{[0111]}$ ($E = 0.0350621$).

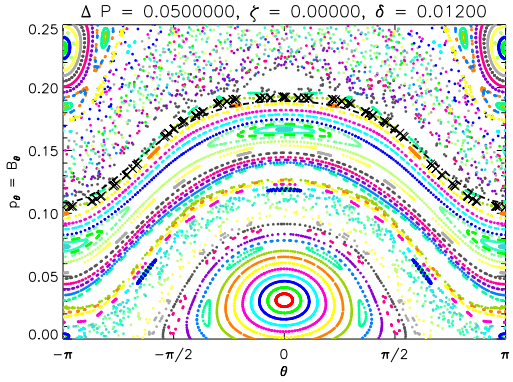

(e) Poincaré diagram of the pressure jump Hamiltonian ($E = 0.0200000$).

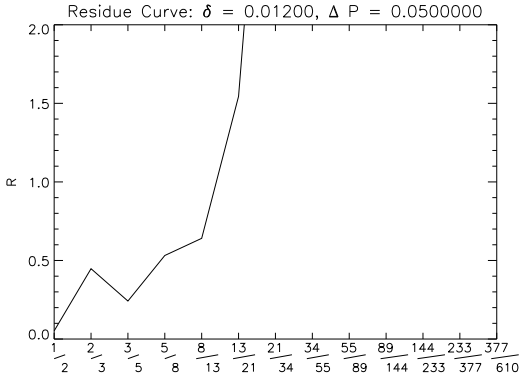

(f) A residue curve for the trajectory $\gamma_{[0111]}$ ($E = 0.0200000$).

Figure 3.2: Figures 3.2(a), 3.2(c) and 3.2(e) are Poincaré diagrams of the pressure jump Hamiltonian trajectories at three different pressures. The dot-dash curve shows the prescribed field and the crosses show Poincaré punctures of the trajectory of the ninth convergent rational ($w = \tau_9^{[0111]} = 0.617977...$) which is very close to the irrational of interest $w = \gamma_{[0111]}$. Figures 3.2(b), 3.2(d) and 3.2(f) are the corresponding residue curves of the $w = \gamma_{[0111]}$ trajectory at those same pressures. There are three possible limiting behaviours of the residue curve, limiting to zero (regular), limiting to 0.25 (critical) and limiting to ∞ (irregular or chaotic).

out along the $p_\theta(\theta)$ "curve". Note that although the irrational trajectory no longer forms an invariant torus, it can be seen that there is probably at least one nearby irrational invariant torus that does, as the chaos above and below the irrational is not connected.

Figure 3.2(d) shows the residues converging to the value 0.25. At this pressure the irrational is said to be *critical*, just on the cusp of destruction so that any further non-trivial deformation will cause the irrational trajectory to trace out a cantorus and no longer correspond to a valid solution. However, it has been shown that cantorii can act as partial barriers through which flux can leak through slowly.[Hud04]

In Figures 3.2(b), 3.2(d) and 3.2(f), one can see the residues take some time to smooth out to the limit. This transient behaviour is due to the low order rationals being so far from the irrational of interest that the convergents do not reflect the residue of the irrational. By inspection, this transient behaviour does give a qualitative idea of how close the irrational is to destruction, or the *resilience* of the orbit (See Section 6.4.2 for a discussion of this in more detail).

There is an important tradeoff to keep in mind when calculating these plots. There is an inevitable decrease in accuracy one succumbs to when integrating long field lines. For example, at the 12th convergent τ_{12} for the interval $[p_1, q_1, p_2, q_2]$, the PJH code must follow the field line $(q_1 + q_2 \times 233)$ times toroidally. Thus field lines need to be long to give an accurate measure of the existence test, but the longer they are the less accurate the numerical calculation is.

One of the reasons the trajectory corresponding to $1/\gamma = \gamma_{[0111]}$ is investigated is because the toroidal transit increase per convergent is the lowest possible, reflecting the fact that the golden mean and its inverse have rationals that approach the irrational the *slowest* of all real numbers, and so is the *most noble*. In contrast, less noble irrationals are approached by their rationals faster, resulting in less transient behaviour in the residue curve, but longer field line tracing for each convergent, and more computational time to determine existence.

3.3.6 Numerical error in calculating the residue

In addition to the accuracy considerations in Section 3.2.1, the calculation of the residue requires more tolerances that affect accuracy.

Tolerance in finding the trajectory with desired winding number

After setting the integration tolerance ν_l, the algorithm is capable of finding a trajectory with a winding number close to the desired with error ε_ι. With ν_l at its minimum possible value, ε_ι was the limiting factor in the accuracy of this ι finding algorithm. Based on experience, $\varepsilon_\iota = 10^{-10}$ was the best value, though the code automatically

p	q	τ_N	$(w-\tau_N)/\tau_N$
1	2	0.500000000000	5.7×10^{-13}
2	3	0.666666666667	-2.2×10^{-12}
3	5	0.600000000000	-3.4×10^{-12}
5	8	0.625000000000	9.2×10^{-13}
8	13	0.615384615385	5.0×10^{-13}
13	21	0.619047619048	1.6×10^{-14}
21	34	0.617647058824	-1.4×10^{-13}
34	55	0.618181818182	-3.9×10^{-12}
55	89	0.617977528090	4.4×10^{-12}
89	144	0.618055555556	1.9×10^{-11}
144	233	0.618025751073	3.5×10^{-11}
233	377	0.618037135279	7.4×10^{-11}
377	610	0.618032786885	-2.7×10^{-10}
610	987	0.618034447822	1.4×10^{-10}
987	1597	0.618033813400	-5.0×10^{-10}

Table 3.1: A table showing the accuracy with which `PJH` finds the trajectory with the descired winding number for $\delta = 0.01200$ and $\Delta P = 0.0350621$ (near criticality) for tolerance $\nu_l = 10^{-15}$ and $\varepsilon_\iota = 10^{-10}$. One can see the error increasing with field line length ($\propto q$). These numbers are small enough so that one can say that the limiting factor of accuracy is the calculation of the residue. This table corresponds to the plot Figure 3.2(d).

relaxed this constraint by a single order of magnitude if the desired winding number wasn't found. If it still was not found for $\varepsilon_\iota = 10^{-9}$, the results were deemed to not be reliable.

Table 3.1 shows the accuracy to which `PJH` was able to find the desired rotational transform for a typical case near criticality (near criticality, Figure 3.2(d)). One can see that the error is often well below the set tolerance level, but begins to have problems for very long field lines. As will be shown later, it is not usually necessary to follow field lines for longer than 100 toroidal transits. In this regime the accuracy of finding field lines is so good that the limiting factor of accuracy of the residue is the integration of the tangent map, rather than the finding of the trajectory with the correct winding number.

Integration tolerance when calculating the tangent map

While ν_l determines the accuracy of field line following, the calculation of the tangent map requires an order of magnitude more calculations and the integrating procedure could not match the accuracy achieved when following the field lines. Thus a second tolerance ν_r was set to determine the accuracy of the tangent map calculation.

Numerical error is a perpetual concern with investigations involving Greene's residue. During integration the error will become worse if the field line is long (when

investigating rational convergents this occurs when N is large), and will also increase for Hamiltonian problem specifications with large perturbations (as the integrating procedure must undergo more calculations).

Table 3.1 shows that the field lines can be found to a high accuracy, which implies that the accuracy is mainly determined by the calculation of the residue, which requires the integration of six equations of motion. As the value of the residue is not known *a-priori*, determining its accuracy by comparing to the expected result is much more difficult.

Numerical error tends to make the trajectory deviate from its true course. This is a concern when calculating Greene's residue because deviations from the invariant torus causes the residue to increase in value. So it can be hard to determine if the increase of the value of the residue is due to a transition to irregularity or to numerical error. A qualitative test was devised to ensure accuracy and this test is outlined in the next section.

It was observed that the integration procedure `D02CJF` would often fail if ν_r was too small, especially if many Fourier components were required. Based on experience, the optimum value was $\nu_r = 10^{-13}$. It is difficult to determine how accurate a given tangent map calculation is because it is not know *a-priori* what the value of the residue should be. For this reason the test in the next section was devised as a rough indicator of accuracy.

3.3.7 Qualitative test for determining accuracy of code

Figure 3.2(b) provides a good oppportunity to determine whether numerical error is affecting the result of the residue, because the true qualitative behaviour of these residue curves is known from Greene's work.[Gre79] In Figure 3.2(b), the residue should] decrease as regularity is assured, if the residue starts to increase, this can be reasonably ascribed to numerical error. Figure 3.3 shows the base ten logarithm of the residue at $\Delta P = 0$. Here the residue increases after $N = 8$, though acceptable accuracy extends to approximately $N = 12$.

In some situations one wishes to calculate the value of the residue and in others one wishes to determine the critical perturbation that makes a trajectory irregular. The accuracy of the residue is limited in the ways described above, so throughout this thesis whenever the residue was calculated the above tests were done manually in an effort to intuit an understanding of how accurate the determination of value of the residue was. In the latter case there are techniques that can be used to precisely determine the critical perturbation without need for more accurate residues, these techniques are covered in Section 5.2.

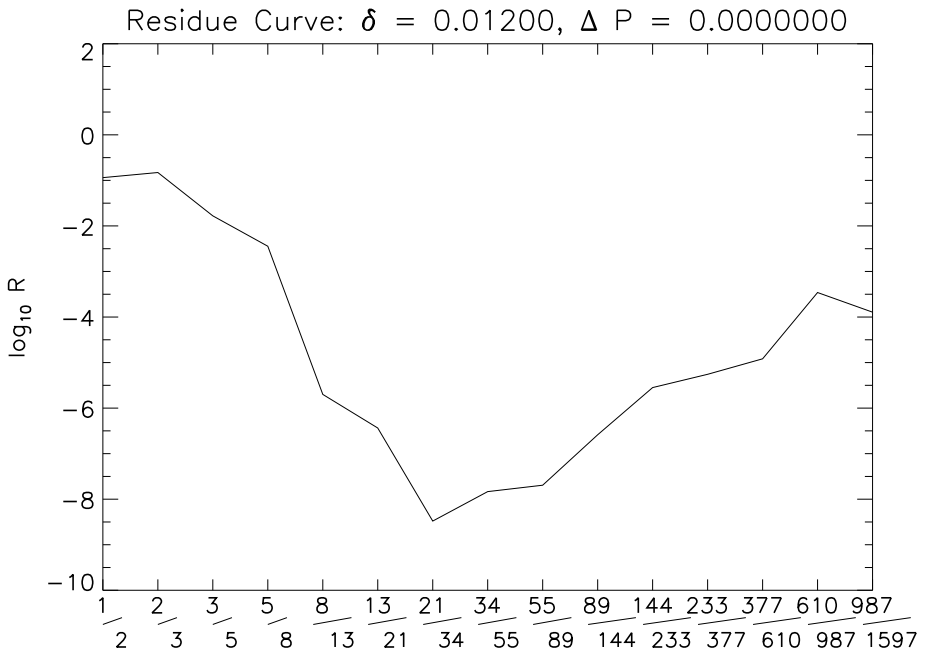

Figure 3.3: A plot of the logarithm of the residue for $E = 0$. The error increases for longer and longer field lines and has the effect of making the residue larger than zero for a trajectory that by construction is known to exist. This plot provides as indication of what value of N past which one should consider the results inaccurate.

3.4 Three cases of interest

3.4.1 The simplified pressure jump Hamiltonian

There is great freedom in defining the Hamiltonian. Although defining R and Z in Fourier form is intuitive, an analytical treatment of the introduction of R_{mn} and Z_{mn} terms quickly becomes untenable. The Fourier sum becomes convoluted when the metric terms g_{ij} are calculated, then these terms are combined to produce the g^{ij} that explicitly appear in the Hamiltonian. This results in a functionally complicated Hamiltonian inappropriate for theoretical exploration. In order to discern some general properties of this Hamiltonian, this freedom must be reduced in a way that retains helpful physical interpretations.

A common simplification to fusion geometries is to take the *cylindrical limit*. This limit occurs as the inverse aspect ratio $\epsilon = r_0/R_0$ approaches zero.

In order for the periodicity length (distance) in the toroidal direction to remain finite as $\epsilon \to 0$, we assume there is a discrete $1/\epsilon$-fold toroidal symmetry of the system (i.e. there are $1/\epsilon$ identical field periods in one toroidal circuit) and take a 2π increment in ζ to correspond to a field period rather than to a full toroidal circuit.

The Cartesian coordinates are required to calculate the metric. In this case the

Cartesian coordinates are

$$x = R(\theta,\zeta)\cos(\epsilon\zeta) - \frac{r}{\epsilon}\ , \tag{3.42a}$$

$$y = R(\theta,\zeta)\sin(\epsilon\zeta)\ , \tag{3.42b}$$

$$z = Z(\theta,\zeta)\qquad . \tag{3.42c}$$

where the the x and z axes are shifted to ensure the cylindrical approximation to the first field period has its axis centered along the y axis.

Simplifying perturbations to the deformation

There are two deformations of interest:

1. Helical deformations of the cross sectional shape (R^δ, Z^δ),

2. Helical deformations of the centroid of the cross section (R^a, Z^a).

Figure 3.4 shows the effects of the two perturbations. The perturbations are applied to $R(\theta,\zeta)$, $Z(\theta,\zeta)$

$$R(\theta,\zeta) = R_0 + r_0\cos\theta + R^a + R^\delta\ , \tag{3.43a}$$

$$Z(\theta,\zeta) = \qquad r_0\sin\theta + Z^a + Z^\delta\ . \tag{3.43b}$$

The deformations to the centroid of the cross section are applied by adding a $(0,1)$ mode to R and Z, as described in Appendix A.3.

$$R^a = \quad a r_0\cos(-\zeta)\ , \tag{3.44a}$$

$$Z^a = -a r_0\sin(-\zeta)\ , \tag{3.44b}$$

so that the centroid draws out a helix of radius ar_0.

Deformations to the cross section can be prescribed by defining the minor radius $r(\theta,\zeta)$. Consider the modifying the minor radius by adding the function

$$r^\delta(\theta,\zeta) = \delta\, r_0\cos(m\theta - n\zeta)\ , \tag{3.45}$$

which applies a "ripple" to the cross section with poloidal period m and toroidal period n. $R^\delta(\theta,\zeta)$ and $Z^\delta(\theta,\zeta)$ are the projections of $r^\delta(\theta,\zeta)$

$$R^\delta(\theta,\zeta) = r^\delta(\theta,\zeta)\cos\theta\ , \tag{3.46a}$$

$$Z^\delta(\theta,\zeta) = r^\delta(\theta,\zeta)\sin\theta\ . \tag{3.46b}$$

By using trigonometric identities, these functions can be written in the form of the Fourier decomposition for R and Z,

$$R^{\delta}(\theta,\zeta) = \frac{\delta}{2} r_0 \left[\cos\left((m+1)\theta - n\zeta\right) + \cos\left((m-1)\theta - n\zeta\right) \right] , \tag{3.47a}$$

$$Z^{\delta}(\theta,\zeta) = \frac{\delta}{2} r_0 \left[\sin\left((m+1)\theta - n\zeta\right) - \sin\left((m-1)\theta - n\zeta\right) \right] . \tag{3.47b}$$

Combining all the above terms, gives

$$\begin{aligned} R(\theta,\zeta) = r_0 \Bigg[& \frac{1}{\epsilon} + \cos\theta + a\cos(-\zeta) \\ & + \frac{\delta}{2}\cos\left((m+1)\theta - n\zeta\right) + \frac{\delta}{2}\cos\left((m-1)\theta - n\zeta\right) \Bigg] , \end{aligned} \tag{3.48a}$$

$$\begin{aligned} Z(\theta,\zeta) = r_0 \Bigg[& \sin\theta - a\sin(-\zeta) \\ & + \frac{\delta}{2}\sin\left((m+1)\theta - n\zeta\right) - \frac{\delta}{2}\sin\left((m-1)\theta - n\zeta\right) \Bigg] . \end{aligned} \tag{3.48b}$$

By substituting Equations (3.43) into Equations (3.42), one can calculate the metric. However, despite only having two harmonics, the form of the metric is still too complicated to provide helpful analytical insight. By expanding the metric functions to first order in ϵ, a and δ, and removing any cross terms in these variables, one finds the simpler but more intuitive metric

$$g^{\theta\theta} \sim \frac{1 - 2\delta\cos\left(m\theta - n\zeta\right)}{r_0^2} , \tag{3.49a}$$

$$g^{\theta\zeta} \sim -\frac{a\cos(\theta - \zeta)}{r_0^2} , \tag{3.49b}$$

$$g^{\zeta\zeta} \sim \frac{1 - 2\epsilon\cos\theta}{r_0^2} . \tag{3.49c}$$

To first order the inverse aspect ratio determines the $g^{\zeta\zeta}$ only, the cross section deformation affects $g^{\theta\theta}$ only and the twist in the centroid axis introduces $g^{\theta\zeta}$.

Simplifying perturbations to the potential function

The simplification is not complete, as the potential function $V(\theta,\zeta)$ has not yet been prescribed. The potential is given by Equation (2.25), expanded here,

$$V(\theta,\zeta) = -\frac{1}{2} g^{\theta\theta}(\partial_\theta f^-)^2 - g^{\theta\zeta}(\partial_\theta f^-)(\partial_\zeta f^-) - \frac{1}{2} g^{\zeta\zeta}(\partial_\zeta f^-)^2 . \tag{3.50}$$

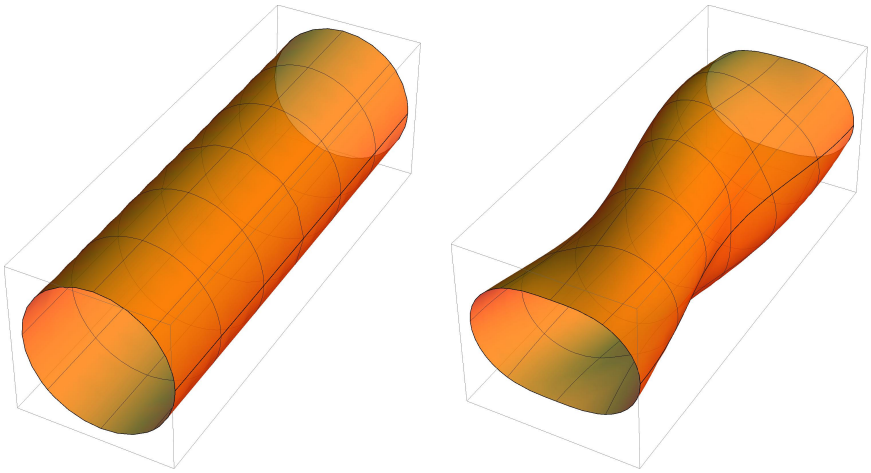

(a) $a = 0$, $\delta = 0$.

(b) $a = 0$, $\delta = 0.1$.

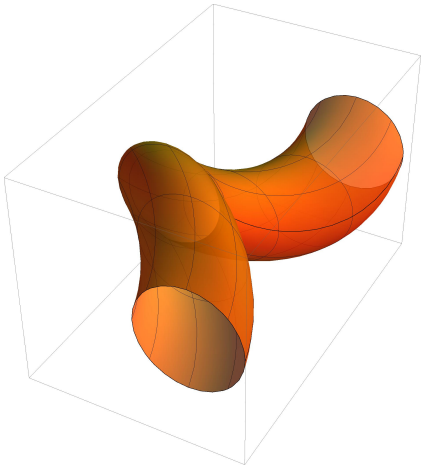

(c) $a = 1.5$, $\delta = 0$.

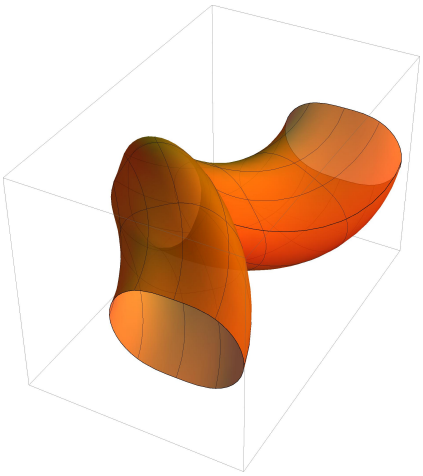

(d) $a = 1.5$, $\delta = 0.1$.

Figure 3.4: Deformations to the cross section (magnitude δ and mode $(1, 1)$) and to the centroid of the cross section (magnitude a) together simulate a deformed surface with only two Fourier components while being consistent with stellarator symmetry.

The general form for f^- was given in Equation (2.21), repeated here

$$f^- = I\theta + G\zeta + \hat{f}_{mn}\sin\left(m\theta - n\zeta\right) \ , \tag{3.51}$$

Where the minus in the superscript has been removed for clarity when f^- is expanded. One can consider a simple perturbation to the potential by selecting one Harmonic, say $(\hat{f}_{mn}, m, n) = (F, m_F, n_F)$ such that

$$f^- = I\theta + G\zeta + F\sin\left(m_F\theta - n_F\zeta\right) \ . \tag{3.52}$$

When this perturbed f^- is substituted into V along with the simplified metric (Equation (3.49)) a complicated epression is then found, which can be reduced by removing higher order terms (i.e. $F^2 \to 0, aF \to 0, \delta F \to 0, \epsilon F \to 0$) to

$$V(\theta,\zeta) \sim -\frac{1}{2}g^{\theta\theta}I^2 - g^{\theta\zeta}IG - \frac{1}{2}g^{\zeta\zeta}G^2 - \frac{F}{r_0^2}(Im_F - Gn_F)\cos\left(m_F\theta - n_F\zeta\right) \ . \tag{3.53}$$

The simplified Hamiltonian

With the above simplifications, the simplified pressure jump Hamiltonian is

$$\begin{aligned} Hr_0^2 = &\frac{1}{2}[1 - 2\delta\cos\left(m\theta - n\zeta\right)](p_\theta^2 - I^2) - a\cos(\theta - \zeta)(p_\theta p_\zeta - IG) \\ &+ \frac{1}{2}(1 - 2\epsilon\cos\theta)(p_\zeta^2 - G^2) - F(Im_F - Gn_F)\cos\left(m_F\theta - n_F\zeta\right) \ . \end{aligned} \tag{3.54}$$

This provides a potentially non-integrable Hamiltonian defined by the variables (r_0, I, G) with perturbation parameters (ϵ, a, δ, F) with a choice of modes $[(m, n) = (m_F, n_F)]$. Unless stated otherwise, when investigating this simplified Hamiltonian $(r_0, I, G) = (1, 1, \gamma)$. I and G are so chosen so that the rotational transform of the prescribed field is $I/G = 1/\gamma$, and setting $I = 1$ ensures the continued trajectory of winding number $1/\gamma$ occurs at $p_\theta = 1$ for the unperturbed Hamiltonian.

If only one of the perturbation parameters is non-zero, the Hamiltonian remains regular, as a transformation may always be made so that the Hamiltonian is separable. By inspection, it is immediately obvious that the Hamiltonian is non-integrable for any combination of two or more perturbation parameters.

The inverse formulation has a simpler form with this first order approximation as

the approximation to the metric contains explicit constant terms. Therefore

$$\begin{aligned} Hr_0^2 = \frac{1}{2}[1 - 2\delta\cos(m\theta - n\zeta)]p_\theta^2 - a\cos(\theta-\zeta)p_\theta p_\zeta \\ + \frac{1}{2}(1 - 2\epsilon\cos\theta)p_\zeta^2 - F(Im_F - Gn_F)\cos(m_F\theta - n_F\zeta) \\ + \delta\cos(m\theta - n\zeta)\, I^2 + a\cos(\theta-\zeta)IG + \epsilon\cos\theta\; G^2 \\ - \frac{1}{2}I^2 - \frac{1}{2}G^2 \,, \end{aligned} \tag{3.55}$$

which has the form of Equation (2.58) with a potential term that can be split into its constant term and fluctuation terms

$$< B_0^2 >= -2 < V > = \left(I^2 + G^2\right) \,, \tag{3.56}$$

$$\begin{aligned} \widetilde{V}(\theta,\zeta) = \delta\cos(m\theta - n\zeta)\, I^2 + a\cos(\theta-\zeta)IG + 2\epsilon\cos\theta\; G^2 \\ - F(Im_F - Gn_F)\cos(m_F\theta - n_F\zeta) \,, \end{aligned} \tag{3.57}$$

and the Hamiltonian for the inverse problem will be

$$\begin{aligned} H' = \frac{1}{2}\left(1 - 2\delta\cos(m\theta - n\zeta)\right)(p_\theta^2 - I^2) - a\cos(\theta-\zeta)(p_\theta p_\zeta - IG) \\ + \frac{1}{2}(1 - 2\epsilon\cos\theta)(p_\zeta^2 - G^2) + \widetilde{V}(\theta,\zeta) \,, \end{aligned} \tag{3.58}$$

where

$$H' = E' = (\Delta P)r_0^2 + \frac{1}{2}(I^2 + G^2) \,. \tag{3.59}$$

Conserving the prescribed rotational transform during deformation

The prescribed f and surface $\mathcal{S}$ define a rotational transform on the surface. Is it possible, within the above first-order model, to relate f and the deformation parameters δ, a, ϵ so that the rotational transform is conserved during deformations? This section shows that it is possible within the simplified formulation to conserve the first order approximation to ι during deformations.

It is hypothesised that the change to the rotational transform under a surface deformation in the modes $a : (1,1)$, $\epsilon : (1,0)$ and $\delta : (m,n)$ could be undone with a change to the prescribed field with the same modes.

$$f(\theta,\zeta) = I\theta + G\zeta + F_\delta\sin(m\theta - n\zeta) + F_a\sin(\theta-\zeta) + F_\epsilon\sin\theta \,. \tag{3.60}$$

The rotational transform is given by the integral

$$\iota = \int_0^{2\pi} \frac{d\theta}{d\zeta}\, d\zeta \ . \tag{3.61}$$

For the prescribed field, the rotational transform can be calculated using

$$\iota = \int_0^{2\pi} \frac{g^{\theta\theta}\partial_\theta f + g^{\theta\zeta}\partial_\zeta f}{g^{\theta\zeta}\partial_\theta f + g^{\zeta\zeta}\partial_\zeta f}\, d\zeta \ . \tag{3.62}$$

Substituting the prescribed deformed field, the integrand becomes, when expanded to first order and removing cross terms

$$\begin{aligned}\frac{d\theta}{d\zeta} \sim \frac{I}{G}\Bigg(1 - 2\delta\cos\left(m\theta - n\zeta\right) + \left[\frac{I}{G} - \frac{G}{I}\right] a\cos(\theta-\zeta) - (1 - 2\epsilon\cos\theta) \\ + F_\delta\left[\frac{m}{I} + \frac{n}{G}\right]\cos\left(m\theta - n\zeta\right) + F_a\left[\frac{1}{I} + \frac{1}{G}\right]\cos(\theta-\zeta) + F_\epsilon\frac{1}{I}\cos\theta + 1\Bigg) \ ,\end{aligned} \tag{3.63}$$

where $\iota = I/G$ in the unperturbed case and the "+1" and "−1" are intentionally left in without cancelling so that the first order metric coefficients can be identified in the equation.

The goal is to have ι not change under perturbations and so the integral in Equation (3.61) must remain equal to ι. The most direct way to do this is to require the integrand to be equal to ι for all θ and ζ. This is a stronger restriction than just requiring ι to be conserved, it additionally requires that (θ, ζ) become straight field line coordinates. Note that this is only a first order expression for ι and so it will only conserve the first order approximation to ι. Equation (3.63) is set to equal I/G and the equation is rearranged to be

$$\begin{aligned}\frac{I}{G} = \frac{I}{G}\Bigg\{ &\left(2\delta + F_\delta\left[\frac{m}{I} + \frac{n}{G}\right]\right)\cos\left(m\theta - n\zeta\right) \\ &+ \left(a\left[\frac{I}{G} - \frac{G}{I}\right] + F_a\left[\frac{1}{I} + \frac{1}{G}\right]\right)\cos(\theta-\zeta) \\ &+ \left(2\epsilon - F_\epsilon\frac{1}{I}\right)\cos\theta\Bigg\} \ .\end{aligned} \tag{3.64}$$

Which allows one to equate like cosine terms for expressions for the coefficients of the

prescribed field perturbations that conserve the rotational transform

$$F_\delta = \quad 2\frac{IG}{In+Gm}\delta \ , \tag{3.65a}$$

$$F_a = -(I-G)a \ , \tag{3.65b}$$

$$F_\epsilon = -2I\epsilon \ . \tag{3.65c}$$

Substituting these expressions into the Hamiltonian gives

$$\begin{aligned} Hr_0^2 = \frac{1}{2}\left(1-2\delta\cos\left(m\theta-n\zeta\right)\right)\left(p_\theta^2-I^2\right) - a\cos(\theta-\zeta)(p_\theta p_\zeta - IG) \\ + \frac{1}{2}(1-2\epsilon\cos\theta)(p_\zeta^2-G^2) - F_\delta\left(Im-Gn\right)\cos\left(m\theta-n\zeta\right) \\ - F_a(I-G)\cos(\theta-\zeta) - F_\epsilon I\cos\theta \ , \end{aligned} \tag{3.66}$$

$$\begin{aligned} Hr_0^2 = \frac{1}{2}\left(1-2\delta\cos\left(m\theta-n\zeta\right)\right)\left(p_\theta^2-I^2\right) - a\cos(\theta-\zeta)(p_\theta p_\zeta - IG) \\ + \frac{1}{2}(1-2\epsilon\cos\theta)(p_\zeta^2-G^2) - 2IG\,\frac{Im-Gn}{Gm+In}\,\delta\,\cos\left(m\theta-n\zeta\right) \\ + (I-G)^2 a\cos(\theta-\zeta) + 2I^2\epsilon\cos\theta \ . \end{aligned} \tag{3.67}$$

3.4.2 MRXMHD Interfaces

Defining the geometry of interfaces

To see how well the simplified Hamiltonian reflects the pressure jump Hamiltonian, the second case involves solving the pressure jump Hamiltonian system for a smoothly deformed surface. Such a deformation simulates one that `SPEC` may apply in an effort to satisfy force balance on an interface as part of its calculation of the equilibrium field. The same deformation as the simplified case, namely a twist in the centroid

$$R^a = \quad ar_0\cos(-\zeta) \ , \tag{3.68a}$$

$$Z^a = -ar_0\sin(-\zeta) \ , \tag{3.68b}$$

and a deformation in the cross section of mode $(1,1)$,

$$r^\delta(\theta,\zeta) = \delta\, r_0\cos\left(\theta-\zeta\right) \ , \tag{3.69}$$

results in

$$R(\theta,\zeta) = R_0 + r_0\cos\theta + ar_0\cos(-\zeta) + \frac{\delta}{2}r_0\left[\cos(2\theta-\zeta)+\cos(-\zeta)\right] , \tag{3.70a}$$

$$Z(\theta,\zeta) = r_0\sin\theta - ar_0\sin(-\zeta) + \frac{\delta}{2}r_0\left[\sin(2\theta-\zeta)-\sin(-\zeta)\right] . \tag{3.70b}$$

Equations (3.70) can be simplified further into two components reflecting the superposition of the two deformations

$$R(\theta,\zeta) = R_0 + r_0\cos\theta + \left(\frac{\delta}{2}+a\right)r_0\cos(-\zeta) + \frac{\delta}{2}r_0\cos(2\theta-\zeta) , \tag{3.71a}$$

$$Z(\theta,\zeta) = r_0\sin\theta - \left(\frac{\delta}{2}+a\right)r_0\sin(-\zeta) + \frac{\delta}{2}r_0\sin(2\theta-\zeta) . \tag{3.71b}$$

It is desirable to reduce the number of perturbative variables so δ will be set equal to a, resulting in

$$R(\theta,\zeta) = R_0 + r_0\cos\theta + \frac{\delta}{2}r_0\left(3\cos(-\zeta)+\cos(2\theta-\zeta)\right) , \tag{3.72a}$$

$$Z(\theta,\zeta) = r_0\sin\theta + \frac{\delta}{2}r_0\left(-3\sin(-\zeta)+\sin(2\theta-\zeta)\right) . \tag{3.72b}$$

By solving the unsimplified pressure jump Hamiltonian system with the deformations in Equations 3.71 and 3.72, the nature of these interfaces under such deformations can be determined, and their investigation should shed light on how they may be chosen and loaded with pressure discontinuities in SPEC.

Calculating the prescribed field on interfaces

The prescribed field f^- still needs to be defined for interfaces. As with the simplified Hamiltonian, deformations to the interfaces will change the rotational transform on those interfaces if V is not corrected.

When ι tracking was required, SPEC was modified to provide this service. SPEC can calculate the f^- required on the prescribed side for each value of the deformation.[1] This f^- was then used as input into the pressure jump Hamiltonian. Two flux surfaces need to be supplied to SPEC. One (say, the outermost one) should be identically the flux surface one wants to evaluate in PJH, with the same RZ description and

[1] The method SPECuses to calculate f^- requires radial derivitives of the magnetic vector function $\boldsymbol{A}$. Details of the method can be found on the online documentation of SPEC.[spe] The method is related to the discussion of straight field line coordinates in Appendix A.2.5.

rotational transform.[2] The inner surface does not have such strict requirements, the only restrictions being that SPEC must be able to find a Beltrami field in between them. To maximise the chances of this happening, a circularly symmetric flux surface with rotational transform similar to or less than the outermost surface was used.

SPEC outputs a `.pj` file that can be used as input into PJH. An example of such a file can be found in Appendix A.7. When SPEC was used to provide an input file, the provided Fourier series sometimes had to be truncated otherwise PJH would run too slowly. Details of the truncation can be found in Section 3.4.3.

3.4.3 Flux surfaces

The third case of interest in this thesis are flux surfaces that are not constructed as interfaces, but naturally appear within the volumes in MRXMHD. SPEC has the ability to extract such flux surfaces from within an MRXMHD volume. Unlike interfaces, such internal flux surfaces may be destroyed by the chaos surrounding them, and are not smoothly and arbitrarily deformed.

This case should provide a more generalised idea of existence under pressure jumps, as the perturbation caused by deformation is no longer an artificial, arbitrary, smooth choice. In this configuration the deformation applied to the flux surface is the result of nearby islands influencing the interior flux surface in a potentially fractal way.

Knowledge of how much pressure an internal flux surface may withstand could be helpful for SPEC if it becomes necessary for SPEC to introduce an extra interface. The internal flux surface could perhaps be tested for robustness before having pressure loaded onto it.

Using SPEC to extract flux surfaces

Consider a volume bounded by two circular axisymmetric flux surfaces of rotational transform ι_0 and ι_1. Under a reasonable assumption of linear shear between the two flux surfaces, one should be able to identify an infinite number of flux surfaces existing between these two prescribed surfaces with rotational transforms corresponding to the real nubers between ι_0 and ι_1. If the interfaces were deformed, flux surfaces would start to be destroyed within the volume but, according to the KAM theorem, a finite measure of the flux surfaces within the volume will persist under these deformations. These surviving flux surfaces are not smoothly perturbed and so considering a pressure discontinuity across these surfaces should represent a more realistic simulation than applying a pressure discontinuity across a smoothy deformed interface.

We calculate the equilibrium field in SPEC by prescribing two axisymmetric interfaces. The outermost surface was given a major radius of 1.0 and a minor radius of

[2]The way PJH stores surfaces and surface potentials as Fourier series is idential to how SPEC does.

$r = 0.3$. The outer surface's minor radius was then perturbed according to

$$r^d = 0.3 + d\cos(2\theta - \zeta) + d\cos(3\theta - \zeta) \ . \tag{3.73}$$

SPEC then calculated the field in the volume between the two interfaces. The inner interface was deformed to satisfy force balance so that the equilibrium field in the interface reflects a global solution. SPEC was used to extract the geometry of a flux surface with $\iota = \gamma_{[1213]}$ for various values of d.

This case has the least number of arbitrary prescriptions in the pressure jump Hamiltonian. While d explicitly parametrises a deformation of the outermost surface, the actual deformation to the extracted flux surface is now implicit in the chaotic mechanisms that can be evinced in SPEC. Of course, there is still some artificiality as the chaotic behaviour in the volume depends on how the outmost surface is warped, and here it is being warped in a smooth, prescribed way.

Truncating the SPEC Fourier series

PJH is limited by the number of Fourier terms it can use. As each term needs to be added multiple times at every evaluation point of the numerical integrator the code slows exponentially as more terms are added. To decide which terms to keep, terms were selected based on the measure

$$W_{mn} = \sqrt{R_{mn}^2 + Z_{mn}^2 + f_{mn}^2} \ . \tag{3.74}$$

calculated from the triplet (R_{mn}, Z_{mn}, f_{mn}). Those terms with large W_{mn} would have the biggest effect on the trajectory and so were kept. PJH was written so that the user may select a number of Fourier terms to keep, or select a minimum W_{min} such that all terms with $W_{mn} > W_{min}$ are kept.

Truncating Fourier terms in this way leads to less accurate results near criticality, as in this regime the functions R, Z, and f have long Fourier tails. The magnitude of the truncation was decided on a case by case basis as there is a tradeoff between more Fourier terms being needed to correctly describe the flux surface, and more Fourier terms leading to more numerical evaluations and higher numerical error. As such the truncation was decided with consideration of the test described in Section 3.3.7.

3.4.4 Summary of accuracy parameters of PJH

Collecting all the mentions of accuracy so far provides four quantities that determine the accuracy of the code. Their default values are provided in Table 3.2.

symbol	value	description
ν_l	10^{-15}	Integration tolerance when following field lines
ε_t	10^{-10}	Minimum error in winding number when finding trajectories with a desired winding number
ν_r	10^{-13}	Integration tolerance when calculating the tangent map
W_{min}	10^{-10}	Minimum size of the RMS of the Fourier terms provided as input

Table 3.2: A table summarising the parameters that determine the accuracy of `PJH`. The first three are computational tolerances that result in random error, W_{min} determines how well the input described the physical situation and so is a source of systematic error.

Chapter 4

Phase space

4.1 Phase space of the simplified pressure jump Hamiltonian

Figure 4.1 shows Poincaré diagrams for the simplified pressure jump Hamiltonian with each of the perturbative set (ϵ, a, δ, F) non zero, and $\Delta P = 0$. For these plots, and all Poincaré sections to follow, the black crosses are the punctures of the continued trajectory with the rotational transform equal to the ninth convergent of the irrational $1/\gamma$ plotted to show the choice of the selected continued field. The dot-dash line is the curve $\partial_\theta f(\theta, 0) = B_\theta$ and can be thought of as a field line or trajectory of the prescribed field (or reference field, in the case of the two sided formulation).

On Poincaré diagrams of perturbed systems, the dot-dash line functions as a reference to the unperturbed case. In the case of a cylinder with no pressure jump [Figure 4.1(a)], the continued field (black crosses) and the prescribed/reference field (black dot-dashed line) are the same, as expected. The continued field is not the same as the reference field in the other four figures, even with no pressure discontinuity because deformations to the geometry or to F in general give the reference field a different rotational transform to the one that is searched for on the other side.

In the case of $(\epsilon, a, \delta, F) = 0$, the Hamiltonian corresponds to a free particle on a cylinder, and as such all trajectories are regular [Figure 4.1(a)]. Introducing δ forms an island according to its harmonic [in this case $(m, n) = (1, 1)$] [Figure 4.1(c)]. The helical twist of the centroid of the surface similarly appears as a harmonic [$(m, n) = (0, 1)$], though the island is smaller than the one caused by δ [Figure 4.1(d)]. Adding a perturbation to the prescribed field by defining (F, m_F, n_F) will add islands corresponding to that mode [Figure 4.1(e)]. By making ϵ non-zero the $(m, n) = (1, 0)$ island appears at the bottom of the Poincaré diagram, which provides the mechanism by which toroidicity may incite chaos [Figure 4.1(b)].

Figure 4.2 shows Poincaré diagrams for the simplified pressure jump Hamiltonian with $(\epsilon, a, \delta, F) = (0.05, 0.05, 0.1, 0)$ and $(\epsilon, a, \delta, F) = (0.15, 0.15, 0.3, 0)$, both for zero pressure jump. In this case the three sources of islands overlap to create

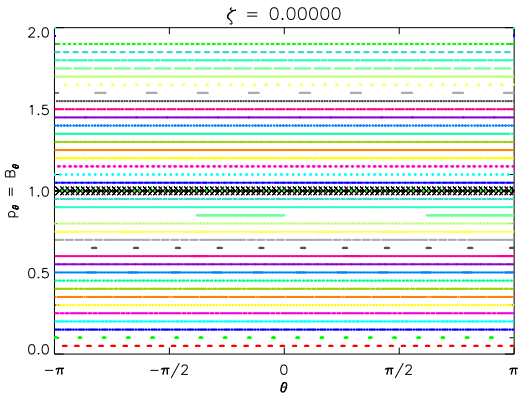

(a) $(\delta, a, \epsilon, F) = (0, 0, 0, 0)$. This corresponds to a free particle on a cylinder.

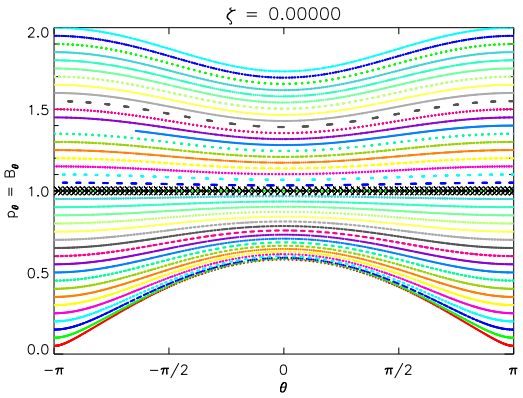

(b) $(\delta, a, \epsilon, F) = (0, 0, 0.1, 0)$. A large aspect ratio torus, the phase trajectories are warped owing to a large island (the $(0, 1)$ island) at $(\theta, p_\theta) = (0, 0)$.

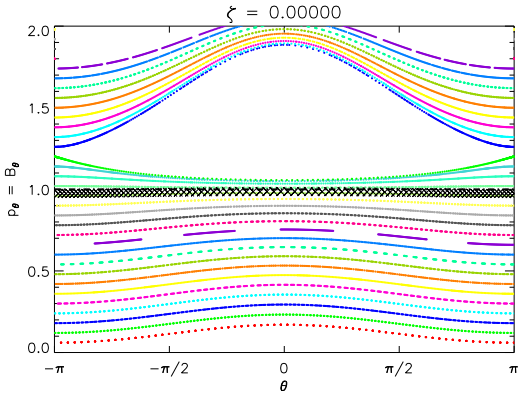

(c) $(\delta, a, \epsilon, F) = (0.05, 0, 0, 0)$. All trajectories are still regular, a large island has been introduced from an elliptic cross sectional deformation $(m, n) = (1, 1)$.

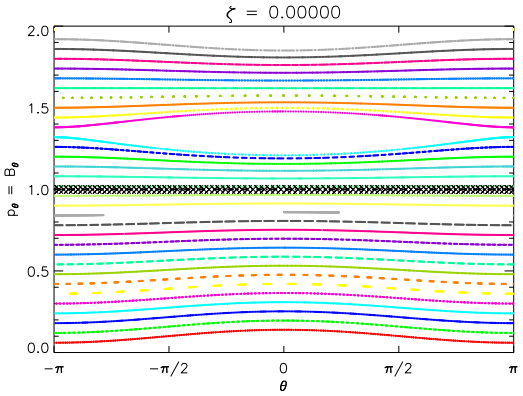

(d) $(\delta, a, \epsilon, F) = (0, 0.05, 0, 0)$. This corresponds to a cylinder that has an axis twisted into a helix of radius $0.05 r_0$.

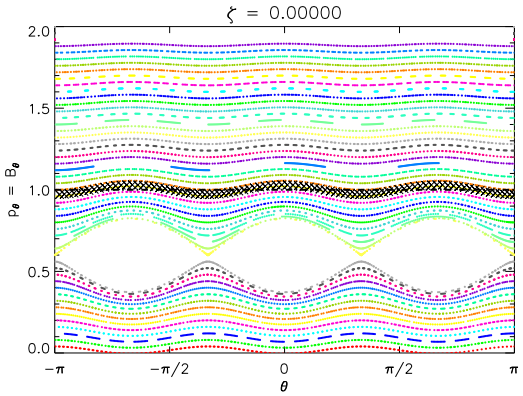

(e) $(\delta, a, \epsilon, F) = (0, 0, 0, 0.01)$. A cylinder, but the prescribed field has been perturbed with the mode $(m_F, n_F) = (3, 1)$.

Figure 4.1: Poincaré sections of the simplified pressure jump Hamiltonian showing the effect of introducing the perturbations. $\delta\, r_0$ is the magnitude of an elliptic cross sectional deformation $[(m, n) = (1, 1)]$, $a r_0$ is radius of the helical twist in the centroid of the cross section and ϵ is the inverse aspect ratio ($\epsilon = 0$ corresponds to the cylindrical limit).

additional islands and regions of chaos. The chaotic regions almost dominate phase space and it looks like the last trajectory to survive is the trajectory with a similar rotational transform to the prescribed field (though, as mentioned, a deformation has changed the rotational transform of the prescribed field so its value is unknown).

4.1.1 The effect of changing energy

Figure 4.3 shows the simplified Hamiltonian system under the perturbations $(\delta, a, \epsilon, F) = (0.01, 0.01, 0.1, 0)$ with positive values for the energy. Increasing the energy increases the magnitude of the pressure jump from the reference case or prescribed side. See Section 2.4.2 for details of how the energy should be interpreted.

Note that once E is non-zero, the prescribed field no longer matches up with the trajectories. From this one can infer that it is impossible to continue the field across a pressure discontinuity without having an associated discontinuity in the field. This reflects the fact apparent in Equation (2.14d).

Increasing energy "stretches" phase space, allowing trajectories with higher momentum and causing the regions of chaos to grow. The effect is qualitatively reminiscent of the Hénon Heiles Hamiltonian under increasing energy, especially the chaotic region in Figure 4.3(d).[Gre80] The regular trajectories toward the top of the phase diagrams have a very high rotational transform and do not feel the low order perturbations. More and more of these are allowed as the energy is increased. This makes sense from a Hamiltonian mechanics point of view, as increasing the energy of the system (increasing the pressure) allows the trajectory possibilities to access more momentum (higher $p_\theta = B_\theta$).

Note that there is a maximum p_θ orbit available, corresponding to the orbit with the highest winding number. This occurs when the equations for p_ζ [Equations (3.7)] becomes imaginary because the term under the square root [the same term as in Equation (2.34)]

$$C = g^{\zeta\zeta}\left[2\Delta P - 2V(\theta,\zeta) - g^{\theta\theta}p_\theta^2\right] + \left(g^{\theta\zeta}p_\theta\right)^2 \tag{4.1}$$

becomes negative. For the equations of motions to remain real, p_θ must satisfy

$$p_\theta^2 < \frac{g^{\zeta\zeta}}{g^{\theta\theta}g^{\zeta\zeta} - (g^{\theta\zeta})^2}\left[2\Delta P - 2V(\theta,\zeta)\right] \ , \tag{4.2}$$

along the entire length of the trajectory. `PJH` may run into this situation, at which stage the code outputs an error.

Figure 4.4 shows the same system but at negative energy levels. Decreasing the energy removes the trajectories with higher momentum, restricting those to lower rotational transform. The decreasing pressure also reverses the phase of the islands,

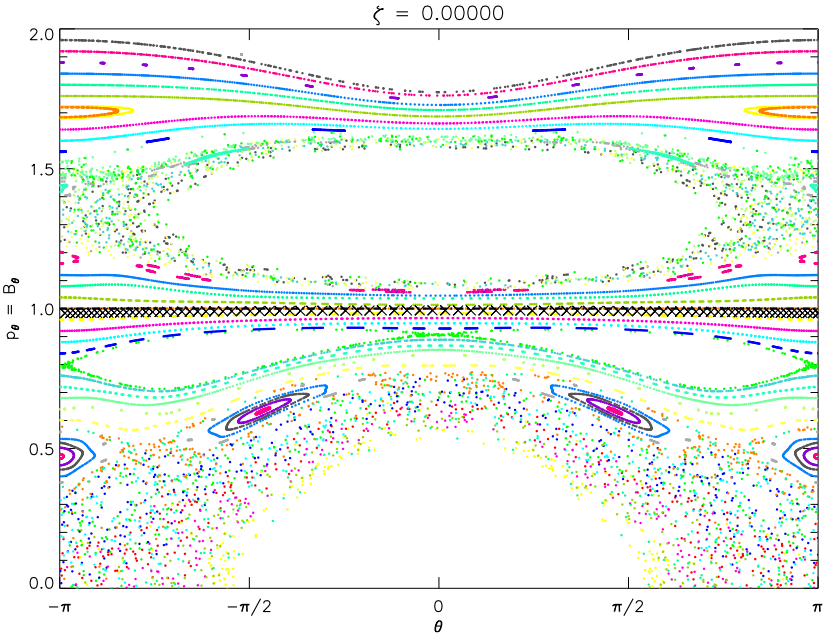

(a) $(\epsilon, a, \delta, F) = (0.05, 0.05, 0.1, 0)$.

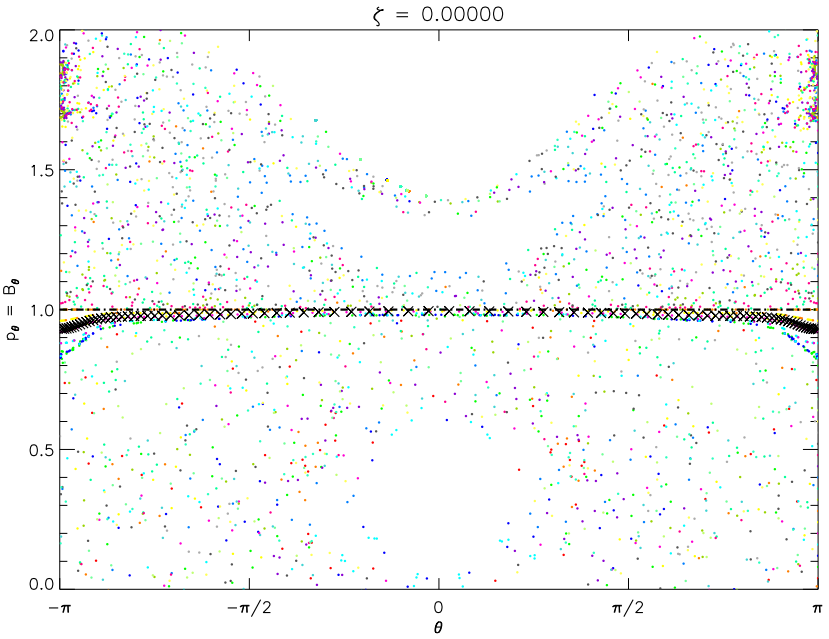

(b) $(\epsilon, a, \delta, F) = (0.15, 0.15, 0.3, 0)$.

Figure 4.2: Poincaré sections of the simplified pressure jump Hamiltonian with $\Delta P = 0$ and with the perturbations such that there is induced chaos. δ is the magnitude of an elliptic cross sectional deformation $[(m, n) = (1, 1)]$, a is radius of the helical twist in the centroid of the cross section and ϵ is the inverse aspect ratio ($\epsilon = 0$ corresponds to the cylindrical limit). The crosses are the punctures of the trajectory whose winding number is the ninth convergent (τ_9) of the irrational $\gamma_{[0111]} = 1/\gamma$.

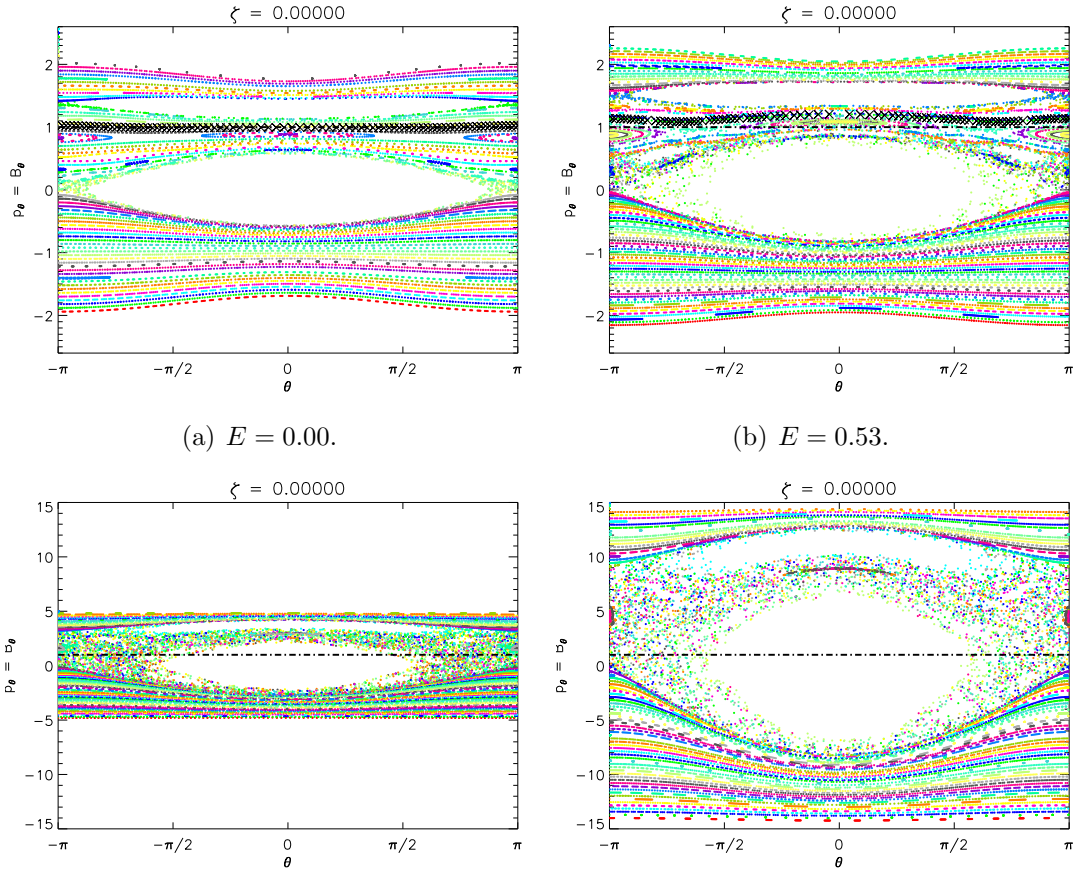

(a) $E = 0.00$.

(b) $E = 0.53$.

(c) $E = 10.00$.

(d) $E = 100.00$.

Figure 4.3: Poincaré sections of the simplified pressure jump Hamiltonian with perturbations $(\delta, a, \epsilon, F) = (0.01, 0.01, 0.1, F)$ for increasing positive values of the energy. In general this expands the phase space to allow more trajectories and at the same time looks to increase the chaos. Large positive values lead to more trajectories with higher rotational transforms that are not affected by the low order perturbations. Note the the scale of the vertical axis is larger in the second row of images, and in these images the energy was so large that the selected continued solution with $w = \tau_9$ could not be found.

and there is a point around $E \approx -0.5$ at which much of the chaos seems to disappear. Decreasing energy past this point results in the islands increasing in size with the opposite phase, introducing chaos that eventually destroys the irrational trajectory of interest. At a low enough energy all energetically available orbits remain within the $(0, 1)$ island.

The increasing pressure does not seem to introduce islands, but it still has a destructive effect. To understand this consider a Hamiltonian trajectory of fixed winding number. If this orbit is regular but has a chaotic region nearby, the scaling of the phase diagram means the chaotic regions expand, possibly overlapping the position of the trajectory of interest. As flux surfaces are defined by their rotational transform, an increase of pressure that causes chaos to expand and overlap with the corresponding Hamiltonian trajectory means that an increase in pressure can effectively make field continuation across the flux surface impossible.

At the lowest energies no orbits can escape the $(1, 0)$ island. The point at which the trajectory can no longer form a rotational invariant surface occurs at some energy $E > E_{min}$. The lowest energy for which a covering is possible should occur at the point $E_r = \max[V(\theta, \zeta)]$, as at energies lower than the maximum value of the potential, the trajectory will not be able to access the points at which the potential is higher than the energy of the particle. Note that this is a necessary condition, but not sufficient as the last trajectory that is able energetically to reach all points of the torus is likely to be already chaotic.

It is likely that each field line configuration will cease to exist at a high enough pressure for any nontrivial deformation, but configurations with higher rotational transforms can exist instead. So although additional high–winding–number orbits are allowed under the increase in energy, the chaotic region expands and tends to destroy low–winding–number orbits. In the supplied Poincaré diagrams, the high iota region is quite clear of chaos, but this is probably due to the simple deformation (which contains only low order resonant Fourier terms) that was applied. More complicated deformations may resonate with high ι rationals. These islands may not be accessible for small pressure jumps, but may appear when E is increased.

It should also be mentioned that, while increasing the energy expands chaotic regions, *some* field line configuration will probably exist no matter how high the energy, so long as one is willing to allow a very high rotational transform on the continued side, and thus a large rotational transform discontinuity. It is not known how physical such a state would be, but there is evidence that discontinuities in rotational transform across flux surfaces are unstable to tearing modes.[MHD09]

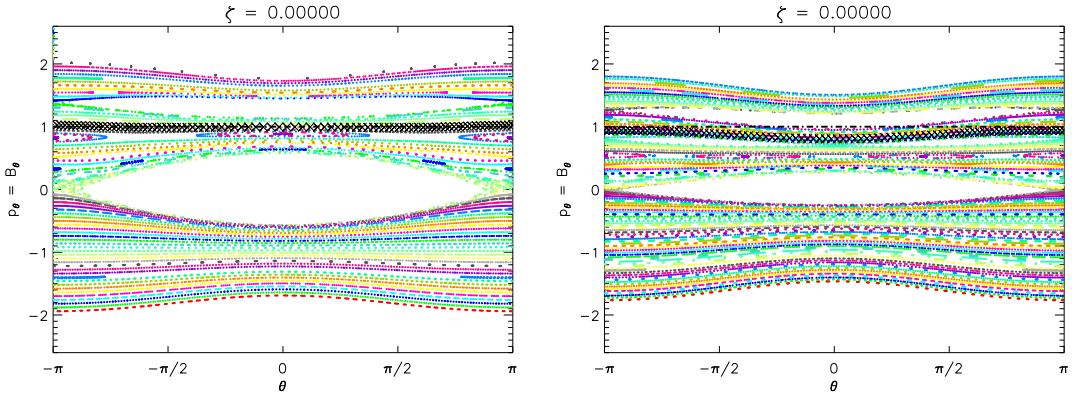

(a) $E = 0.00$.

(b) $E = -0.4$.

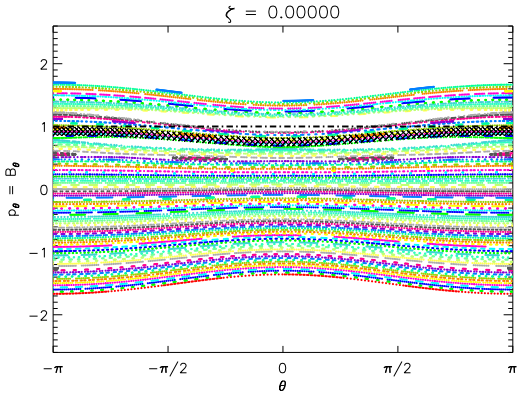

(c) $E = -0.5$.

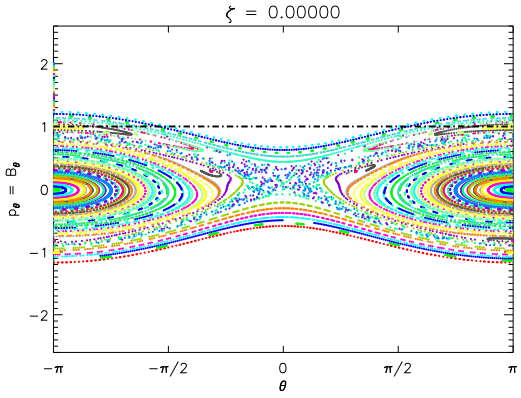

(d) $E = -1.3$.

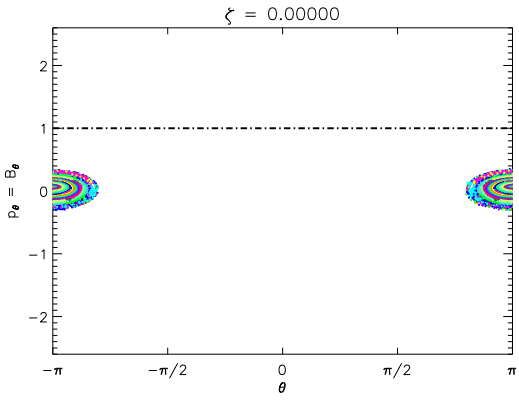

(e) $E = -2.0$.

Figure 4.4: Poincaré sections of the simplified pressure jump Hamiltonian with perturbations $(\delta, a, \epsilon, F) = (0.01, 0.01, 0.1, 0)$ for values of the energy decreasing from zero. The lower energies reverse the phase of the islands leading to much less chaos, the amount of chaos appears to reach a minimum around $E = -0.5$. Past this point the islands start to increase in size with the opposite phase, increasing the amount of chaos. At the same time the lower energy brings the maximum and minimum p_θ values toward zero. Eventually the only energetically available orbits reside in and cannot escape the $(0, 1)$ island. This latter case corresponds to a field line that "wiggles" like a sine curve about $\theta = \pi$ on the innermost edge of the torus.

Comparison to double pendulum Hamiltonian

As mentioned in Section 2.4.3, a comparison to the double pendulum Hamiltonian may help to visualise the trajectories of the pressure jump Hamiltonian.

Each pendulum can either *librate* (swing back and forward) or *rotate* (do a full spin around its fixed point). Both these behaviours can be seen for the angles in the pressure jump Hamiltonian. Librational motion can be seen most obviously in the large island in Figure 4.4(d). A trajectory in this island never reach the point $\theta = 0$. When mapped to configuration space the field lines are seen to "wriggle" along the inner edge of the torus ($\theta = pi$). These librational trajectories do not have an irrational rotational transform and so the corresponding field line cannot be considered a solution to field balance by the restrictions in Section 3.2.5.

This also provides a visualisation of the effect of reducing the island size. With reference to Figure 4.4, at $E = 0$ a low-momentum trajectory hamonically oscillates (librates) about the curve $\theta = 0$, the outermost geodesic on the surface, as ζ increases. By reducing the enery to $E = -0.5$, it looks as if even the lowest momentum trajectories can rotate completely around with a well defined rotational transform. As the energy is increased past this point, the low momentum orbits start oscillating around the shortest geodesic on the torus, the $\theta = \pi$ curve.

The double pendulum is a non-integrable Hamiltonian system that becomes integrable in the low and high energy limits. At the low limit, a small angle approximation can be made, and nonlinear terms may be ignored leading to a pair of linear oscillators.[RWB09] In the high energy regime, the kinetic term dominates and the pendulums fully extend and spin together as a fixed rotor. To be considered solutions to force balance, trajectories of the pressure jump Hamiltonian require an irrational rotational transform and so both angles must undergo rotation [Section 3.2.5]. In the case of the high energy limit of the double pendulum, both angles rotate at the same rate, which, in the force balance problem would correspond to a field line of $\iota = 1$. Field lines with other rotational transforms would correspond to a double pendulum with rotational motion in both angles, with the two angles rotating at a different rate.

4.1.2 The effect of conserving rotational transform

The constraint to conserve rotational transform adds fluctuations to the prescribed field that compensate for the deformation to the surface and ensure that under deformations the rotational transform of the prescribed field remains constant. This may be of importance if one wishes to determine continuation for a field of a given rotational transform under deformations.

Typically, trajectories with irrational rotational transform are more robust to chaos.[Gre79] Intuitively one may think that forcing the prescribed field to have an

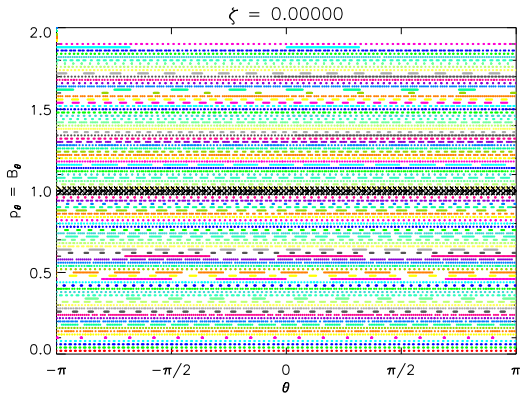

(a) $(\delta, a, \epsilon) = (0, 0, 0)$. Unperturbed system with unperturbed prescribed field.

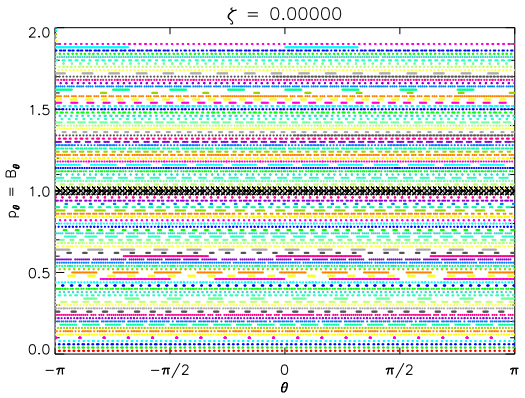

(b) $(\delta, a, \epsilon) = (0, 0, 0)$. Unperturbed system with conserved prescribed rotational transform.

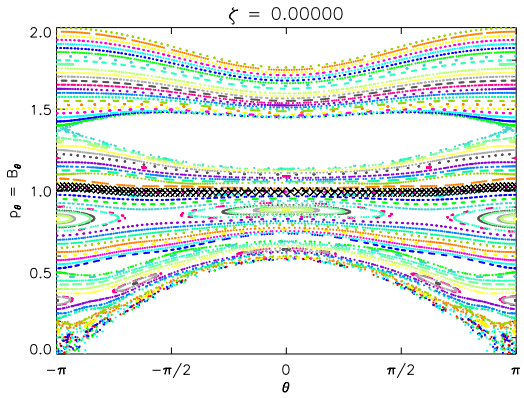

(c) $(\delta, a, \epsilon) = (0.010, 0.010, 0.1)$. Perturbed system with unchanged prescribed field f^-.

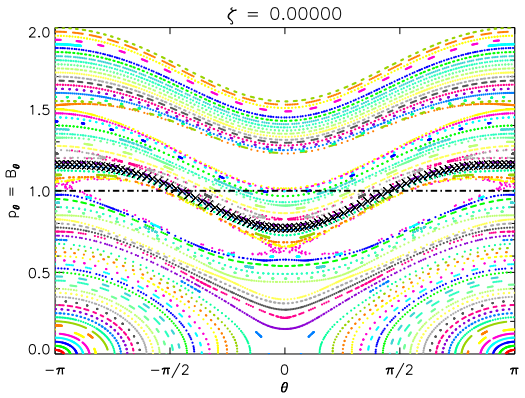

(d) $(\delta, a, \epsilon) = (0.010, 0.010, 0.1)$. Perturbed system with prescribed field changed to conserve prescribed rotational transform.

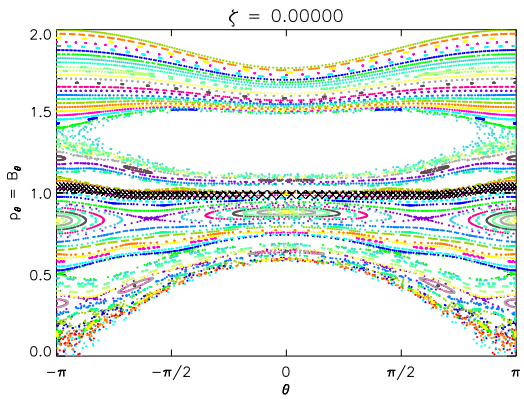

(e) $(\delta, a, \epsilon) = (0.015, 0.015, 0.1)$. A more perturbed system than above, still with unchanged prescribed f^-. The trajectory remains regular.

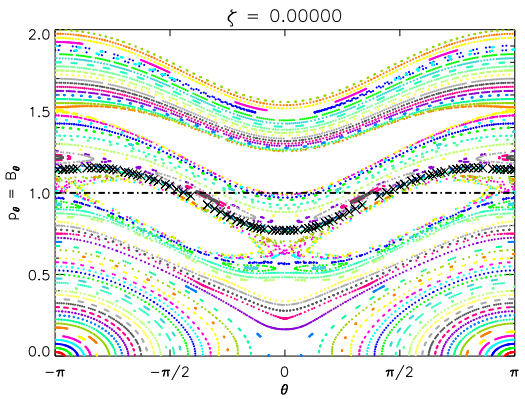

(f) $(\delta, a, \epsilon) = (0.015, 0.015, 0.1)$. A more perturbed system than above with f^- conserving prescribed rotational transform. At this point the convergent to the irrational suggests the continued trajectory is critical.

Figure 4.5: Poincaré sections of the simplified pressure jump Hamiltonian with $\Delta P = 0$ showing the effect of conserving the rotational transform of the prescribed field. In general it was observed that continuation occurs for smaller energy values when the rotational transform of the prescribed field is constrained via Equations (3.65).

irrational rotational transform may reduce the chaos in the Hamiltonian. Figure 4.5 shows the phase space at three levels of increasing deformation at $\Delta P = 0$. The right column of plots show the system with rotational transform conservation and the left column shows the same perturbations without ι conservation. In this case the ι conservation increases the amount of chaos for a given perturbation and results in the continued field configuration becoming critical at a lower deformation.

Looking at the Hamiltonian under ι conservation, the fact that it has a prescribed field perturbation at all is probably the cause of the increased chaos. Alternatively the intuitive thought may be incorrect because this phase space is unlike other Hamiltonian systems in that, at $H = \Delta P = 0$, continuation is always allowed for the solution for the same rotational transform. Prescribing this rational must suppress any islands that would ordinarily destroy it in the $H = 0$ case. This constructed ensured existence for the rational is unnecessary in the two-sided formulation, and so is avoided unless continuation from a certain prescribed field is required. Perhaps the restriction of Equations (3.65) is too strong, or that the first order conservation of the rotational transform is insufficient.

4.2 Phase space of SPEC interfaces

The previous section investigated the simplified pressure jump Hamiltonian system. We now move back to the unsimplified Hamiltonian system and investigate the phase space of a Hamiltonian that represents the prescribed interfaces that would be used in MRXMHD and in `SPEC`. To allow some comparison to the previous section, we deform the surface in the following way

$$\mathcal{S} = \left[\begin{array}{cccc} m & n & R_{mn} & Z_{mn} \\ \hline 0 & 0 & 1.0 & 0.0 \\ 1 & 0 & 0.2 & 0.2 \\ 0 & 1 & \frac{3}{2}\delta & -\frac{3}{2}\delta \\ 2 & 1 & \frac{1}{2}\delta & \frac{1}{2}\delta \end{array}\right] . \tag{4.3}$$

The prescribed field in these cases was found using `SPEC` for each of the above deformations, and so at each deformation the f^- is such that its rotational transform is $\iota^- = \gamma_{[0111]} = 0.618033....$ See Section 3.4.2 for more information on how the case of `SPEC` interfaces were defined.

At the largest deformation, 40 Fourier terms were found to provide a scan indistinguishable by eye from cases with less truncation Section 3.4.3. The plots in this section were done with 60 Fourier terms.

4.2.1 Phase space under specific deformation of interface

Figure 4.6 shows the phase space of the pressure jump Hamiltonianfor the surface defined in Equation (4.3). The trajectory with winding number $\iota = \tau_9$ for the interval [0111] was selected as the continued solution in each plot. The maximum deformation for which `SPEC` could calculate the prescribed field was $d = 0.02870$.

The most obvious change to the phase space is that chaotic structures begin to appear and that these chaotic structures get more numerous and larger as the deformation increases. The large islands visible in the centre of the Poincaré diagrams correspond to the harmonics of the deformation, which is easiest seen when the deformation is written in the form of Equation (4.3). The position of the chaos on the Poincaré diagram was observed to be highly sensitive to the form of the deformation array, suggesting that the existence of regular orbits was dependent on the deformation in a very complicated way.

The phase diagrams are reminiscent of, but sufficiently different from the simplified version to suggest that the simpified version is unsuitable as an approximation. Instead the simplified system should be considered a "toy problem" reflecting the basic chaotic nature of the pressure jump Hamiltonian.

As the deformation increases further, more and more of the phase space becomes chaotic. It was not possible to increase the deformation until the entire volume became chaotic at a pressure jump of zero, because `PJH` makes its calculations predicated on the existence of f^-, which `SPEC` is required to calculate first. In situations where `PJH` used customised f^- functions not taken from `SPEC`, it was possible to concoct geometries and prescribed fields in which the only possible solution was $f^- = f$.

As each orbit corresponds to a field line configuration, it is clear that increasing the deformation of the flux surface results in less candidate field line configurations that can satisfy the pressure jump condition. Also, there is a maximum limit to the rotational transform that would satisfy the pressure jump condition, and this limit decreases with increasing deformation.

4.2.2 Phase space under change in energy

Figure 4.7 shows Poincaré diagrams for the surface defined by Equation (4.3) for different values of the energy. Again the continued solution is the same as the prescribed field, which is calculated using `SPEC`. The three plots show the phase space for the minimum energy for which a solution can be found, zero energy and the maximum energy for which the continued solution can be found respectively.

The qualitative behaviour is similar to the simplified version, supporting the latter's role as a toy problem.

Increasing the energy can certainly have a destructive effect on trajectories, mean-

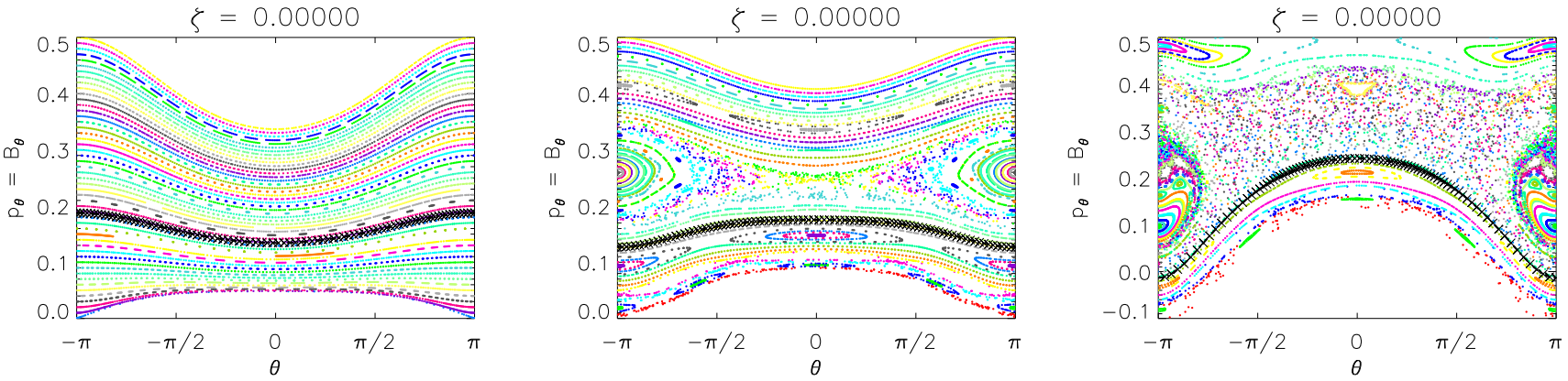

(a) $\delta = 0$. Like the simplified Hamiltonian, only the $(1, 0)$ island appears.

(b) $\delta = 0.01061$.

(c) $\delta = 0.02870$. At the maximum deformation for which SPECcould calculate the prescribed field, the continued trajectory is not critical, but close to it considering the nearby chaos.

Figure 4.6: Poincaré sections of the pressure jump Hamiltonian with $\Delta P = 0$ for the interface defined in Equation (4.3). At each deformation SPECwas used to calculate the f required to ensure the rotational transform of the prescribed field was $\gamma_{[0111]}$.

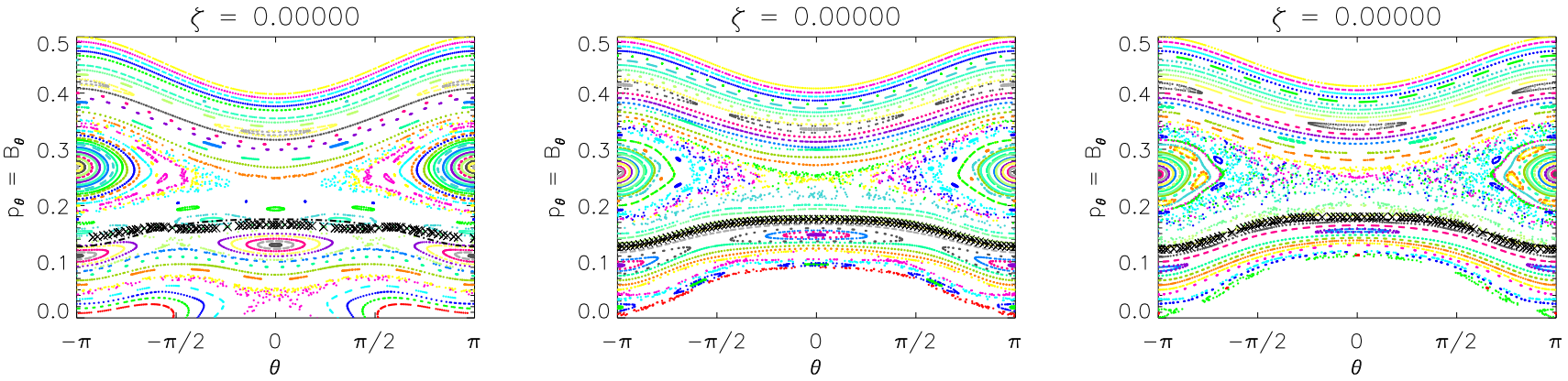

(a) $E = -0.14$. The continued field is critical at this energy.

(b) $E = 0$.

(c) $E = 0.06$. The continuted field is critical at this energy.

Figure 4.7: Poincaré sections of the pressure jump Hamiltonian for an interface defined in Equation (4.3) with $\delta = 0.01061$. `SPEC` was used to calculate the f^- required to ensure the rotational transform of the prescribed field was $\gamma_{[0111]}$. The first and third plots show how `PJH` can identify the energy at which the continued trajectory no longer corresponds to a valid solution.

ing that large pressure discontinuities across SPEC interfaces do make continuation less likely. Inspecting phase space cannot provide many more answers than this, so the next chapter considers the range of parameters for which continuation is possible.

4.2.3 Phase space for different prescribed fields

Figure 4.8 shows Poincaré diagrams for the deformation $\delta = 0.01061$ where each case has the prescribed f^- such that the prescribed field has a different ι_- in each plot. The continued solution is selected as the one whose winding number ι is the same as the prescribed rotational transform.

The prescribed fields have a rotational transform from the following list

- $\gamma_{[0111]}$ (Figure 4.8(a)),
- $\gamma_{[0113]}$ (Figure 4.8(b)),
- $\gamma_{[1211]}$ (Figure 4.8(c)),
- $\gamma_{[1121]}$ (Figure 4.8(d)),
- $\gamma_{[2311]}$ (Figure 4.8(e)),
- $\gamma_{[1132]}$ (Figure 4.8(f)).

The left column of Poincaré diagrams in Figure 4.8 have prescribed fields with rotational transforms that belong to the class of irrationals from the interface $[c, c+1, 1, 1]$ for $c \in \mathbb{N}$. Irrationals in this class approach unity as $c \to \infty$ and as they do they become less noble. Comparing cases of members of this set will allow comparison between irrationals of decreasing irrationality as c increases. The other irrationals in the above list are selected to provide a variety of cases for contrast.

Generally f^- dictates the contours of the $p_\theta(\theta)$ curves. This is because in the trivial case $p_\theta(\theta) = f(\theta, 0)$. However from Figure 4.8 it is clear that different versions of f^- interact with the same deformation to produce quite different chaotic regions. This effect is lost in the simplified system, where the first order approximation to V arising from perturbations in f^- ignored the interaction between the metric (which is a function of the deformation) and the f^-.

4.3 Phase space of flux surfaces

In this case the phase space of flux surfaces extracted from between two interfaces in SPEC is visualised. In contrast to the simplified Hamiltonian earlier in the chapter and the interfaces in the previous section, these flux surfaces are not smoothly deformed.

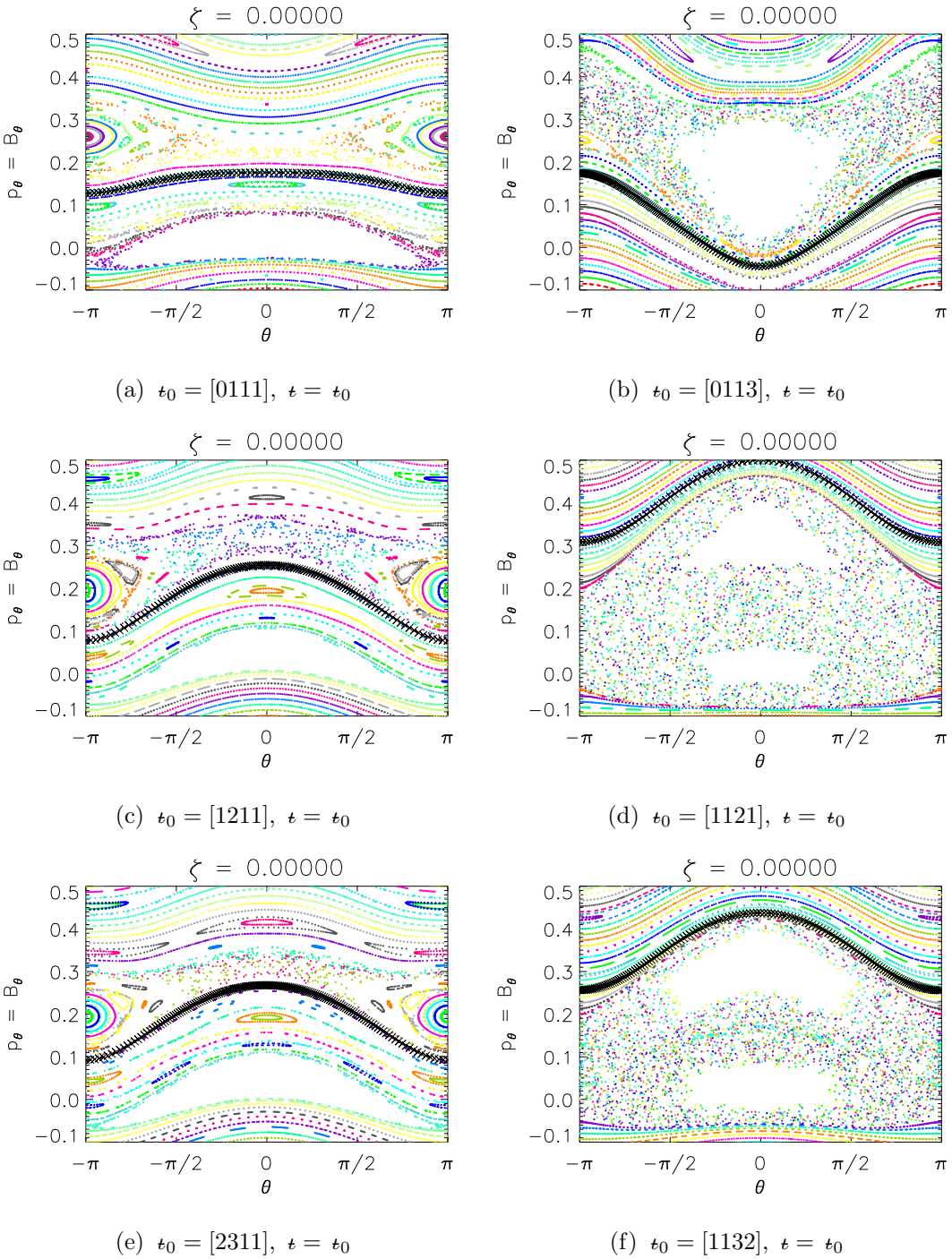

(a) $\iota_0 = [0111]$, $\iota = \iota_0$

(b) $\iota_0 = [0113]$, $\iota = \iota_0$

(c) $\iota_0 = [1211]$, $\iota = \iota_0$

(d) $\iota_0 = [1121]$, $\iota = \iota_0$

(e) $\iota_0 = [2311]$, $\iota = \iota_0$

(f) $\iota_0 = [1132]$, $\iota = \iota_0$

Figure 4.8: Poincaré sections of the pressure jump Hamiltonian system with $\Delta P = 0$ for an interface defined in Equation (4.3) with $\delta = 0.01061$ for prescribed fields of various rotational transform. The continued field is chosen to have a winding number the same as the prescribed transform in each case.

Instead the surface is deformed by the islands and chaotic structures that naturally appear in a plasma region as its outer boundary is deformed. For more information about how these flux surfaces were extracted, and the details of the deformation, see Section 3.4.3.

At the largest deformation ($d = 0.00153$), 60 Fourier terms were found to provide a scan indistinguishable by eye from cases with less truncation Section 3.4.3. The plots in this section were done with 70 Fourier terms.

The three Poincaré diagrams in Figure 4.9 show the effect of the increasing deformation. In contrast to the previous sections, there are fewer and smaller islands. Instead the "contours" of $p_\theta(\theta)$ are very intricate. In contrast to the earlier cases, Figure 4.9 suggests that the small but numerous deformation harmonics result in a complicated and intricate prescribed f^-. In the case of flux surfaces, the phase space is affected by the deformation less through the metric (which the previous cases has shown creates islands and chaos), and more through the prescribed field (which were shown to affect more the contours of the invariant tori).

4.3.1 Effect of changing energy

Figure 4.10(e) shows the effect of changing the energy for the Hamiltonian defined on a extracted flux surface for the case where the outer interface was deformed by $d = 0.00050$. In configuration space, this would correspond to loading a pressure discontinuity across the flux surface that itself lies within the plasma volume.

Destruction comes about mainly through the increasing chaos around the $(1, 0)$ island. As shown in the simplified case, this island is primarily caused by the toroidicity. Perhaps the main determinant of continuation is the aspect ratio. The island suppression and reversal is also present and shown in Figures 4.10(a,b,c).

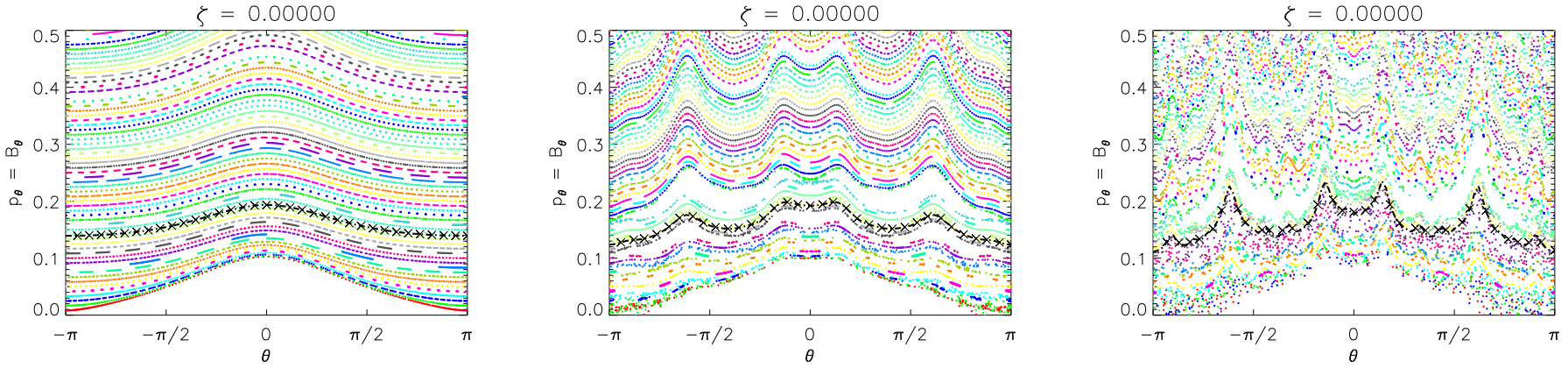

(a) $d = 0.00000$. In this case the inner and outer boundary are axisymmetric and as a result the extracted flux surface is also axisymmetric.

(b) $d = 0.00100$. A deformed outer boundary leads to the flux surface being warped (which generates the islands). The prescribed f^- leads to an intricate $p_\theta(\theta)$.

(c) $d = 0.00153$. This is the last deformation for which `SPEC` could extract the desired rotational transform.

Figure 4.9: Poincaré sections of the pressure jump Hamiltonian for a surface extracted from a `SPEC` volume at $E = 0$. There are less and smaller islands than in the simplified Hamiltonian and the interface cases. Instead the complicated prescribed f^- leads to highly warped invariant tori.

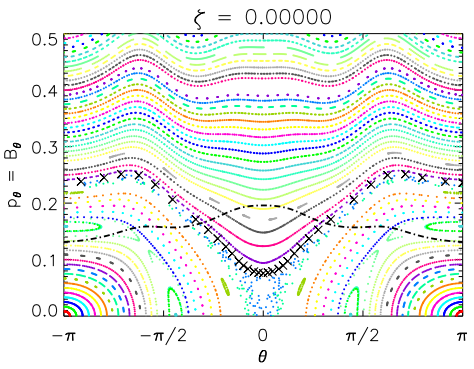

(a) $E = -3.47$. The minimum energy for which the continued field can still be found. It is on the edge of chaos from the $(1, 0)$ island and is critical.

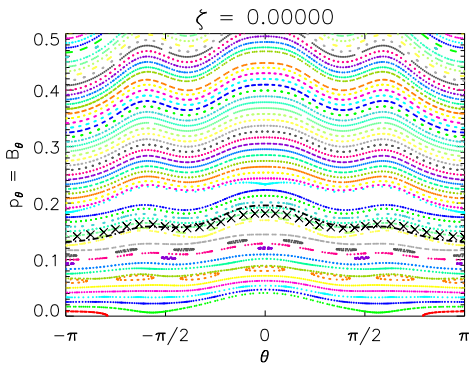

(b) $E = -0.34$. The energy for which the $(1, 0)$ island appears to be most suppressed, akin to the effect noticed in the simplified Hamiltonian system.

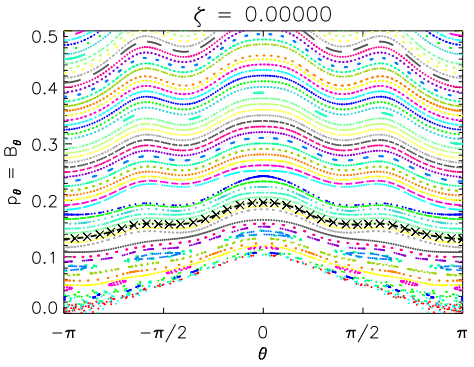

(c) $E = 0$. The trivial continuation of no pressure jump where $< B^2 >=< B_0^2 >$.

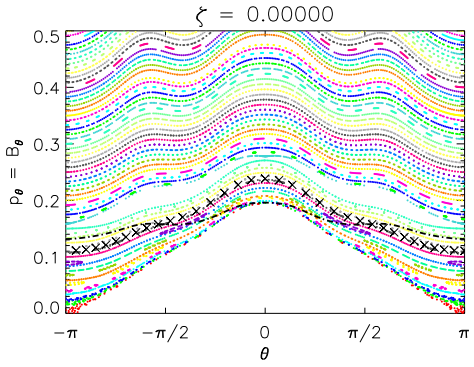

(d) $E = 1.0$. The effect of increasing energy continues. The difference between the prescribed field (dot-dashed line) and the potential field configurations shows the magnitude of the change.

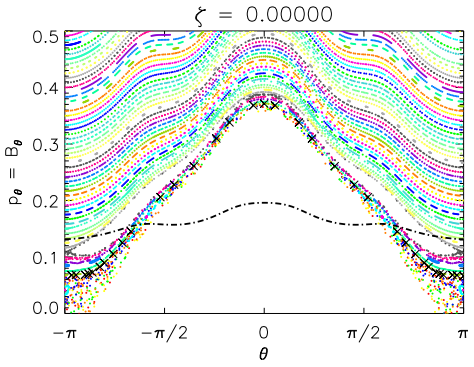

(e) $E = 4.5$. The continued field is just past critical. The chaos causing this criticality mainly comes from the $(1, 0)$ island like in the negative energy case.

Figure 4.10: Poincaré sections of the pressure jump Hamiltonian for a surface extracted from a `SPEC` volume with the outer interface of the volume deformed with $d = 0.00050$. `PJH` can load a pressure discontinuity across this flux surface by setting the energy of the pressure jump Hamiltonian $E \neq 0$.

Chapter 5

Robustness

5.1 Robustness

5.1.1 Concept of robustness

With solutions to the pressure jump Hamiltonian system now calculated, the applicability of the solutions resolved, and a test to determine if such solutions are regular, it is now possible to investigate the conditions of regularity for a given trajectory.

Beyond the concern of how close a given trajectory is to destruction, is the more general question of which trajectories are most resilient to the most number of perturbations. The (global) property of a trajectory to survive under a range of perturbations is referred to as *robustness*, to distinguish it from the (local) property of how close to destruction the trajectory is for a given pressure and deformation, i.e. the trajectory's *resilience*.

To visualise this reliability of a flux surface under all perturbations, this section introduces the concept of a *robustness graph*, which plots the regularity of the pressure jump Hamiltonian trajectory as a function of the perturbations to the system. Such a plot requires an automated test of regularity, described in the next section.

5.2 Determining critical perturbation in an automated way

It will become necessary to determine the regularity of a vast number of trajectories under different perturbations and so an automated test of existence must be used. While most investigations into criticality are concerned with determining an accurate value for the perturbation at which the orbit of interest becomes irregular, this thesis is only concerned with collecting general information regarding the conditions for which the Hamiltonian system gives regular solutions.

An irrational is selected (using the nomenclature in Appendix A.6) by selecting the interval $[p_1q_1p_2q_2]$ for which the noble path gives the irrational number $\gamma_{[0111]}$. The sequence of rational numbers that converge to the noble irrational is $\{\tau_N^{[p_1q_2p_2q_2]} \mid N \to$

$\infty\}$.

Although only the limit of the residues of the infinite series of rational trajectories provides the value of the residue of the irrational trajectory (Section 3.3), it was noted that this limit is usually obvious from a "high enough" convergent. The simplest way to determine the regularity of an irrational orbit is to select a convergent, say the Nth one, then calculate that convergent's residue $r_N(\tau_N^{[p_1q_1p_2q_2]})$ and check that it is small compared to 0.25.[Hud04] It was observed that doing this provided a reasonable and repeatable measure of the existence of the desired irrational. This dovetails with the findings of MacKay where various methods of averaging the residues were tried, but simply considering a close enough convergent was sufficient.[MS92] It has been observed in the simpler systems in which Greene's residue method has been implemented that searching for the N such that $r(N) = 0.25$ gives the quickest measure of criticality for the trajectory with w equal to the golden mean.[Mac86]

MacKay's residue criterion

A more advanced test for the critical perturbation was introduced by MacKay[Mac86] as an extension to Greene's residue criterion. For two convergent orbits with rotational transform $\tau_{N-1}^{[p_1q_2p_2q_2]}$ and $\tau_N^{[p_1q_2p_2q_2]}$, calculate the residues $r(\tau_{N-1}^{[p_1q_2p_2q_2]})$ and $r(\tau_N^{[p_1q_2p_2q_2]})$. Then calculate the quantity

$$\rho_N([p_1q_1p_2q_2]) = \frac{1}{\gamma^2}\ln|r(\tau_N^{[p_1q_2p_2q_2]})| + \frac{1}{\gamma}\ln|r(\tau_{N-1}^{[p_1q_2p_2q_2]})|\,, \tag{5.1}$$

The trajectory is regular if

$$\rho_N([p_1q_1p_2q_2]) \ll \ln(0.2500888)\,. \tag{5.2}$$

This test is referred to as *MacKay's residue criterion*.

In 1994, Paul *et al* compared the above two tests. They investigated the Hamiltonian of the double pendulum because it cannot be written in such a way as to apply perturbation theory to the Hamiltonian, nor can one construct a mapping with which other methods may be applied.[PR94] Their goal was to compare Greene's method to the more theoretically developed MacKay's residue criterion. It was found that MacKay's residue criterion was superior because it did not require long periodic orbits to be followed, though the double pendulum did prove simple enough for Greene's method to "not be inaccurate". The similarity in nature between the double pendulum and the pressure jump Hamiltonian system descrbed in Section 2.4.3 and Section 4.1.1 lend encouragement to the idea that tests based on Greene's residue are appropriate for the pressure jump Hamitlonian. In this thesis we choose to use MacKay's residue criterion based on Paul *et al*'s findings.

5.2.1 Testing the accuracy of the criteria

Although there are similarities, the pressure jump Hamiltonian is more computationally complicated than the double pendulum so we produced a comparison similar to that of Paul *et al.* Figure 5.1 shows the result of the test for the critical perturbation (in this case the critical value of $E^C = \Delta P^C$ as a function of the orbits convergent to the irrational $\iota = \gamma_{[0111]} = 1/\gamma$) for a SPEC interface under the deformation in Equation (3.72). The data points for Greene's residue provide the ΔP for which the residue of the convergent orbit was equal to 0.25. The solution is not accurate at low convergents, but the critical ΔP becomes quite accurate for longer trajectories. The points corresponding to MacKay's residue criterion provide the value of ΔP for which $\rho = \ln(0.2500888)$. The method converges to the same critical perturbation value at a lower convergent in this case, and in all other cases observed.

The difference in Figure 5.1 may not be great, but the difference becomes more pronounced in highly chaotic systems. The more chaotic the system was, the more difficult it was to find convergent orbits with long field lines. MacKay's method can provide accurate results with shorter convergent orbits, but one needs to find *two* shorter orbits.

The decision as to which fixed convergent N' was used was made on a case by case basis, by comparing the robustness graphs using one convergent less $(N'-1)$ and one convergent more $(N'+1)$. If the robustness graph was observed to not be sensitive to the convergent used, then (N') was used. If the robustness graph was sensitive, then the deformation or the prescribed field are too complex for PJH to give reliable results.

For the purposes of this thesis, whose goal is to determine general behaviour, it was found that using the MacKay residue criterion at $N = 6$ would provide accuracies indistinguishable by eye on robustness graphs from the higer convergent tests. In addition the lower convergent curves tended to be smoother, as high convergent trajectory tracing was very difficult and often failed to find the rational convergent. Also the rate at which ρ increased as a critical perturbation (say E) was reached was lower for the lower convergents. Conversely, for long convergents $\rho(\delta)$ approached a step function, making the critical perturbation quite difficult to find.

As a shooting code, `PJH` is especially prone to numerical error during the tracing of long trajectories. This issue tended to *overestimate* irregularity, as numerical errors in following the irrational path would be more likely to deviate from the invariant torus, increasing the trace of the tangent map leading to a larger residue.

In an attempt to sidestep the issue of accuracy brought about by using a shooting code, another version of the code was devised that takes a different approach to calculating the field line. Based on a variational principle, the formulation as-

sumed a piecewise linear field line whose points can be varied to satisfy the pressure jump condition. This formulation, its advantages and disadvantages are outlined in Section 6.3.1.

5.2.2 Problems with the test

At low deformations, it is possible for the energy to be low enough so as not to allow the high rotational transform orbits that would be affected by the $(1,1)$ island. This means that the island does not appear in phase space, so at the point of criticality only the $(1,0)$ is encroaching on the continued irrational orbit. Above the orbit there is no discernible chaos and below there is. If τ_{N-1} is a rational convergent to γ and $\tau_{N-1} > \gamma$, then $\tau_N < \gamma$ and so the residue ${}^{\tau_N}r$ may be large, while ${}^{\tau_{N-1}}r$ will be small. This ruins the convergence of the relied on assumption from Greene's paper that the residues of the convergent rationals with converge to the residue of the irrational. In this case the test was less reliable. This problem was only present at low negative energies and so the robustness graphs to follow are cut off at negative energies, producing a flat bottom at which the this difficulty rendered the results inaccurate.

5.3 The Robustness graph for the simplified pressure jump Hamiltonian system

The simplified system has the perturbative parameters (δ, a, ϵ, F). The following sections explore the robustness of the simplified pressure jump Hamiltonian system under various combinations of these parameters.

5.3.1 Robustness plot for a torus

For $\epsilon = 0.1$ and $F = 0$, Figure 5.2 shows a robustness graph that visualises the regimes in which field continuation in possible, for changing energy and deformation. The two deformations δ and a are set equal to each other to allow one parametrisation of surface deformation.

The plot is a contour plot of $\rho_6([0111])$ with its axes the two perturbations of interest E and $\delta = a$. The brightness of the blue is propotional to ρ_6 with a bright blue colour representing a large negative value of ρ_6, and white representing large positive values of ρ_6. The points at which $\rho_6 = \ln 0.2500888 = -1.38594$ is traced out with a black line that represents at which point the continued trajectory is critical. For situations within the black curve, the continued solution exists, for situations outside, the continued solution does not exist.

Figure 5.2 shows that for zero deformation, an infinite pressure discontinuity is allowed, and, in agreement with Section 4.1.1 there is a minimum negative energy at which the trajectory of the same rotational transform can be found. The MacKay residue criterion experiences difficulties in this area, which causes the perfectly flat sections at the bottom. This difficulty was described in Section 5.2.2.

The point $E = 0$ corresponds to a pressure discontinuity of zero and provides the trivial continuation, where the continued field is equal to the prescribed field. Field continuation is not possible for all deformations, because once $\delta \neq 0$ a rotational transform discontunity occurs. This ι discontinuity comes about because, as mentioned before, a deformation changes $g^{ij} = g^{ij}(\delta)$, but f_0 remains the same. A change in δ modifies the rotational transform of the prescribed field, but the continued field will always have a rotational transform of $\gamma_{[0111]}$ because this is the irrational trajectory searched for.

In Figure 5.2 there is a region of existence pointing out from the otherwise smooth curve for negative energies. This strucure appears often, and will be referred to as a *wisp*, to reflect its appearance. This structure represents a small range of deformations for which the energy may destroy the continued field of interest, but then as the energy is made even more negative the continued field exists again. To visualise what may be happening, Figure 5.3 contains Poincaré diagrams for three points on the robustness graph along the $\delta = 0.031$ line. Figure 5.3(a) shows the continued field for $E = -0.4$ and it is past critical. If the energy is decreased further (making the pressure more different on the continued side than the reference case) the continued trajectories becomes regular again, an example of this is shown in Figure 5.3(b) for $E = -0.58$. Further increasing the pressure to $E = -0.6$ [Figure 5.3(c)] results in the continued trajectory no longer being regular again.

This effect will be referred to as *energy healing* or *pressure healing*, as it results in field configurations coming back into existence as the pressure discontinuity is made larger. It is thought that the poorly–understood interaction between the deformation and the energy combine in such a way so as to suppress chaos near the irrational of interest. In particular the islands above the continued trajectory at $E = -0.58$ look to diminish.

5.3.2 Pressure jumps in the inverse formulation

Selecting a value for the energy at a given deformation and prescribed field determines the pressure discontunity between the prescribed side and the continued side. However from the point of view of the inverse formulation, the prescribed side can be considered to be a reference case, and two continuations [defined by (w_1, E_1) and (w_2, E_2)] can be selected and placed on each side. A simple continuation is the special case where

$(w_1, E_1) = (\iota^-, 0)$. However in the more general inverse formulation two energies can be selected and the pressure jump becomes the difference in the two energies $E_1 - E_2$.

Any two values of energy for which the trajectory exists can be selected. In the case of $d = 0.1$ in Figure 5.2, one can select two energies between the two critical energies E_a^C and E_b^C. The maximum pressure jump allowed is then $\Delta P = E_a^C - E_b^C$, and any jump lower than this is allowed $(-|E_a^C - E_b^C| < \Delta P < |E_a^C - E_b^C|)$.

However, for $d = 0.031$ there are four critical energies $(E_a^C, E_b^C, E_c^C, E_d^C)$ and two ranges of energies that have regular solutions. Selecting energies within these two ranges results in bands of allowed pressure jumps. These bands are discussed further in Section 6.1.3.

5.4 The robustness of MRXMHD interfaces

With MRXMHD in mind, one desires interfaces that would be robust to a range of perturbations. This is especially important in SPEC, as the interfaces need to be able to support pressure discontinuities *and* surface deformations during the optimisation, which will continuously distort and redistribute pressure among the interfaces. For more details on how the SPEC algorithm works, see Section 6.1.2 .

This section contains robustness plots of the unsimplified pressure jump Hamiltonian for interfaces that are smoothly deformed in order to simulate a deformation that may be produced in SPEC.. A more detailed description of this case can be found in Section 3.4.2. All plots were again symmetric about $\delta = 0$, so only the positive values of deformation are shown.

Many types of deformations were investigated, with vastly different robustness plots. Trends were noticed and the plots below were selected to reflect the observed trends.

5.4.1 Truncation

SPEC was used to create the input files to ensure that the prescribed rotational transform was constant under deformations. The input files were generated with $m_{max} = 14$, $n_{max} = 7$ resulting in 218 Fourier terms, all of which were included in the following calculations.

5.4.2 Robustness of an interface

Figure 5.4 shows the robustness plot for a SPEC interface with a prescribed field calculated using SPEC to have a rotational transform of $\iota_0 = \gamma_{[0111]}$. As before, the existence of the continued field with rotational transform $\iota = \iota_0$ is tested by calculating ρ_6 for various values of deformation and energy.

Figure 5.4 suggests that the simplified Hamiltonian does function as a good toy problem as far as robustness is concerned as the plot have the same general behaviour. The major difference is that there are no wisps, though there is a hint at a small wisp for negative energy around $\delta = 0.0157$. Other interface deformations were seen to have wisps, though they are not included for brevity.

The region of existence is cut off at $\delta = 0.02870$, which was the maximum deformation for which `SPEC` could provide the prescribed field. The range of energies at this point is small but non-zero, from which we can infer that the field is likely to exist for deformations larger than `SPEC` could access.

5.4.3 Robustness of interfaces with different rotational transforms

The two robustness plots in Figure 5.5 show two different prescribed fields on the same interface.

Figures 5.4 and 5.5 follow the same exponential behaviour with no wisps. The case with prescribed field $\gamma_{[1211]}$ [Figure 5.5(b)] can maintain a larger pressure jump at lower deformations, but continuation with the prescribed $\gamma_{[0111]}$ is possible for larger deformations. Thus there is no simple way to compare robustness as a whole, as some system specifications can be more resilient than others in different regimes of perturbation.

However in general it was observed that the more irrational the prescribed surface was, the higher the deformation it could withstand. At lower deformations the advantage can reverse, with cases like the prescribed $\gamma_{[1211]}$ [Figure 5.5(b)] capable of being continued across a larger pressure discontinuity at smaller deformations than the more irrational $\gamma_{[0111]}$.

Figure 5.6 shows two more robustness plots with prescribed rotational transforms $\gamma_{[2311]}$ and $\gamma_{[3411]}$ and where $\iota = \iota_0$. One can see that these irrationals (along with the case $\gamma_{[0111]}$ in Figure 5.4) are the noble irrationals for the intervals $[c, c+1, 1, 1]$, $c \in \mathbb{N}$. As c increases, these irrationals become less irrational because their partial fractions get larger as the irrational numbers approach the rational $1/1$. (See Appendix A.6 for more information). Comparing the robustness graphs for all four interfaces shows that in this case decreasing the irrationality of the prescribed field results in a configuration that can withstand higher pressures at very small deformations, but can withstand less of a pressure discontinuity at higher deformations.

Figure 5.5(a) is cut off as `SPEC` had difficulty calculating f^- for this combination of ι_0 and δ. The robustness plot shows that indeed it was close to destruction, as at the maximum available δ, the maximum E is close to zero. However, the critical curve is not symmetric about $E = 0$ at this maximum deformation. It is possible that

the region of existence extends past this maximum deformation, but below $E = 0$. In this regime, $<B^2> \ll <B_0^2>$ meaning the continuation would only be possible if a pressure jump is set up across the interface. This is tantalising evidence that in some cases a pressure discontinuity *allows* a field to be continued across the surface when it would not be possible for a continuous field.

5.4.4 Robustness of interfaces with rotational transform discontinuities

Figure 5.7 shows robustness plots for continued fields of different winding number for the same prescribed field $\gamma_{[0111]}$. The robustness plots are much more intricate in this case, especially Figure 5.7(a), which has wisps in which pressure healing occurs multiple times.

Figures 5.4, 5.7(b), 5.8(a) and 5.8(b) can be compared in the same manner as the prescribed fields were in Section 4.2.3, namely that the contined winding numbers decrease in their irrationality. There is a corresponding decrease in the ability to withstand pressure jumps at high deformation. In fact the maximum deformation at which these discontunitous continued fields exist occur at a negative energy. At these deformations the field requires a pressure discontinuity to allow the jump in rotational transform.

5.5 Robustness of flux surfaces

This section shows a robustness plot for a flux surface that has been extracted from a MRXMHD volume calculated by `SPEC`. For more details about how the flux surface was calculated in `SPEC`, see Section 3.4.3.

5.5.1 Truncation

The flux surface with $\iota = \gamma_{[1213]}$ was extracted for deformations d from zero to 200. `SPEC` used $(m_{max}, n_{max}) = (50, 25)$ resulting in $2,576$ Fourier terms. Figure 5.9 shows the number of Fourier components that must be kept in order to include all Fourier terms greater than W_{min}, as a function of the deformation.

The limit $W_{min} = 10^{-10}$ was sufficient to get accurate residues. The `PJH` code became too slow for more than 700 Fourier components and so results only include the range $d = 0, 0.00150$. This limit also passed the test described in Section 3.3.7 in that 700 Fourier components did not lead to decreased numerical accuracy from the added calculations.

5.5.2 Robustness of flux surface with same continuous rotational transform

Figure 5.10 shows a robustness plot for the extracted flux surface with rotational transform $\gamma_{[1213]}$, the horizontal axis denotes d, the deformation of the outermost boundary which now is a parameter for the destruction of the flux surface. The existence of the continued field configuration is tested using $\rho_6(1213)$ so that the continued field has the same rotational transform.

The robustness plot of the flux surface has a complex structure at negative energy, but for positive energy it has the same exponential like behaviour as has been seen before. Only deformations up to $d = 0.00150$ are shown, although `SPEC` could calculate up to $d = 0.00200$, the Fourier tails for cases higher than $d = 0.00150$ would require too many Fourier terms for `PJH`. The fact that there is still a large range of energies that are allowed suggests that indeed that the surface will likely survive past $d = 0.00150$.

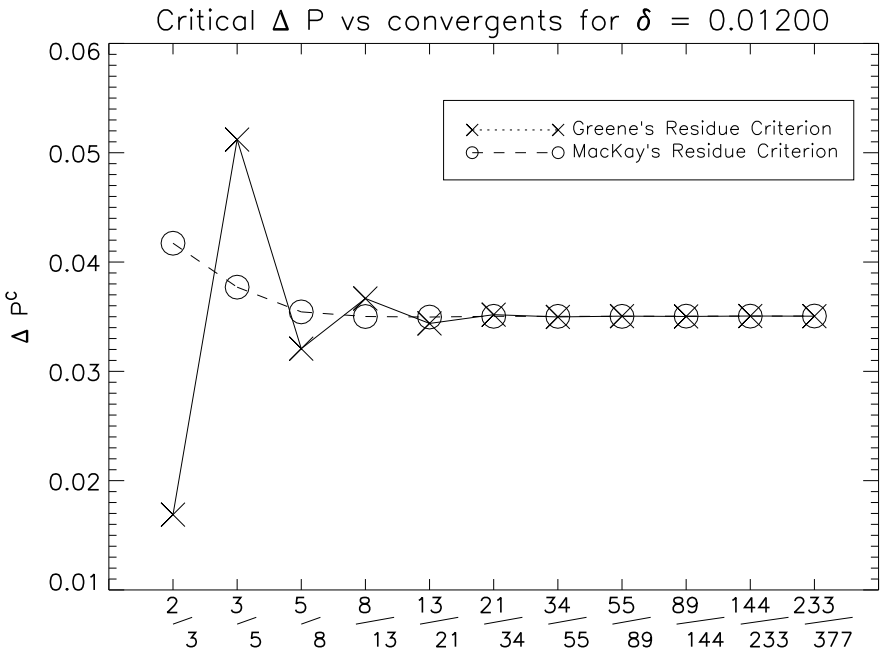

Figure 5.1: The critical energy determined by the Greene's residue test and MacKay's residue criterion as a function of the convergent at which the test is applied. MacKay's test is superior in this case. Low convergent tests using MacKay's criterion tend to overestimate the critical value, but are sufficient if the critical point does not need to be determined precisely.

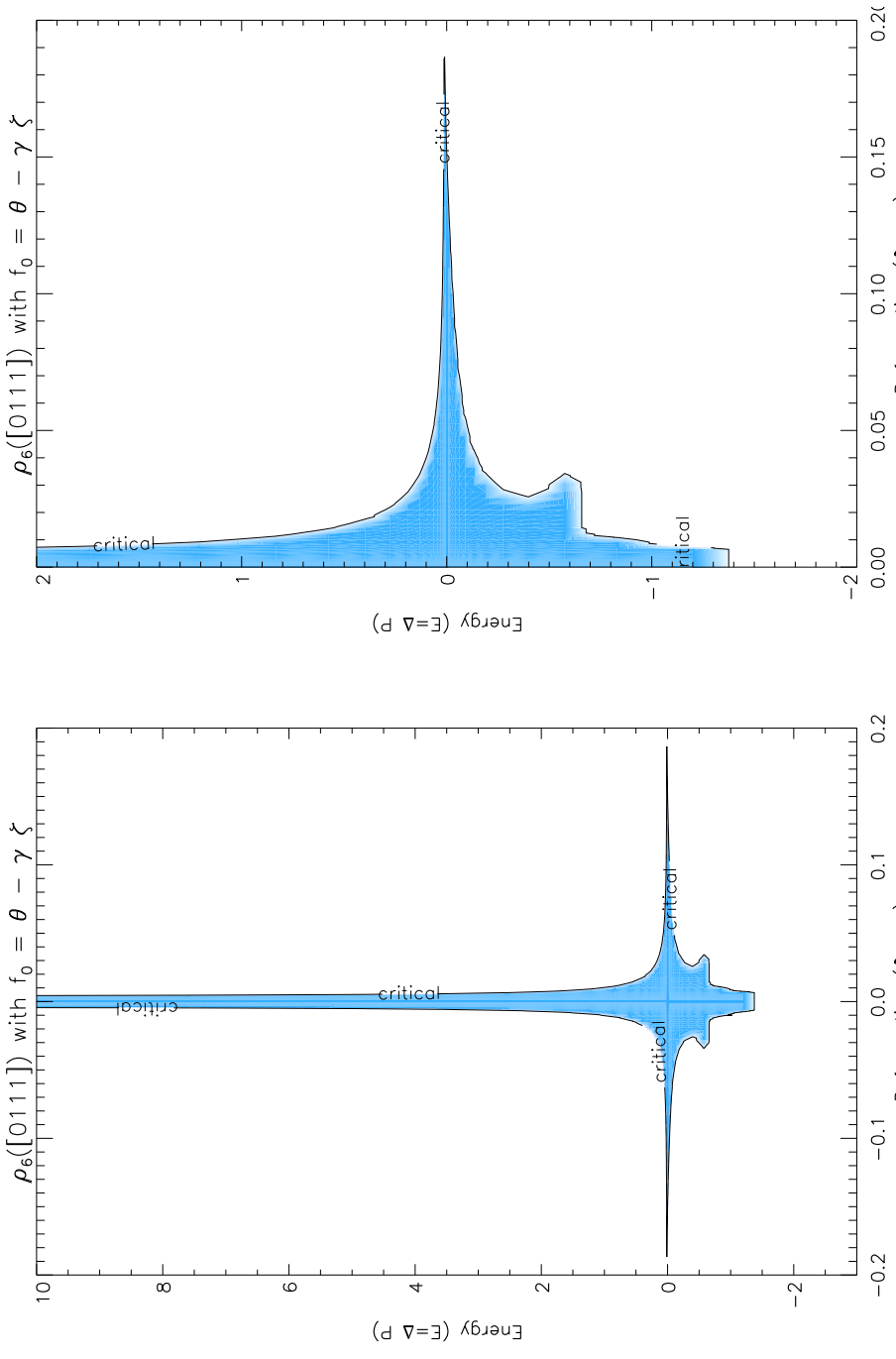

(a) The regime for which the continued trajectory is regular.

(b) A detailed view of the low energy cases, the plot is symmetric in δ and so only one side need be shown.

Figure 5.2: Robustness plots for the simplified Hamiltonian with $\delta = a$ and $\epsilon = 0.1$. This contour plot shows the value of $\rho_6([0111])$ as a function of deformation and energy. The critical line shows the locus of $\rho_6([0111]) = \ln 0.2500888$, and shows where the continued field can be assumed to be critical.

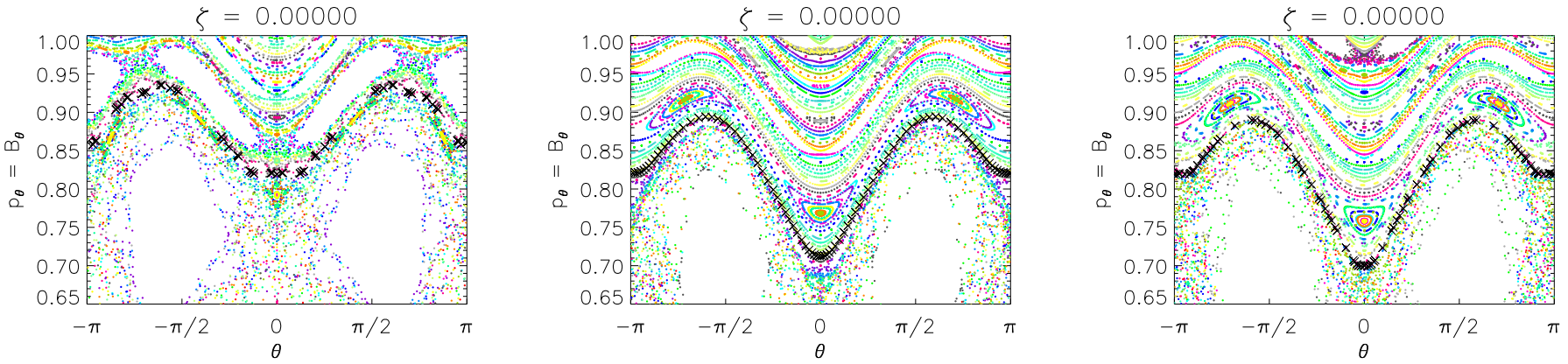

(a) $E = -0.4$. The continued field does not exist.

(b) $E = -0.58$. The continued field exists again, despite the energy decreasing (despite the pressure jump becoming larger).

(c) $E = -0.60$. The continued field is destroyed again, and remains destroyed for all $E < -0.6$.

Figure 5.3: Poincaré sections taken along the $\delta = 0.031$ line, at three negative and decreasing energies. At $E = -0.4$, the continued field is destroyed, but exists again at $E = -0.58$, then is destroyed again at $E = -0.6$.

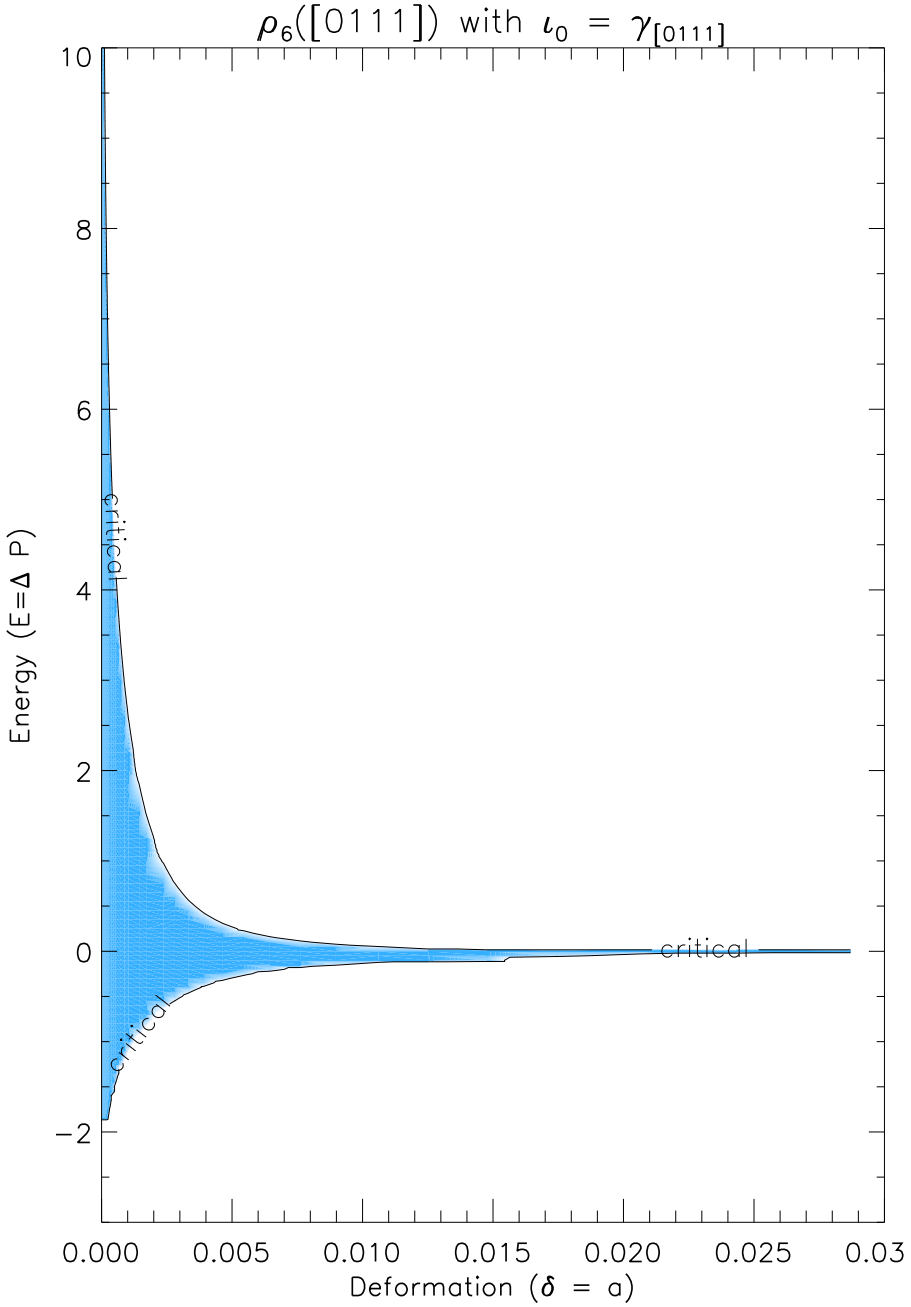

Figure 5.4: Robustness plot for a `SPEC` interface with prescribed field $\iota_0 = \gamma_{[0111]}$ and continued field $\iota = \iota_0$ tested by calculating ρ_6. The overall behaviour of the plot is similar to the simplified system, with an exponential–like decrease in energy allowed for increasing deformations. Note in this case there are no regions of healing.

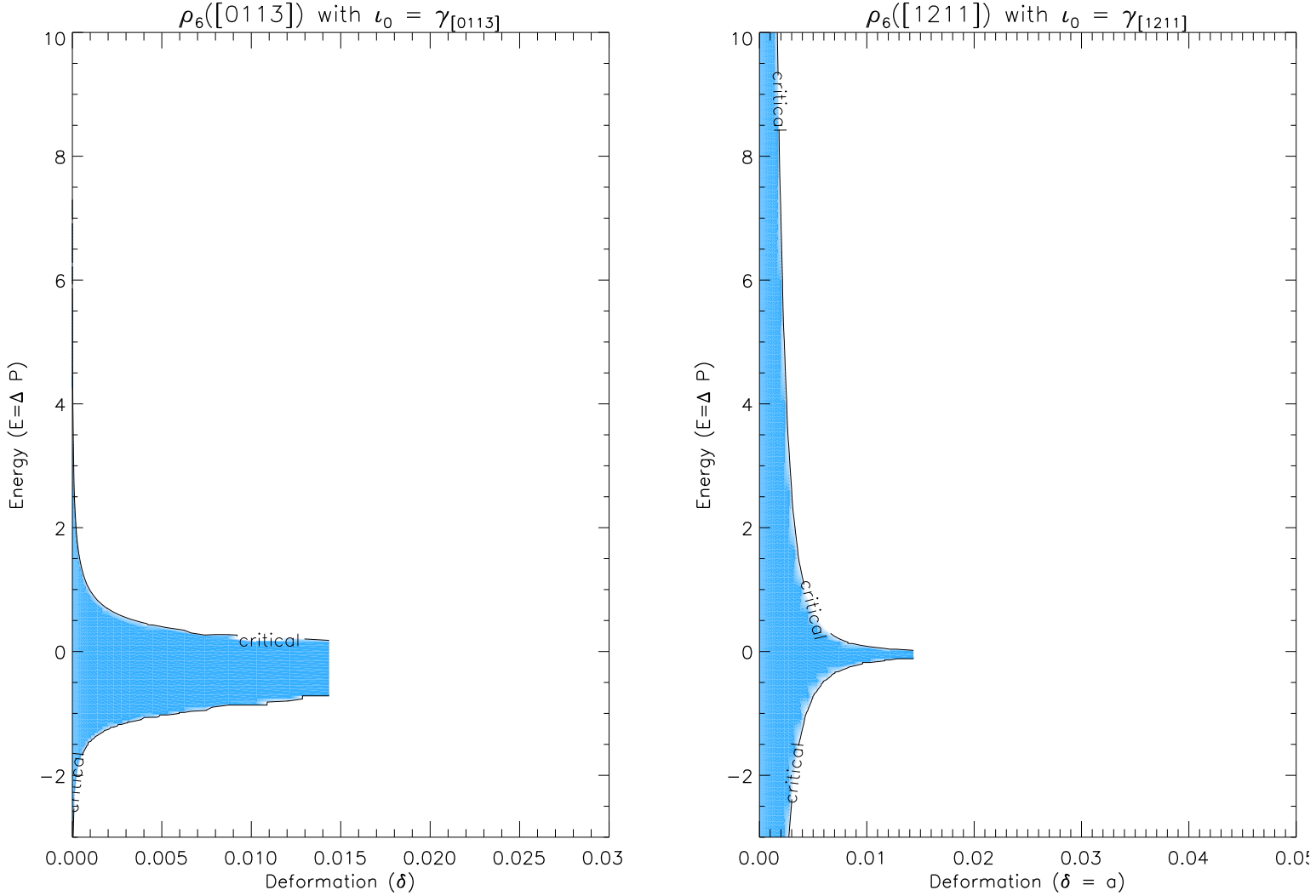

(a) Robustness plot for an interface with prescribed field $\iota_0 = \gamma_{[0113]}$. The continued field $\iota = \iota_0$.

(b) Robustness plot for an interface with prescribed field $\iota_0 = \gamma_{[1211]}$. The continued field $\iota = \iota_0$.

Figure 5.5: The two robustness plots give an idea of how different rotational transforms prescribed on the same surfaces can have different robustness properies.

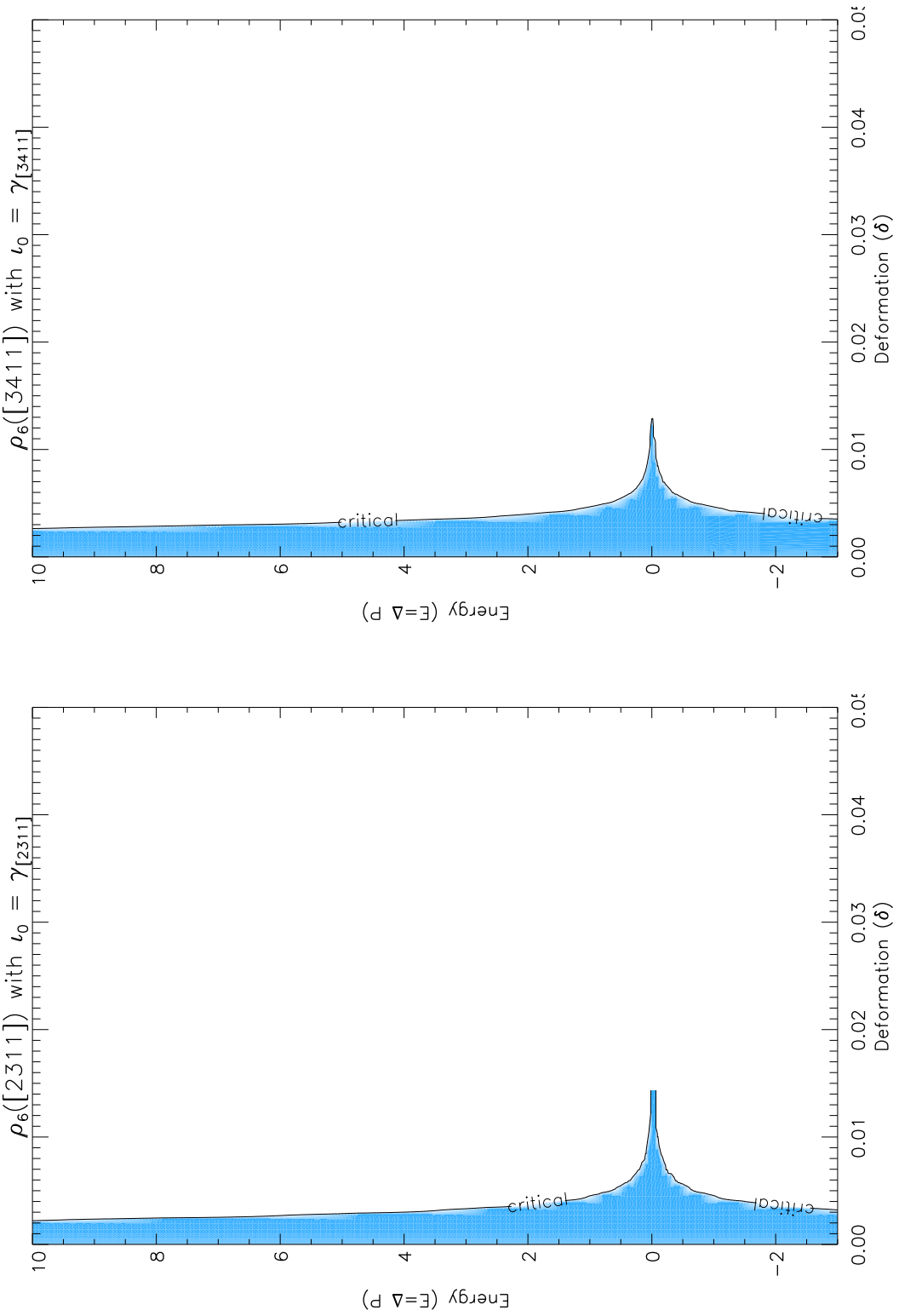

(a) Robustness plot for an interface with prescribed field $\iota_0 = \gamma_{[2311]}$. The continued field is $\iota = \iota_0$.

(b) Robustness plot for an interface with prescribed field $\iota_0 = \gamma_{[3411]}$. The continued field is $\iota = \iota_0$.

Figure 5.6: The two robustness plots are of situations with prescribed field of differing irrationaliy. The more irrational, the more presure at higher deformation it can withstand, however the less irrational field configurations can withstand higher pressure jumps at low deformations.

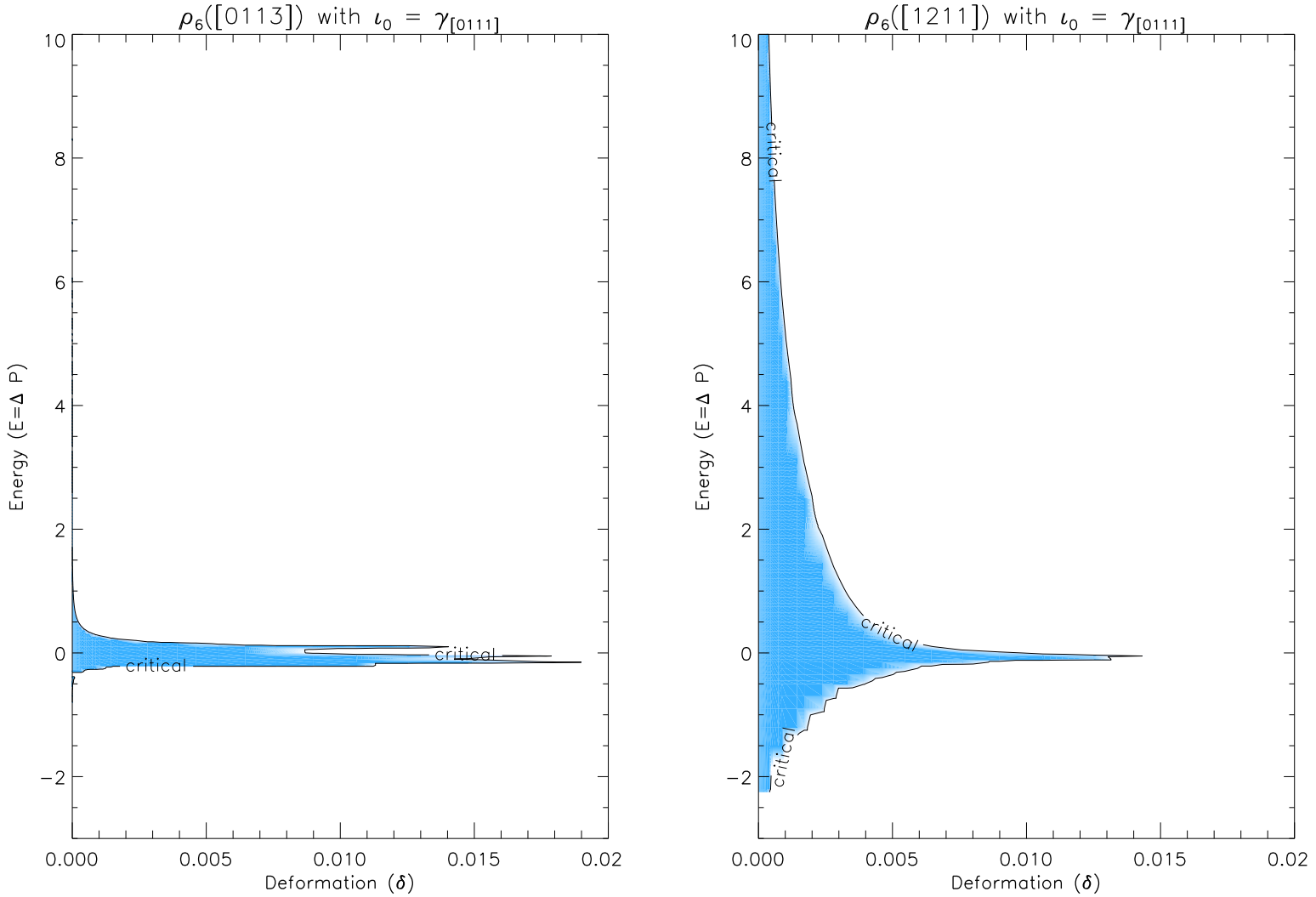

(a) Robustness plot for an interface with prescribed field $\iota_0 = \gamma_{[0111]}$. The continued field is $\iota = \gamma_{[0113]}$

(b) Robustness plot for an interface with prescribed field $\iota_0 = \gamma_{[0111]}$. The continued field is $\iota = \gamma_{[1211]}$.

Figure 5.7: Robustness plots for SPEC interface with rotational transform jumps

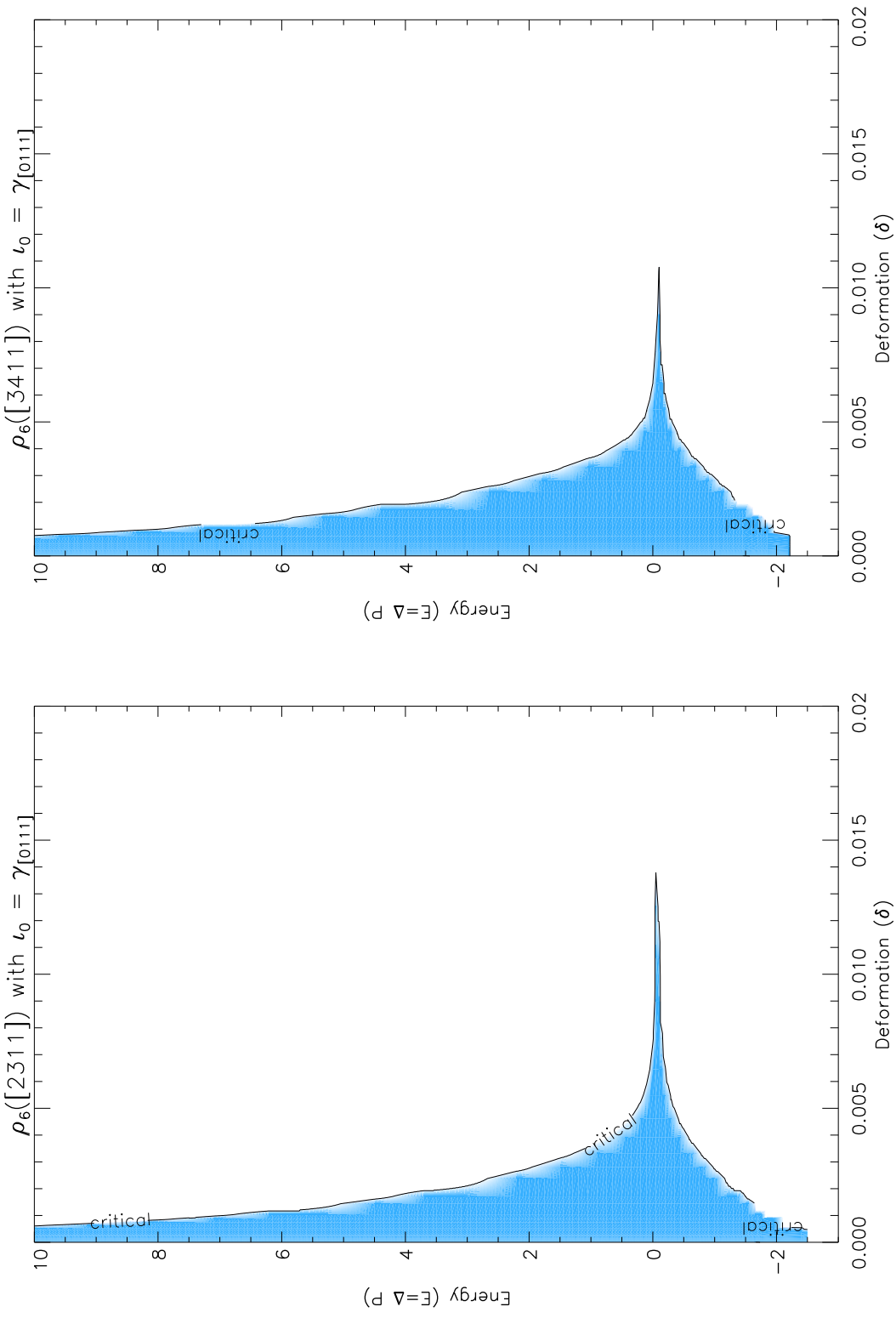

(a) Robustness plot for an interface with prescribed field $\iota_0 = \gamma_{[0111]}$. The continued field is $\iota = \gamma_{[2311]}$.

(b) Robustness plot for an interface with prescribed field $\iota_0 = \gamma_{[0111]}$. The continued field is $\iota = \gamma_{[3411]}$.

Figure 5.8: Robustness plots for SPECinterface with rotational transform jumps

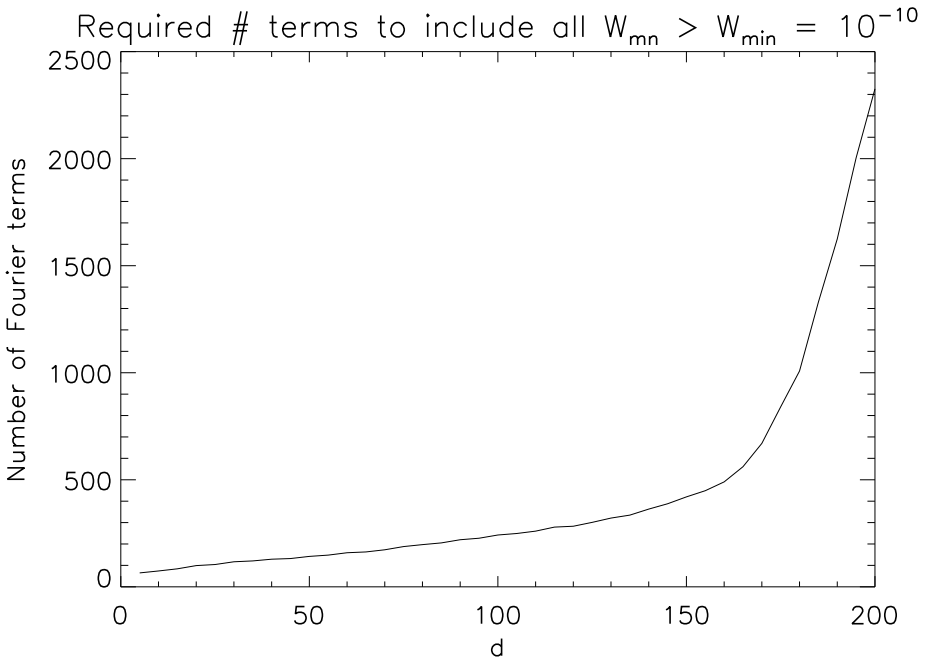

Figure 5.9: The number of Fourier component triplets (R_{mn}, Z_{mn}, f_{mn}) whose size measure W_{mn} have a value larger than $W_{min} = 10^{-10}$. W_{min} was observed to be a good minimum limit for which the residues behaved as expected.

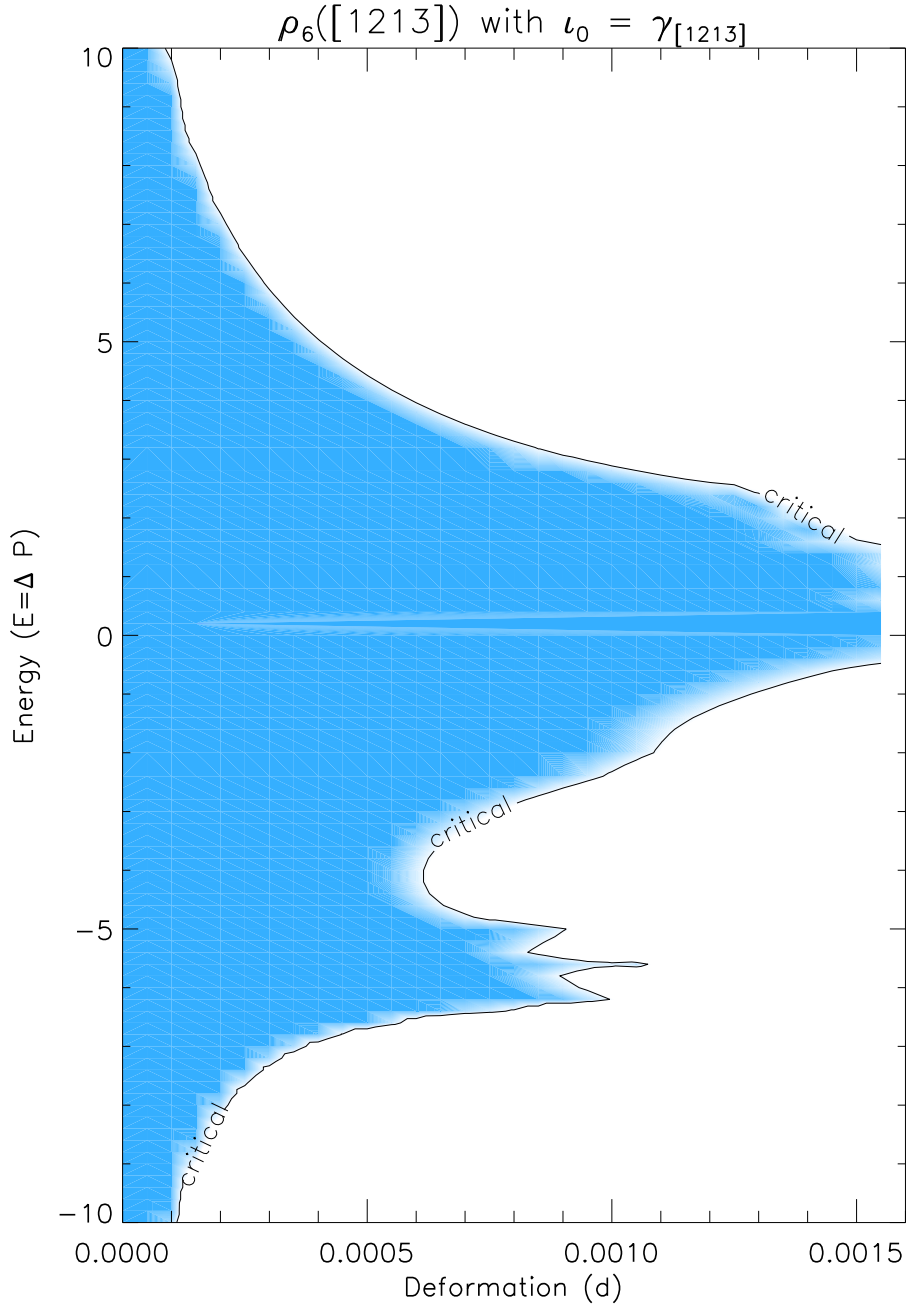

Figure 5.10: The robustness graph for a flux surface that is being warped by the appearance of islands and chaos in the plasma volume. There are many more wisps, stemming from the additional harmonics present in this more complicated case.

Chapter 6

Implications and future work

6.1 Implications for SPEC and MRXMHD

6.1.1 Original motivation of thesis

The original motivation that led to the work in this thesis was the need to understand the nature of flux surfaces withstanding pressure jumps for the purposes of both the `SPEC` code and to inform the MRXMHD formulation.

Throughout this section the pressure jump Hamiltonian will be considered in the context of the entire plasma volume. As a result two Hamiltonian systems and therefore two different sources of chaos will be discussed. See Appendix A.4 for more information about the differences between the two systems. The reader must keep in mind that the pressure jump Hamiltonian can only be defined on each flux surface, and the trajectories determine whether the field can be connected across the pressure discontinuity, whereas the magnetic field line Hamiltonian is defined in the entire volume, and the trajectories are the field lines and determine make up equilibrium field. The trajectories of each Hamiltonian must agree on the two sides of each interface.

6.1.2 How SPEC works

As mentioned earlier, `SPEC` considers the fusion plasma to contain a set of interfaces which represent assumed-to-exist nested flux surfaces $\mathcal{S}_l$ each defined by a rotational transform ι_l, where $l \in \mathbb{Z}$, $l = 0, N$ where N is the outermost boundary and $l = 0$ gives the magnetic axis. These surfaces are then used as boundaries for a modified Taylor relaxation to determine the Beltrami field between each of the flux surfaces.[HHD07] This modified Taylor relaxation shows that there is a constant pressure within each volume. As a result all the pressure changes occur on the interfaces and thus there is a discontinuity in the pressure at each of the flux surfaces.

In general, after the relaxation, the Beltrami field calculated in each volume will not necessarily satisfy force balance on each of the surfaces $\mathcal{S}_l$. The next step then is to warp the boundaries (by modifying the quantities R_{mn}, Z_{mn}) to match force balance. Of course, this will change the prescribed fields on the interfaces that act

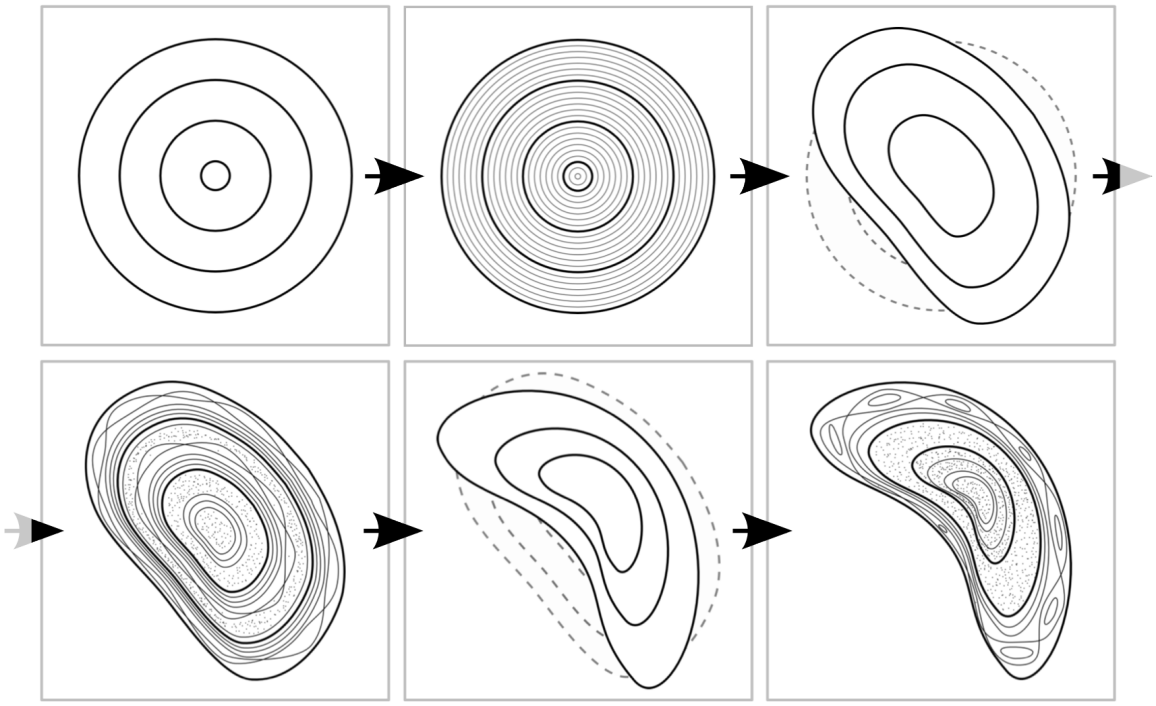

Figure 6.1: A stylised version of the principles by which SPEC works. One solves for the Beltrami field in the volumes between a set of flux surfaces set as interfaces. Then one modifies the shape of the flux surfaces to satisfy force balance. This changes the boundary conditions for the calculation of the Beltrami field, which must be repeated. This iteration convergences to the equilibrium field.

as boundaries for the internal Beltrami field. Thus the Beltrami field will need to be recalculated with the new boundaries. This process is iterated until force balance is satisfied at which point the union of the resultant Beltrami fields gives the equilibrium field. Figure 6.1 shows a stylised illustration of the algorithm.

However, there is an assumption that the iteration will converge with a set of smooth interfaces consistent with force balance. Whether this is true was not clear and indeed the basic nature of pressure discontinuous flux surface was not clear. This led to the formulation of the pressure jump Hamiltonian system and consequently the PJH code. The pressure jump Hamiltonian system gives a necessary condition for such convergence in SPEC. Since work started on this thesis, convergence testing has been done with SPEC with promising results.[HDHM12] The PJH code complements these findings by utilising Hamiltonian theory to explore the domains over which the necessary condition of force balance holds. The computational results of the previous chapters provide evidence to the following findings relevant to the progression of SPEC.

6.1.3 Results that have implications for SPEC and MRXMHD

There is a Hamiltonian formulation for internal flux surfaces

The pressure jump Hamiltonian system derived in Section 2.3 is a generalisation of the Hamiltonian formulation of force balance on the last closed flux surface proposed originally by Berk *et al*[BFL+86] to force balance on a flux surface residing inside the plasma.

Results from the pressure jump Hamiltonian do map homeomorphically back to configuration space

Using the Birkhoff theorem in Section 2.3.6 it was shown that trajectories map homeomorphically to field lines on the surface, and the winding number of the trajectories is conserved so that it is equal to the rotational transform of the resulting field line.

The simplified Hamiltonian is suitable as a toy problem

The simplified version of the pressure jump Hamiltonian reduces the number of harmonics present in the Hamiltonian and results in a system in which the effect of each perturbation can be identified. The system was shown to have the same general behaviour as the original problem, though its simplifications are too strong for it to make any predictions about realistic cases.

The conservation of the rotational transform is in principle possible, but the attempt made in this thesis was not successful. It may be that the conservation results in many f components, which would defeat the purpose of the simplified model. Despite this the simplified Hamiltonian was helpful in explaining the effects of the perturbations of the system.

The simplified Hamiltonian is an interesting Hamiltonian in its own right. It is easily visualised and provides multiple perturbative parameters.

Flux surfaces may be destroyed during warping

The statement here that flux surfaces may be destroyed during warping may seem obvious from the KAM theorem. However the "smooth and small" perturbations that ensure some tori persist within JAM theory, can not easily be identified with the perturbations to the pressure jump Hamiltonian (g^{ij}, f^-). That is it is not clear how a modification of the geometry of a flux surface can be designed so that it is "smooth and small" enough to ensure that force balance is still possible.

Currently, `SPEC` uses a steepest descent method to warp the surfaces. In this case the Fourier components of the shape of the surface are modified to reduce the discrepancy in the pressure jump condition from zero in the least steps possible. The

numerical investigation of this thesis suggests that it may be important to apply a constraint of smoothness to the steepest descent algorithm, lest the algorithm sharply warp the flux surface and make force balance impossible. SPEC's behaviour in such a situation is not well understood. We suspect that convergence will become difficult if no solution is possible for the pressure jump and rotational transform prescribed. In this case it may be necessary to re-start the calculation with other prescribed boundaries that are more likely to persist.

There is another advantage to a smoothness constraint on the flux surfaces during the iterations and that is purely computational. The more Fourier components required, the more computational time is needed to perform any calculations. Computation time is extremely sensitive to the number of Fourier components as the corresponding Fourier series often appear as convolutions or as quadratic quantities in the SPEC code.

Higher pressure jumps tend to destroy flux surfaces

It was shown that, in general there is a maximum pressure jump for which continuation is possible for a given reference field. In some cases though, increasing the pressure jump further past the point at which it can no longer be continued resulted in the continuation becoming possible again for a small range of larger pressures. These appeared as "wisps" in the robustness plot and seemed to be more likely to be present in situations where the deformation had many Fourier components (i.e. complex geometries).

From the perspective of the inverse formulation, the results show that the maximum pressure discontinuity (maximum difference between the average of the squares of the fields) in general becomes smaller as the surfaces are warped. The existence of wisps shows that the decrease is not smooth. Indeed, as one is free to select any two continuations from the reference case, wisps correspond to *energy bands* for which the inverse problem may be solved. These bands have an analogue in quantum mechanics as *Brillouin zones*, and in the pressure jump Hamiltonian problem the width of these bands correspond to the maximum pressure jump that is allowed for force balance to be satisfied.

The rotational transform of the surfaces should be kept constant during their deformation

It has been shown that the resilience of flux surfaces is highly sensitive to their rotational transform, as implied by the KAM theorem. As SPEC relies on the existence of the flux surfaces during deformation, it is important to maintain ι on $\mathcal{S}$ otherwise the interfaces will become a different flux surface with a different robustness profile.

The requirement that ι be kept constant under deformation of the interface, however, is theoretically inconsistent with Helicity conservation. One possible solution to this problem is to slightly relax one of the other constraints in Equation (2.8) (mass, entropy or helicity conservation) to allow more freedom in the deformation. The problem of helicity *and* rotational transform conservation has been noted as a difficulty since the early development of `SPEC`[HHD07] and remains unsolved[HDHM12].

Rotational transform of flux surfaces should be strongly irrational

One of the issues with an equilibrium code like `SPEC` is that one is trying to determine the chaotic structure of a Hamiltonian system (the field line Hamiltonian, see Appendix A.4) that is highly perturbed to begin with. This is different from other systems in which one may start with an unperturbed, smooth system and perturb it to determine information about its nature (an investigation of this form allows one to appeal to the KAM theory). When applying `SPEC` one is confronted with an unknown and highly chaotic system and needs to somehow determine which flux surfaces exist so that one can use these flux surfaces as interfaces (and thus for this task we cannot use the KAM theory). It is important then to have a method to determine which flux surfaces should be prescribed that would 1) exist and 2) continue to exist under perturbations.

The KAM theory does however answer part 2), as it has proved the most irrational are most likely to survive smooth and small perturbations. As it was shown that the winding number of Hamiltonian trajectories is conserved during the mapping to a field line on the surface, the KAM result that the most-likely-to-persist-invariant tori are irrational can itself be mapped to configuration space to imply that flux surfaces with irrational rotational transform are the most robust to sufficiently smooth and small perturbations.

In general it was observed that the more irrational the continued field, the higher the deformation it could survive. The effect of energy was less obvious and it was possible for less irrational continued fields to be continued across larger pressure discontinuities for small deformations. This suggests that pressure jumps should be portioned amongst interfaces depending on the irrationality of the field either side. Though just how to do this is not clear. The results in this thesis suggest that highly deformed surfaces are likely only to exist if they are highly irrational, and in that case only a small pressure discontinuity could be loaded on that interface. For less deformed surfaces the situation is less clear, as rotational transforms of less irrationality may hold more pressure at low deformations. Further work is required to clarify this.

Greene's residue can be utilised to predict imminent destruction

Before a force balance iteration of SPEC, it would be desirable to know whether force balance is possible at all. As mentioned in Section 6.1.3, SPEC would likely have difficulty converging if force balance is not possible and this would only be apparent with a convergence test that would check how force balance is satisfied as more Fourier components are included. However we have provided evidence that Greene's reside could be used to check if force balance can be satisfied without the need for a convergence test.

It would likely be beneficial to include a more specialised version of PJH as a module in SPEC that can monitor the flux surfaces by following the field lines and computing Greene's residue. This would allow SPEC to adapt its algorithm to ensure it is not wasting time attempting to satisfy force balance when its solution is not possible. Further, in situations similar to Figure 5.5(b), a scan of Greene's residue for various perturbations will provide a domain of pertubrations to g^{ij}, f^- and ΔP that are allowed, allowing SPEC to change the pressure and find a solution.

However, the use of PJH in SPEC is not the most efficient way to determine the closeness of a flux surface to destruction. This is because PJH is highly computationally intensive and uses a shooting method. While SPEC has the capability to follow orbits, it uses a variational approach on the Fourier decomposition of the 3D magnetic field $B(\theta, \zeta, s)$ when calculating the equilibrium field. This means that when SPEC considers the flux surfaces, it considers not the field lines, but the two dimensional magnetic field $B(\theta, \zeta; s_l)$ and by extension the surface potential $f_l(\theta, \zeta)$. All the information about the magnetic field is contained in f_l, and so following the field lines would be wasted computation. Instead one could either 1) adapt PJH to use a variational principle (see Section 6.3.1 for the issues with this) or calculate some other quantification of resilience directly from f (see Section 6.4.2 for suggestions in this vein).

Multiple pressure jumps can be applied across a given surface

Most discussion so far has assumed that one can load whatever pressure one desires on each interface. Surely though there must be some constraint that determines how much of a pressure discontinuity should be loaded. One suggestion has been that every surface has a pressure discontinuity such that it is critical. However the energy healing observed in Chapter 5 shows that this is not unique, as the critical line can be multi-valued for a given deformation.

While there is some ambiguity, the results also showed that in general the pressure jumps should be kept small.

6.1.4 Suggestions for SPEC code

Listed here is a summary of possible modifications to SPEC that the pressure jump Hamiltonian formulation investigation has suggested may help its accuracy and stability.

1. Ensure the interfaces have a highly irrational (noble) ι.
2. Apply a smoothness constraint to the descent algorithm that modifies the Fourier coefficients of the prescribed surfaces to satisfy the pressure jump condition.
3. The PJH code can be inserted into SPEC as a diagnostic tool to ensure not just that the invariant torus exists, but that it is not close to destruction. A more elegant improvement in this vein would be to calculate a quantity such as the analyticity width directly from $f(\theta, \zeta)$ (See Section 6.4.2).
4. Using one side of the interface as the reference case, the inverse formulation allows one to test both sides of the surface at the same time, the iteration in which the surfaces are warped may benefit from this formulation.
5. The conservation of the rotational transform of the interfaces is important, and so a modification to the relaxation formulation that ensures this is the case during modification of the boundaries is suggested. Perhaps allowing small leakages of ideally conserved quantities through the flux surface during deformation may allow this to occur.

6.2 Other uses for PJH

6.2.1 Used to investigate high–n stability of flux surfaces

The PJH code has already been used to further research on the nature of flux surfaces in the MRXMHD formulation in a manner that was not originally intended when it was formulated. In 2010 Barmaz used PJH to aid in their investigation the high–n stability of flux surfaces with pressure discontinuities.[Bar11]

This work investigated the question how stable flux surfaces are to displacements of the interface when the surfaces held a pressure discontinuity. While this thesis asks questions about whether flux surfaces exist or are likely to exist by making the first variation of the MHD energy vanish, this complementary MHD stability investigation asks how stable the surfaces are to deformations using the second variation of the MHD energy.

The work of Barmaz[Bar11] generalised a stability treatment of Bernstein *et al*[BFKK58] of an interface with a vacuum magnetic field on one side. Barmaz generalised it to

the situation of a flux surface with a plasma either side. This is analagous to the generalisation of the pressure discontinuity condition of Berk *et al* to the more general plasma–plasma boundary derived in this thesis.

First Barmaz determined that a flux surface in a plasma at equilibrium is stable to deformations unless there are points of zero shear (where $\boldsymbol{B}^- \parallel \boldsymbol{B}^+$). Axisymmetric surfaces can have zero shear everywhere, but for a three dimensionally deformed surface it can be the case that there are lines (or points, though they are very rare) in which the inner field is parallel to the outer field and thus susceptible to instability under further deformation.

To investigate these instabilities, Barmaz was able to run `PJH` and identify lines of zero shear. In these neighbourhoods the results from `PJH` could be inserted into the energy variation equation to compare the interaction between curvature and the stability of the surface. From this it was determined that a high curvature in the low magnetic shear region can keep the surface stable while undergoing geometric deformation.

6.3 Suggested improvements and extensions to the PJH code

6.3.1 Use of a variational integrator

In order to address issues that arise from using a shooting code for finding periodic orbits, work was done toward a variational version of the code. Given a Hamiltonian system, one can construct the discrete Lagrangian which solves the Hamilton-Jacobi equation exactly and this discrete Lagrangian can be solved for an exact solution.[MW01] Such a method is superior to the shooting method for finding trajectories of certain winding numbers because the boundary conditions of the configuration variables set the rotational transform and so a search is not required. Variational integrators also avoid the problem that shooting codes face, in which the problem becomes stiff for long orbits, especially those orbits with high Lyapunov number.[Jac91]

Using the pressure jump Hamiltonian Equation (2.22), one can assume a pointwise-linear magnetic field line consisting of θ and p_θ values at certain points of ζ, so $(\theta, p_\theta) = [\theta(\zeta_i), p_\theta(\zeta_i)]$ for $i \in \mathbb{Z}$, $i = 0, N$ with $\zeta_0 = 0$ and $\zeta_N = 2\pi$. The momentum is periodic so $p_\theta(\zeta_N) = p_\theta(0)$. The initial values for the functions were set to

$$\theta(\zeta_i) = \iota\zeta_i \ , \tag{6.1}$$

$$p_\theta(\zeta_i) = f(\iota\zeta_i, \zeta_i) \ . \tag{6.2}$$

Care would need to be taken with trajectories with high winding numbers as it

these trajectories would require more points, though a swap to θ as the independent variable for trajectories with $\iota = 1$ would remedy this problem. As would the fundamental long Fourier tails difficulties finding orbits near criticality. The difficulty of resolving orbits near criticality will still be present as more and more Fourier terms are required in this domain.

However the biggest difficulty in using a variational method is the determination of Greene's residue. Variational equivalents of the residue criterion can be found in the Lagrangian-derived method of Meiss and MacKay.[MM83] However for more than one dimension the expression becomes very complicated involving determinants of determinants. The author's conversations with MacKay suggested that a higher-dimensional solution is in principle possible, but the determination of its form proved too difficult.

There is an alternative expression for a variational measure like Greene's residue in Bountis' PhD thesis.[Bou78] However it came to our attention too late for this thesis.

6.4 Suggested future work

6.4.1 Further investigate energy healing

If the precise mechanism for energy healing could be determined, it may provide methods for which the phenomenon could be avoided (perhaps by constraining how the interfaces are warped) or exploited (allowing access to larger pressure jumps).

6.4.2 Use of analyticity width to quantify resilience

Resilience information in residue curves

The limit of the residue curve implies the nature of the Hamiltonian trajectory, however there is more information in the residue curves than simply a litmus determination of regular/not regular. Consider Figure 6.2, which shows the residue curves of a certain irrational trajectory at various stages of increasing deformation of the flux surface. Note that all residue curves limit to zero, so at each of the deformations the field line configuration satisfies the pressure jump condition. However, as the deformation increases the number of convergents required before the curve can be confidently said to be limiting to zero also increases, which is reflected in a slower approach of the curve to zero in the graphs.

This correlation between residue decay rate and how close the trajectory is to being not regular has been observed and commented on before.[Gre79][SK81][Mac92]

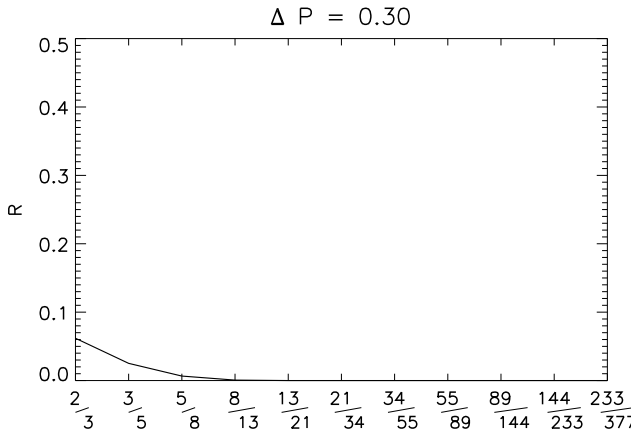

(a) The residue curve for $\Delta P = 0.3$.

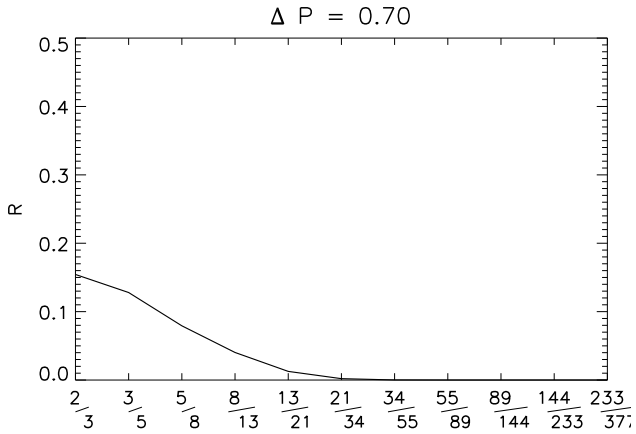

(b) The residue curve for $\Delta P = 0.7$.

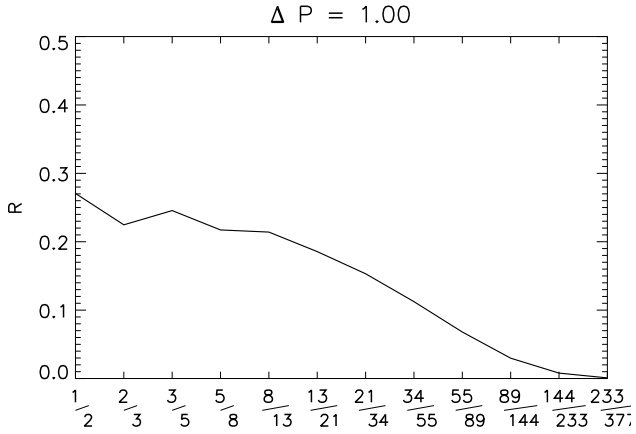

(c) The residue curve for $\Delta P = 1.0$.

Figure 6.2: At each of these pressures the trajectory is regular, but the residue takes longer to converge to zero. Thes are taken from the simplified Hamiltonian with perturbation $(\delta, a, \epsilon, F) = (0.01, 0.01, 0.1, 0)$.

Some of these papers suggested quantifications of the residue decay rate which are investigated in Section 6.4.3.

This thesis submits that this information can be used to determine how resilient the field line configuration is. Further, the *analyticity width* is identified as a quantification of resilience.

Analyticity width

The *analyticity width* is a measure of how "difficult" the transformation to action angle coordinates is. This would amount to a method of quantifying how close a surface is to destruction. Such a quantity would provide a measure of resilience, allowing one to ignore the specific sensitivities to certain perturbations caused by the changes in the Hamiltonian system specification. That is, there would be no need for a multi-parameter robustness investigation, instead the analyticity width a could be used as a single measure of closeness to destruction. The practical use of the analyticity width in this manner was first suggested by Stuart Hudson in a private conversation and has since been discussed with Robert MacKay, leading to the following findings.

Definition of analyticity width

In Section 3.2.4 it was shown how the ability to make a transformation to straight field line coordinates determines whether the trajectory is chaotic or not. However, while the transformation is either possible or not, it is possible to extract a measure of how close the transformation is to being impossible.

In Arnol'd 's proof of the KAM theorem he proves that, when the invariant torus is written parametrically as a function of the action-angle variables, the invariant torus is analytic within a complex band of the real axis.[GP81] So that not only can a transformation to action angle coordinates be defined, but such a transformation can be done in a finite region into the complex plane.

To be more precise, a solution to a Hamiltonian system can be written as the mapping

$$\theta \mapsto M\theta \ , \tag{6.3}$$

as the mapping brings the trajectory back to where it started, M is then a periodic mapping. The mapping can be written in general form as[DM92]

$$M(\theta) = \theta + \iota + m(\theta) \ , \tag{6.4}$$

where $m(\theta)$ some function with periodicity 2π.

There may be a diffeomorphism transforming the mapping $M(\theta) = \theta + \iota + m(\theta)$ to a *circle mapping*

$$\mathcal{R}\Theta = \Theta + \iota \, . \tag{6.5}$$

This circle mapping acts on a new set of coordinates Θ, identified as action angle coordinates. The diffeomorphism between $\mathcal{R}$ and M exists if the parametrisation

$$\theta = X\Theta = \Theta + x(\Theta) \, . \tag{6.6}$$

exists for Θ extending into the complex plane. In this case $\mathcal{R}$ and M are said to be *topologically conjugate*.

This conjugacy needs only to be proved for a single mapping, because if

$$X\mathcal{R} = MX \, , \tag{6.7}$$

then

$$X\mathcal{R}^N = M^N X \, . \tag{6.8}$$

The maximum extent to which Θ can be complex and the parametrisation still exist defines the *analytic width* or analyticity width $\alpha > \text{Im } \theta$.[Mac92]

The parametrisation X is the conjugacy between the mapping [Equation (6.3)] and rigid rotation [Equation (6.5)]

$$X\mathcal{R} = MX \, , \tag{6.9}$$

The conjugacy also applies to continuous solutions like pressure jump Hamiltonian trajectories, in which case ζ has been declared as the time coordinate, matched with the timing of the mapping.

To find the analytic width of X, one complexifies $X(\Theta)$ to ${}^{C}X = X(\Theta_r + i\Theta_i)$, and finds the maximum Θ_i for which the X still exists, i.e. the distance Θ_i to the nearest singularity.

Greene and Percival have shown that the analyticity width decreases in magnitude along with increases in destructive perturbations, and an analyticity width of zero successfully predicts the breakup of a surface for the standard map.[GP81] There is no proof that the analyticity width has the same behaviour for more complex Hamiltonians, but Greene and Percival conjecture that it behaves the same way for general nonintegrable systems.

Calculating analyticity width for field line configurations

The analyticity width can be calculated by complexifying the transformation to action angle coordinates. In the pressure jump Hamiltonian formulation the action angle coordinates were seen to be equivalent to straight field line coordinates (See Appendix A.2.5). It states that one can transform to straight field line coordinates via the transformation

$$\theta = \Theta - \frac{f(\hat{\theta}, \zeta)}{I} \ , \tag{6.10}$$

$$\zeta = \zeta \ , \tag{6.11}$$

which amounts to removing the periodic deviations away from f so that it is linearised to $f(\Theta, \zeta) = I_\Theta \Theta + G_\zeta \zeta$. This leads to the magnetic field components $\boldsymbol{B}_\Theta$, $\boldsymbol{B}_\zeta$ becoming constant as a function of the new angular variables, hence straight field line coordinates.

The f_{mn} terms that describe the action of the solution trajectory can be calculated from

$$p_\theta(\theta, \zeta) = I + \sum_{m,n}^{\infty} m f_{mn} \cos\left(m\theta - n\zeta\right) \ , \tag{6.12}$$

which comes from the relation in Equation (2.26).

In principle the process of calculating the analyticity width involves transforming Equation (6.10) to the form of Equation (6.6). One must then complexify the resulting function X using the coordinate $\Theta = \Theta_r + i\Theta_i$. The result will be an expression for the analyticity width that is a function of f_{mn}.

Calculating the analyticity width of a trajectory of even the most simple Hamiltonian system is a highly computationally intensive task. For instance Rosengaus and Dewar[RD82] showed that the Fourier tail of conjugate expansions must be followed to a large value of m, and even then the behaviour of the coefficients is not monotonic, and the limit is not well defined. The pressure jump Hamiltonian is extremely complicated for any reasonably realistic conditions and so the calculation of the analyticity width is left as future work, with pessimism toward it being practically calculable without some new derivation.

Analyticity width in the magnetic field line Hamiltonian

In principle the analyticity width can be calculated for the magnetic field line Hamiltonian too. The analyticity width in the magnetic field line Hamiltonian would again represent how resilient the field line is, but would not contain information about the effect of the pressure discontinuity. The perturbations to the magnetic field line

Hamiltonian are solely due to the deformation of the flux surfaces, and so the associated analytic width would tell how resilient the flux surface is to deformations only. The pressure jump Hamiltonian in contrast can only be defined on a flux surface, but the analytic width represents the resilience with regard to deformation and the pressure jump.

6.4.3 Other measures of resilience

Because of the difficulty of reliably measuring the analyticity width, other measures have been suggested in the literature that may provide an approximate measure. Studies of Greene's residue criterion have spawned various attempts to quantify "closeness to destruction". The definitions that follow are theoretical approximations or computational measures that have been shown to be correlated with resilience. The advantage of these measures is that they are much more computationally tractable than the analyticity width, but of course are merely approximations to it.

Shenker technique

Shenker and Kadanoff looked at residue curves and came to the same observation as outlined in Section 6.4.2, that the behaviour of the residue curve reflects how close the trajectory is to being chaotic.[SK81] Shenker and Kadanoff found that the following equations matched the residues "quite closely" in the limit of large q_i and small $\epsilon = E^C - E$[SK81]

$$R_i^e \sim R_\infty^e \, \iota^{(E^C - E)\beta_0 q_i} \tag{6.13}$$

$$R_i^h \sim R_\infty^h \, \iota^{(E^C - E)\beta_0 q_i}. \tag{6.14}$$

where the two parameters to fit are β_0, R_∞^e. There are two equations, one for the elliptic (positive) residue R_i^e and one for the hyperbolic (negative) residue R_i^h.

MacKay technique

Another model has been introduced by MacKay. This model has a more rigorous definition, it is a predicted expression for the asymptotic behaviour of the residue, relying on the fact that the analyticity extends continuously to the analytic boundary. The model is the asymptotic (large q) expression [Mac92]

$$R \sim \pm R_\infty(q, |\iota - p/q|) e^{-q\alpha}. \tag{6.15}$$

where $R_\infty(q, |\iota - p/q|)$ depends on the convergent (parametrised by q) and the closeness of the convergent to the irrational it is approximating ($|\iota - p/q|$). The nature

of the function R_∞ is "unknown"[Mac92], but the exponential envelope can be fitted to give a value for the analyticity width. The $\pm$ implies there is a separate fit for hyperbolic and elliptic orbits, like the Shenker fit.

This expression for the residue agrees with Greene and Percival when they showed that the rates of exponentiation of $R(q)$ agreed to 4.5 figures to the analyticity width calculated by studying the behaviour of the Fourier tail. There is numerical evidence that MacKay's model is correct for the inverse golden mean in the semistandard map.[GP81]

More accurate than the previous two measures (but strongly related) is MacKay's theorem 4,[Mac92] that

$$\limsup_{n\to\infty} q_n^{-1} \log |R_n| = \mu(\iota) \leq -\alpha \ , \tag{6.16}$$

which gives a minimum value for the analyticity width α.

The above methods may provide a simpler and faster way to infer resilience for a trajectory, which would be a helpful diagnostic for `SPEC`. However their application has only been compared for the standard map, and more work would be required to ensure they are applicable as replacements for the analyticity width.

6.4.4 Edge localised modes

The break up of a flux surface sustaining a large pressure discontinuity could provide a simple mechanism for edge localised modes. The redistribution of pressure that would need to occur when a flux surface withstanding a pressure discontinuity breaks up may result in the destruction of nearby flux surfaces. If this starts a chain reaction the net result may be the translation of pressure radially outward and eventually out of the outermost flux surface, where the mass would escape confinement.

This explanation would fit with observations that show a reduction in the severity of edge localised modes when chaotic modes are induced in the outer plasma region. A simulation of this effect should be possible with `SPEC` in the near future.

6.4.5 Current sheets in other physical systems

Flux surfaces sustaining a pressure or rotational transform jump are an example of *current sheets*, which have been observed particularly in astrophysics where magnetic forces push currents and localise them along two-dimensional surfaces. While this thesis concentrated on toroidal surfaces, current sheets have investigated in many other topologies (e.g. linear and hyperbolic).[Par94]

An analogous Hamiltonian system for these geometries may shed light on their nature. Including determining a necessary condition for when these sheets may exist

in equilibrium.

6.4.6 Further investigation into the idea of a "Hamiltonian within a Hamiltonian"

The pressure jump Hamiltonian is defined on an invariant torus of the magnetic field line Hamiltonian. This is a strange formulation which sees a non-integrable Hamiltonian system imbedded within another non-integrable Hamiltonian system.

This can be seen in the structure of the Hamiltonian:

$$\Delta P = \frac{1}{2} g^{ij} p_i p_j - \frac{1}{2} g^{ij} \partial_i f_- \partial_j f_- \ . \tag{6.17}$$

The potential function is of the form of the kinetic term, which is itself the form of the problem of finding geodesics on a torus. The magnetic field line Hamiltonian influences this Hamiltonian through the metric terms, which describe an invariant torus of the magnetic field line Hamiltonian dynamics.

This situation was reflected in the robustness plots based off `SPEC` equilibria in this thesis. These plots showed how the stability of the pressure jump Hamiltonian depend on how close the invariant torus of the magnetic field line Hamiltonian was to destruction. Past this it is not clear what could be done to garner some fundamental knowledge of this situation, but this peculiar construction that sees "chaos within chaos" may be worth further investigation.

Appendices

Appendix

A.1 Covariant and contravariant representations

Consider a position vector $\boldsymbol{R}$. We can define the vector function $\boldsymbol{R}_c$ to convert a set of cartesian coordinates x, y, and z to give $\boldsymbol{R}$, but we want to instead use a new general coordinate system defined by the three numbers u^1, u^2, and u^3, for which one would need a function $\boldsymbol{R}_{\boldsymbol{u}}$,

$$\boldsymbol{R} = \boldsymbol{R}_u(u^1, u^2, u^3) = \boldsymbol{R}_c(x, y, z) \ . \tag{A.1}$$

This implies there must exist functions

$$u^1 = u^1(x, y, z) \tag{A.2a}$$
$$u^2 = u^2(x, y, z) \tag{A.2b}$$
$$u^3 = u^3(x, y, z) \ , \tag{A.2c}$$

that transform the Cartesian coordinates to our general curvilinear coordinates. As Cartesian coordinates are a valid coordinate system, the condition for u^1, u^2, and u^3 to be a valid coordinate system is that the transformations between them [Equations (A.2)] be one to one, i.e., there must be one u^1, u^2, and u^3 point for every x, y, and z point.[1]

Providing the new coordinate set is valid, it is helpful to define the *basis vectors* of the coordinate system. The $\mathbf{e}_i$ basis vectors point in the direction in which $\boldsymbol{R}_u$ changes with respect to u^i, thus the basis vectors of the u^i set are

$$\mathbf{e}_1 = \frac{\partial \boldsymbol{R}_u}{\partial u^1}, \qquad \mathbf{e}_2 = \frac{\partial \boldsymbol{R}_u}{\partial u^2}, \qquad \mathbf{e}_3 = \frac{\partial \boldsymbol{R}_u}{\partial u^3}. \tag{A.3}$$

[1] A transformation to a toroidal topology would need the functions in Equations (A.2) to be multiple valued, this is allowed.[DHCS91]

Now we can write the position $\boldsymbol{R}$ as

$$\boldsymbol{R} = x\ \mathbf{e}_x + y\ \mathbf{e}_y + z\ \mathbf{e}_z \Leftrightarrow (x, y, z) \tag{A.4}$$

$$= u^1\mathbf{e}_1 + u^2\mathbf{e}_2 + u^3\mathbf{e}_3 \Leftrightarrow (u^1, u^2, u^3)\ , \tag{A.5}$$

note that the right hand side uses brackets for different basis sets, which basis set should be used should be clear from the context.

This choice of basis vectors is not the only choice. For any curvilinear coordinate system it can be helpful to define another set of basis vectors $\mathbf{e}^i$, that points in the direction that u^i changes with respect to the vector $\boldsymbol{R}_u$. defined by

$$\mathbf{e}^1 = \frac{\partial u^1}{\partial \boldsymbol{R}_u} = \nabla u^1, \qquad \mathbf{e}^2 = \frac{\partial u^2}{\partial \boldsymbol{R}_u} = \nabla u^2, \qquad \mathbf{e}^3 = \frac{\partial u^3}{\partial \boldsymbol{R}_u} = \nabla u^3. \tag{A.6}$$

So we can write $\boldsymbol{R}$ as

$$\boldsymbol{R} = x\ \mathbf{e}_x + y\ \mathbf{e}_y + z\ \mathbf{e}_z = (x, y, z) \tag{A.7}$$

$$= u_1\mathbf{e}^1 + u_2\mathbf{e}^2 + u_3\mathbf{e}^3 = (u_1, u_2, u_3)\ . \tag{A.8}$$

To aid in visualisation, the basis vectors $\mathbf{e}_i$ are tangent to the u^i coordinate curves, whereas the basis vectors $\mathbf{e}^i$ are perpendicular to the coordinate surface $u^i = \text{const}$, as shown in Figure A.1.

The two definitions of basis vectors seem similar and indeed they are stongly

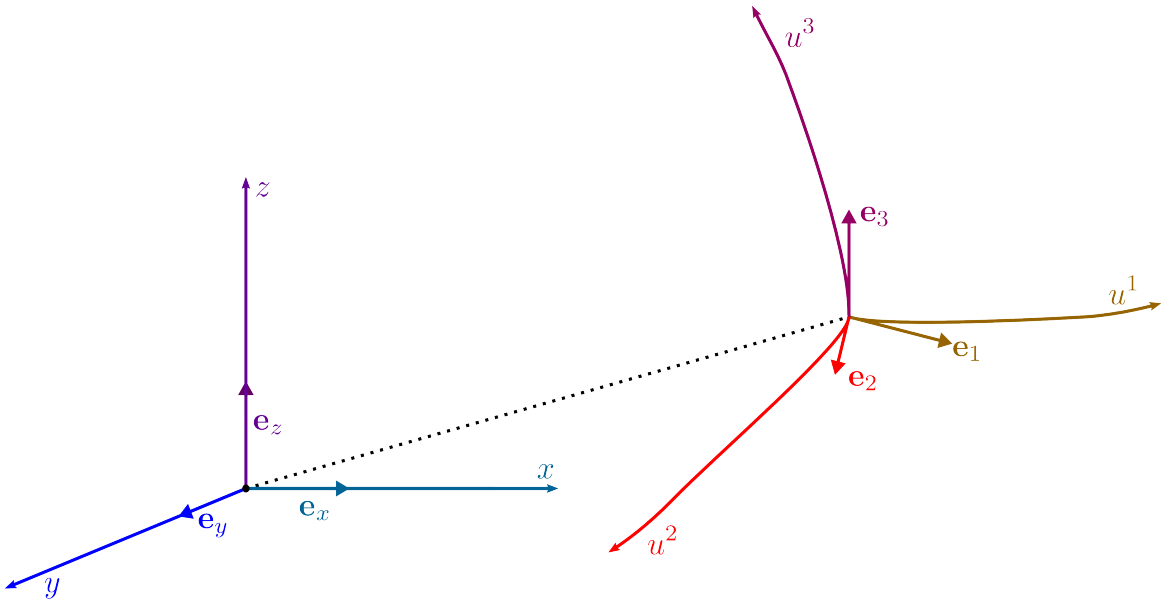

Figure A.1: An example of a transformation of a point in space in Cartesian coordinates to the *same point in space* in curvilinear coordinates. Here the basis vectors $\mathbf{e}_i$ are in the direction in which $\boldsymbol{R}_u$ changes with respect to u^i, i.e., tangent to the u^i coordinate curve.

related. In fact it is simple to show that with the above definitions, that

$$\mathbf{e}^i \cdot \mathbf{e}_j = \delta^i_j \ , \tag{A.9}$$

where δ^i_j is the Kronecker delta. This orthogonal relation means conversion between the two basis sets can be trivial, so the two sets of bases are very helpful when dealing with curvilinear coordinate systems. Because of the relation in Equation (A.9), the two sets are referred to as *reciprocal* basis sets (a name that is more fitting when one campares their original definitions).

As these two basis sets span $\mathbb{R}^3$, any three dimensional vector can be written in either of the two bases by writing the vector as a linear combination of the basis vectors like so,

$$\boldsymbol{D} = D_1\mathbf{e}^1 + D_2\mathbf{e}^2 + D_3\mathbf{e}^3 = (u_1, u_2, u_3) = D_i\mathbf{e}^i \tag{A.10a}$$

$$= D^1\mathbf{e}_1 + D^2\mathbf{e}_2 + D^3\mathbf{e}_3 = (u^1, u^2, u^3) = D^i\mathbf{e}_i \ , \tag{A.10b}$$

here the vectors are written in Einstein notation.

The two representations in Equations (A.10) are identified by the script (super or sub) of the components. Components of a vector with a subscript (e.g. D_i) are referred to as *covariant components*. Components of a vector with a superscript (e.g. D^i) are referred to as *contravariant components*. Thus, the first representation [Equation (A.10a)] is referred to as the *covariant representation* of the vector $\boldsymbol{D}$ because the components of the vector has subscripts (D_i), and the second representation is the *contravariant* representation of the vector $\boldsymbol{D}$ because the components of the vector has superscripts (D^i).

One can determine the covariant or contravariant components of a vector by simply taking the dot product with the corresponding basis vectors.

$$D_i = \boldsymbol{D} \cdot \mathbf{e}_i \tag{A.11a}$$

$$D^i = \boldsymbol{D} \cdot \mathbf{e}^i \ . \tag{A.11b}$$

To transform from, say the covariant representation $D_i\mathbf{e}^i$ to the contravariant representation, $D^j\mathbf{e}_j$, one would need to first determine the contravariant components D^j. This is done by combining Equation (A.11a) to Equation (A.10a)

$$D^j = \boldsymbol{D} \cdot \mathbf{e}^j \tag{A.12}$$

$$= (D_i\mathbf{e}^i) \cdot \mathbf{e}^j \tag{A.13}$$

$$= D_i g^{ij} \ , \tag{A.14}$$

where

$$g^{ij} = \mathbf{e}^i \cdot \mathbf{e}^j \ , \tag{A.15}$$

is a *metric coefficient*. As one might expect, transforming the other way, from contravariant components to covariant components uses metric coefficients

$$g_{ij} = \mathbf{e}_i \cdot \mathbf{e}_j \ . \tag{A.16}$$

The metric coefficients contain information about the transformation between the two representations. They inherit nice properties from the vectors that make them up, including

$$g^{ij} = g^{ji}, \qquad g_{ij} = g_{ji} \ , \tag{A.17}$$

and

$$g_{ij} g^{jk} = \delta_i^k \ . \tag{A.18}$$

The metric is mainly used for transforming between representations. As well as transforming vector components, one can transform the basis vectors themselves using metric coefficients

$$\mathbf{e}_i = g_{ij} \mathbf{e}^j \tag{A.19a}$$
$$\mathbf{e}^i = g^{ij} \mathbf{e}_j \ . \tag{A.19b}$$

One less common terminology used in this thesis is referring to a transformation that results in a transformation that converts a component or vector with a subscript to a superscript as *raising* the indices, and referring to the opposite transformation as a *lowering* of the indices.

The metric coefficients g_{ij} can be collected into a matrix $[g_{ij}]$, the i, jth element being g_{ij}. Similarly, one can also create a matrix $[g^{ij}]$. When these matrices are multiplied, we get a result that mirrors Equation (A.18)

$$[g_{ij}][g^{ij}] = I \ , \tag{A.20}$$

where I is the identity matrix. The determinant of each of these matrices are inverses

of each other

$$g = \det[g_{ij}] \tag{A.21a}$$
$$g^{-1} = \det[g^{ij}] \, . \tag{A.21b}$$

The determinant of the matrix is important, because it is related to the Jacobian of the transformation from Cartesian coordinates to the curvilinear coordinate system. The Jacobian of the transformation from (x, y, z) to (u^1, u^2, u^3) is

$$\mathcal{J} = \begin{vmatrix} \frac{\partial x}{\partial u^1} & \frac{\partial x}{\partial u^2} & \frac{\partial x}{\partial u^3} \\ \frac{\partial y}{\partial u^1} & \frac{\partial y}{\partial u^2} & \frac{\partial y}{\partial u^2} \\ \frac{\partial z}{\partial u^1} & \frac{\partial z}{\partial u^2} & \frac{\partial z}{\partial u^3} \end{vmatrix} \, . \tag{A.22}$$

Writing out the definition of the components of the metric matrix and simplifying gives the following relation

$$\mathcal{J} = \sqrt{g}. \tag{A.23}$$

There are other ways to write the Jacobian, including

$$\mathcal{J} = \mathbf{e}_1 \cdot \mathbf{e}_2 \times \mathbf{e}_3 = \sqrt{g} \tag{A.24}$$
$$\mathcal{J}^{-1} = \mathbf{e}^1 \cdot \mathbf{e}^2 \times \mathbf{e}^3 = \sqrt{g}^{-1} \, . \tag{A.25}$$

A.1.1 Other helpful relations

There are further advantages to using covariant and contravariant representations. Dot products are simplified when using reciprical representations:

$$\boldsymbol{C} \cdot \boldsymbol{D} = C^i D_j \delta_i^j \tag{A.26}$$
$$= C_i D^j \delta_j^i \, , \tag{A.27}$$

or

$$\boldsymbol{C} \cdot \boldsymbol{D} = C^i D^j g_{ij} \tag{A.28}$$
$$= C_i D_j g^{ij} \, . \tag{A.29}$$

A common form for cross products uses raising and lowering operations to calculate cross products. Expanding in either the covariant or the contravariant representation,

$$\boldsymbol{C} \times \boldsymbol{D} = C^i D^j \mathbf{e}_i \times \mathbf{e}_j = C_i D_j \mathbf{e}^i \times \mathbf{e}^j \, , \tag{A.30}$$

you can find the covariant or contravariant component of the resultant vector by dotting with the corresponding basis vector Equations (A.11),

$$(\boldsymbol{C} \times \boldsymbol{D})_k = (C^i D^j \mathbf{e}_i \times \mathbf{e}_j) \cdot \mathbf{e}_k \tag{A.31}$$

$$= \varepsilon_{ijk} \sqrt{g} C^i D^j \ , \tag{A.32}$$

where ε_{ijk} is the Levi-Civita symbol. Similarly,

$$(\boldsymbol{C} \times \boldsymbol{D})^k = \varepsilon^{ijk} \frac{1}{\sqrt{g}} C_i D_j \ . \tag{A.33}$$

The torus $\mathcal{S}$ is embedded in an ambient, 3-dimensional Euclidean space with its own metric, G^{ij} say. If (θ, ζ, ψ) are curvilinear coordinates in this ambient space such that $\psi = \text{const}$ on $\mathcal{S}$, then the covariant components G_{ij}, $i, j \in \{\theta, \zeta\}$, are identical to g_{ij} on $\mathcal{S}$, but the contravariant components are different, they would be

$$g^{ij} = G^{ij} - \frac{G^{\psi i} G^{\psi j}}{G^{\psi\psi}} \text{ for } i, j \in \{\theta, \zeta\} \ . \tag{A.34}$$

A.1.2 Why curvilinear coordinates are so helpful in Fusion theory

he coordinates one sets when treating a fusion plasma should be chosen to follow the contours of the plasma. For instance, the radial direction is often parametrised by a nested set of surfaces of constant flux. This way the coordinate contours are flux surfaces. This is always done with equilibrium codes that assume nested surfaces, but becomes difficult when some flux surfaces cease to exist due to the presence of chaos.

By virtue of the coordinates following the contours of the plasma, the Jacobian (and by extension the metric) of the transformation contains all information about the transformation from cartesian coordinates to curvilinear coordinates, and thus contains all the information of the geometry of the fusion plasma.

When the geometry of the flux surface is defined as in Section 2.2.1, it completely defines the metric. Conversely, inspection of a given metric can tell you everything about the surface.

A.2 Coordinate systems used in fusion theory

A.2.1 General comments on toroidal coordinate systems

Toroidal topology is two–fold symmetric, and so a point on a torus can be uniquely defined by

$$u = u \mod 2\pi \tag{A.35}$$

$$v = v \mod 2\pi\ . \tag{A.36}$$

Obviously these are extremely general, and in fact are underdefined leaving opportunity to define coordinates to suit certain tasks. For instance, one can redefine these coordinates to minimise the Fourier terms you need in a Fourier description of a torus (this is described in Appendix A.3).[HL86]

A.2.2 Cartesian coordinates

We assume the Cartesian coordinates of a point $\boldsymbol{r}$ to be given by $\boldsymbol{r} = x\boldsymbol{e}_x + y\boldsymbol{e}_y + z\boldsymbol{e}_z$.

A.2.3 s, θ, ζ coordinates

These are the simplest coordinates from a geometric point of view and are given by (s, θ, ζ). The poloidal direction (short way round) is parameterised by θ. Similarly the toroidal direction is parametrised by the angle ζ.

The radial coordinate s can also be used when dealing with a toroidal volume. To simplify matters, the contours of the flux surfaces within the plasma volume are defined to be surfaces of constant s. This way a choice of $s = \text{const}$ specifies a flux surface, and θ and ζ then parameterise the points on the flux surface. That the level surfaces of s coincide with flux surfaces means that s effectively 'labels' the flux surfaces.

Consider a surface $s = \text{const}$. A point on this surface is defined by (θ, ζ), but theta and zeta are still largely undefined. It is often simpler not to think of them as angles from the centre axis, but to think of them as simply parameterisations of a distance along the surface $\mathcal{S}$, which we refer to as *angle–like*. As the majority of this thesis is concerned with single flux surfaces, s will commonly not be mentioned.

A.2.4 RZ coordinates

We use the term RZ coordinates to refer to the set (R, ϕ, Z) where

$$R = R(s, \theta, \zeta) \tag{A.37}$$
$$Z = Z(s, \theta, \zeta) \tag{A.38}$$
$$\phi = \zeta \ , \tag{A.39}$$

as shown in Figure 2.1(a).

$R(\theta, \zeta)$ gives the distance of the point on the surface $s = \text{const}$ to the vertical axis, while $Z(\theta, \zeta)$ gives the distance of the point on the surface to the horizontal plane. The relationship between the RZ coordinates and Cartesian coordinates is given by

$$x = R(s, \theta, \zeta)\cos(\zeta) \tag{A.40}$$
$$y = R(s, \theta, \zeta)\sin(\zeta) \tag{A.41}$$
$$z = Z(s, \theta, \zeta)\sin(\theta) \ . \tag{A.42}$$

These coordinates are especially helpful at constant ϕ, where such an intersection results in an (R, Z) Cartesian description of the plasma cross section.

These coordinates can be used to prescribe surfaces as shown in Section 2.2.1.

A.2.5 Straight field line coordinates (SFLC)

Consider an integrable field $\boldsymbol{B}$ such that invariant tori (good flux surfaces) are smoothly nested. We then choose the level surfaces of s to be these invariant tori. In this case $\boldsymbol{B} \cdot \boldsymbol{\nabla} s \equiv 0$, i.e. $B^s \equiv 0$. Combined with the fact that the magnetic field is divergence free, gives

$$\nabla \cdot \boldsymbol{B} = \frac{1}{\mathcal{J}} \left[\frac{\partial}{\partial \theta}(\mathcal{J} B^\theta) + \frac{\partial}{\partial \zeta}(\mathcal{J} B^\zeta) \right] = 0, \tag{A.43}$$

where $\mathcal{J}$ is the Jacobian.

This implies that

$$\mathcal{J} B^\theta = -\frac{\partial \nu(s, \theta, \zeta)}{\partial \zeta} \quad \text{and} \tag{A.44}$$
$$\mathcal{J} B^\zeta = -\frac{\partial \nu(s, \theta, \zeta)}{\partial \theta} \ . \tag{A.45}$$

Thus wherever the magnetic field is divergence free (i.e. everywhere), the field can be written as the spatial derivative of a potential. As the field is the derivative of this

potential function, it must be linear and periodic in the angle coordinates,[DHCS91]

$$\nu = u(s)\theta + v(s)\zeta + \hat{\nu}(s,\theta,\zeta)\ , \tag{A.46}$$

where θ and ζ are the previously defined periodic coordinates with the above mentioned freedom and where $\hat{\nu}$ is a function that is periodic in θ and ζ.

The goal then in defining SFLCs is to find the angles for which the surface potential does not have this periodic part. This is done by linearly transforming the coordinates, so as to cancel the periodic terms like so:

$$\theta = \Theta - C_\Theta \frac{\hat{\nu}}{u(s)}, \tag{A.47}$$

$$\zeta = \phi - C_\phi \frac{\hat{\nu}}{v(s)}, \tag{A.48}$$

where $C_\Theta + C_\Phi = 1$.

This gives the desired form for ν

$$\nu = u(s)\Theta + v(s)\phi\ . \tag{A.49}$$

In MRXMHD $u(s)$ and $v(s)$ are not well defined because we allow chaotic structures to form between flux surfaces, indeed single good flux surfaces surrounded (perhaps infinitely closely) by chaos. In this situation ν is only defined on flux surfaces and is given by the *surface potential* $f(\theta,\zeta)$.

A.3 The Fourier representation of a toroidal surface

The pressure jump Hamiltonian problem is defined on a flux surface of some geometry. A method of prescribing a flux surface is desired that is both intuitive and takes up little storage in computer memory.

Consider the (R,ϕ,Z) coordinate system introduced in Section A.2.4,

$$R = R(s,\theta,\zeta) \tag{A.50}$$

$$Z = Z(s,\theta,\zeta) \tag{A.51}$$

$$\phi = \zeta\ . \tag{A.52}$$

By setting the level surfaces of s to coincide with the invariant tori of the pressure jump Hamiltonian system, the choice $s = \text{const}$ selects a toroidal surface whose geometry

is given by

$$x = R(\theta, \zeta)\cos(\zeta)\ , \tag{A.53}$$

$$y = R(\theta, \zeta)\sin(\zeta)\ , \tag{A.54}$$

$$z = Z(\theta, \zeta) \qquad . \tag{A.55}$$

Now the surface is completely defined by only two functions $R(\theta, \zeta)$ and $Z(\theta, \zeta)$. One can take the Fourier transform of these functions

$$R = \sum_{n=-N}^{N} \sum_{m=0}^{M} R_{mn} \cos\left(m\theta - n\zeta\right)\ , \tag{A.56}$$

$$Z = \sum_{n=-N}^{N} \sum_{m=0}^{M} Z_{mn} \sin\left(m\theta - n\zeta\right)\ , \tag{A.57}$$

so that the functions are defined using the sets of coefficients

$$R = \begin{pmatrix} R_{11} & R_{12} & \dots & R_{1M} \\ R_{21} & \ddots & & R_{2M} \\ \vdots & & \ddots & \vdots \\ R_{NM} & \dots & \dots & R_{NM} \end{pmatrix}\ , \quad Z = \begin{pmatrix} Z_{11} & Z_{12} & \dots & Z_{1M} \\ Z_{21} & \ddots & & Z_{2M} \\ \vdots & & \ddots & \vdots \\ Z_{N1} & \dots & \dots & Z_{NM} \end{pmatrix}\ . \tag{A.58}$$

This Fourier representation allows a smooth toroidal surface to be stored on a computer with $n_{max} + 1 + m_{max}(2n_{max} + 1)$ terms, where $m \geq 0$ and $|n| \leq m$.[HW83]

Not only does it provide a convenient way to store toroidal surfaces computationally, this prescription also allows a more intuitive description of a surface. For instance, an axisymmetric torus with major radius R_0 and minor radius r_0 can be given by the components $R_{00} = R_0$, $R_{10} = Z_{10} = r_0$.

The surface as a whole can be represented with a *surface array*, for example:

$$\mathcal{S} = \left[\begin{array}{cccc} m & n & R_{mn} & Z_{mn} \\ \hline 0 & 0 & R & 0 \\ 1 & 0 & r_0 & r_0 \\ 0 & 1 & \delta & -\delta \\ 2 & 1 & \delta & \delta \end{array}\right]\ . \tag{A.59}$$

The surface array in Equation (A.59) is used in this thesis for deforming an interface in Section 3.4.2.

Magnetic field line Hamiltonian	Pressure jump Hamiltonian
P implicit	P explicit
Defined throughout plasma volume	Defined on a given magnetic surface
Phase space and time a representation of Euclidean 3-space	Phase space a combination of a Riemannian 2-space = magnetic surface (configuration space) and field components (momentum space)
All orbits are field lines	Orbits are not field lines, projections of regular orbits with specified ι onto configuration space are field lines

Table A.1: A table summarising the differences between the magnetic field line Hamiltonian and the pressure jump Hamiltonian.

A.4 Comparison of Hamiltonians

In this section we compare the magnetic field line Hamiltonian system often used in the literature to the pressure jump Hamiltonian system introduced in this paper.

The magnetic field in the plasma volume be written as [Boo83]

$$\boldsymbol{B} = \nabla\psi \times \nabla\theta + \nabla\zeta \times \nabla\chi \,. \tag{A.60}$$

Using the equation of the field line $d\boldsymbol{r}/dt = \boldsymbol{B}(\boldsymbol{r})$, one finds [Boo04]

$$\frac{d\theta}{d\zeta} = \frac{\partial\chi}{\partial\psi} \tag{A.61}$$

$$\frac{d\psi}{d\zeta} = -\frac{\partial\chi}{\partial\theta} \,, \tag{A.62}$$

which are of the form of Hamilton's equations. Thus each field line can be described as the solution of the magnetic field line Hamiltonian χ, in a phase space with the poloidal angle θ and toroidal flux function ψ as canonical variables.

Trajectories of this Hamiltonian correspond directly to magnetic field lines within the plasma volume. Trajectories that lie on invariant tori correspond to field lines that draw out flux surfaces. Trajectories that are chaotic correspond to chaotic field lines that fill the chaotic regions of the plasma.

The pressure enters *implicitly* into the magnetic field line Hamiltonian system, exciting currents that determine the flux functions. The field line dynamics feed back into the determination of the pressure as a function of position.

In contrast, the pressure is explicitly prescribed in the pressure jump Hamiltonian as the magnitude of the pressure discontinuity across the surface, and functions as the Hamiltonian energy. While the trajectories of this Hamiltonian system are not

identically the field lines, the projection of the phase trajectories onto the 3D torus are field lines of the given rotational transform. If the surface potential can be found, then the surface is a flux surface.

The two Hamiltonian systems are related in that the pressure jump Hamiltonian system may be "embedded" into the magnetic field line Hamiltonian system. An invariant torus of the magnetic field line Hamiltonian system corresponds to a flux surface in the plasma volume. The pressure jump Hamiltonian may be used to investigate the effect of setting a pressure discontinuity across this flux surface. The geometry of the invariant torus of the magnetic field Hamiltonian system is supplied to the pressure jump Hamiltonian through the metric coefficients g^{ij}. The pressure discontinuity is introduced by setting the energy of the pressure jump Hamiltonian to be non-zero.

A summary of the differences of the Hamiltonian systems in given in Table A.1.

A.5 A general derivation of the pressure jump condition

This section contains a general derivation to complement the SPEC-motivated derivation in Section 2.3. This is provided mainly to show that the condition has more relevance than may be immediately discerned from the SPEC context.

As in plasma equilibrium theory, the plasma is assumed to be static (i.e. mass flow is negligible) and the ion and electron Larmor radii to be negligible. There is no minimum scale length model and discontinuities are in principle possible, provided the net force density at each point $\boldsymbol{r}$ in the plasma vanishes (the *force balance condition*). Also, a corollary of the assumed flowless state is that electric fields are also negligible.

We assume the kinetic stress is described by the isotropic pressure tensor $P(\boldsymbol{r})\mathsf{I}$, where I is the unit dyadic. Adding the electromagnetic stress, the total stress tensor is

$$\mathsf{T} \equiv P\,\mathsf{I} + \frac{B^2}{2}\mathsf{I} - \boldsymbol{B}\boldsymbol{B}\ , \tag{A.63}$$

where $\boldsymbol{B} \equiv \boldsymbol{B}_{\mathrm{SI}}(\boldsymbol{r})/\sqrt{\mu_0}$, $\boldsymbol{B}_{\mathrm{SI}}$ being the magnetic field in SI units and μ_0 the permeability of free space. The force balance condition is then [Fre87]

$$\boldsymbol{\nabla}\cdot\mathsf{T} = 0\ . \tag{A.64}$$

If P and $\boldsymbol{B}$ are differentiable, Equation (A.64) may be written in the more usual form $\boldsymbol{\nabla}P = (\boldsymbol{\nabla}\times\boldsymbol{B})\times\boldsymbol{B}$; but at surfaces of discontinuity P and $\boldsymbol{B}$ are step functions and $\boldsymbol{\nabla}\times\boldsymbol{B}$ contains a Dirac delta function component, corresponding to a

sheet current at the discontinuity. Then $(\boldsymbol{\nabla} \times \boldsymbol{B}) \times \boldsymbol{B}$ is not well defined and it is better to regard Equation (A.64), interpreted in the weak sense of distribution theory, as the fundamental form of the force balance relation.

Consider a surface $\mathcal{S}$, defined as $\varsigma = 0$ where ς is the distance from $\mathcal{S}$. For the purposes of deriving the pressure jump condition, the definitions of $\boldsymbol{B}^{\pm}$ are extended radially so they are both smooth everywhere (i.e. not by themselves discontinuous) and remain bounded in both volumes. The discontinuous pressure profile $P(\boldsymbol{r})$ and the corresponding discontinuous complete magnetic field $\boldsymbol{B}(\boldsymbol{r})$ can then be expressed as

$$P = P_{-}(\boldsymbol{r})h(-\varsigma) + P_{+}(\boldsymbol{r})h(\varsigma) \,, \tag{A.65}$$

$$\boldsymbol{B} = \boldsymbol{B}_{-}(\boldsymbol{r})h(-\varsigma) + \boldsymbol{B}_{+}(\boldsymbol{r})h(\varsigma) \,, \tag{A.66}$$

where h is the unit Heaviside step function, which causes the discontinuity in $\boldsymbol{B}$, as both $\boldsymbol{B}^{\pm}$ are themselves not discontinuous. Such a form for P and $\boldsymbol{B}$ gives

$$\nabla P_{\pm} = \boldsymbol{j}_{\pm} \times \boldsymbol{B}_{\pm} \,, \tag{A.67}$$

where $\boldsymbol{j}_{\pm} = \boldsymbol{\nabla} \times \boldsymbol{B}_{\pm}$ are the associated currents. Dotting Equation (A.67) with $\boldsymbol{B}_{\pm}$ gives $\boldsymbol{B}_{\pm} \cdot \nabla P_{\pm} = 0$, which implies the pressure is constant along a magnetic field line. As a flux surface is composed of a single magnetic field line, we have the condition that on both sides of the surface

$$P_{\pm} = \text{const} \,. \tag{A.68}$$

Substitution of Equation (A.66) into $\nabla \cdot \boldsymbol{B} = 0$ gives

$$\nabla \cdot \boldsymbol{B} = \tag{A.69}$$

$$\boldsymbol{\varsigma} \cdot [\![\boldsymbol{B}]\!]\, \delta(\varsigma) + \nabla \cdot \boldsymbol{B}_{-} h(-\varsigma) + \nabla \cdot \boldsymbol{B}_{+} h(\varsigma) \,, \tag{A.70}$$

where $\boldsymbol{\varsigma}$ is the unit normal to $\mathcal{S}$ and where $[\![x]\!]$ is the jump of x across the interface, $[\![x]\!] = x_{+} - x_{-}$. The divergence can only be zero if

$$[\![B_{\varsigma}]\!] \equiv \boldsymbol{\varsigma} \cdot [\![\boldsymbol{B}]\!] = 0 \,, \tag{A.71}$$

i.e., the normal component of the magnetic field must be continuous.

Similarly, when Equations (A.65 - A.66) are substituted into the stress tensor in Equation (A.64),

$$\boldsymbol{\varsigma} \cdot \left[\!\!\left[P\boldsymbol{I}\left(\frac{1}{2}B^2 - \boldsymbol{B}\boldsymbol{B}\right)\right]\!\!\right] = 0 \,. \tag{A.72}$$

Substituting Equation (A.71) into the above and dotting with $\boldsymbol{\varsigma}$ gives the condition

$$\left[\left[P + \frac{1}{2}B^2\right]\right] = B_\varsigma \left[\left[B_\varsigma\right]\right] = 0 \,, \tag{A.73}$$

removing the middle equality gives the *pressure jump condition*.

As B_ς is continuous, Equation (A.73) can be written as

$$\left[\left[(\boldsymbol{\varsigma} \times \boldsymbol{B})^2\right]\right] = -2 \left[\left[P\right]\right] \,, \tag{A.74}$$

so long as $[\![P]\!] \neq 0$,

$$\left[\left[\boldsymbol{\varsigma} \times \boldsymbol{B}\right]\right] \neq 0 \,. \tag{A.75}$$

Crossing Equation (A.72) with $\boldsymbol{\varsigma}$ gives

$$B_\varsigma \left[\left[\boldsymbol{\varsigma} \times \boldsymbol{B}\right]\right] = 0 \,. \tag{A.76}$$

Combining Equation (A.75) with Equation (A.76) implies

$$\boldsymbol{\varsigma} \cdot \boldsymbol{B}_\pm = 0 \,. \tag{A.77}$$

Thus, if there is a pressure discontinuity across a surface, the field lines must lie on that surface.

The plasma in the neighborhoods either side of the surface is assumed to be force free, so that $\nabla P = 0$. Equation (A.67) then implies that $\boldsymbol{j}_\pm$ is parallel to $\boldsymbol{B}_\pm$, which on comparison with Equation (A.77) implies

$$\boldsymbol{\varsigma} \cdot \boldsymbol{j}_\pm = \boldsymbol{\varsigma} \cdot (\boldsymbol{\nabla} \times \boldsymbol{B}_\pm) = 0 \,. \tag{A.78}$$

Thus, if there is a pressure discontinuity across a surface, the curl of the magnetic field must be parallel to the surface at all points on the surface.

A.6 Irrational numbers and their representations

A.6.1 Importance of different rational and irrational number representations

The idea of degrees of irrationality is not well known outside of number theory, and is best explained using certain representations of real numbers. In this appendix, two representations of real numbers and how they each quantify degrees of irrationality

are explained. The representations also provide ways to identify and group sequences of rationals and irrationals which provide standards by which to base comparisons between their associated orbits.

A.6.2 The number line

The real number line is composed of *rational* and *irrational* numbers. A rational number w is one that can be written as a fraction $w = \frac{m}{n}$. For example

$$1/1 = 1 \,, \tag{A.79}$$
$$1/2 = 0.5 \,, \tag{A.80}$$
$$2/3 = 0.(6) = 0.6666... \,, \tag{A.81}$$
$$13/21 = 0.(619047) \,, \tag{A.82}$$
$$89/144 = 0.6180(5) \,, \tag{A.83}$$

where (x) refers to the repeating decimal string x.

An irrational number on the other hand cannot be written as a fraction. For instance

$$\sqrt{2} = 1.41421... \,, \tag{A.84}$$
$$\pi = 3.14159... \,, \tag{A.85}$$
$$e = 2.71828... \,, \tag{A.86}$$
$$\gamma = 1.61803... \,. \tag{A.87}$$

Rational numbers are *countably infinite*, i.e. there are an infinite number of them but there is one rational for every integer. Irrationals are *uncountably infinite* in that there are infinitely more irrationals than there are rationals. Thus *almost all* real numbers are irrational.

A.6.3 The continued fraction representation of real numbers

One can write any real number b in the form[Niv56][Mei92]

$$b = a_0 + \cfrac{1}{a_1 + \cfrac{1}{a_2 + \cfrac{1}{a_3 + ...}}} = [a_1, a_2, a_3, ...] \,. \tag{A.88}$$

This representation is known as the *continued fraction representation* and the a_i are referred to as the *partial fractions* of b.

Any sequence of integer partial fractions will give a real number. The nomenclature is to represent the number as a sequence of integers in square brackets.

Only a rational number can be written as a fraction, so the number b is rational if and only if the continued fraction terminates at some a_n, for example, $b = [a_0, a_1, ..., a_n]$ is a rational. The number is irrational if it requires an infinite number of partial fractions to obtain it.

A.6.4 Farey tree representation of real numbers

The Farey tree technique is a method of organising irrationals and allows a more visual representation. A Farey tree is defined from some *Farey interval* $\mathcal{I}$, consisting of two rational numbers p_1/q_1, and p_2/q_2; the interval is written as $[p_1q_1p_2q_2]$. Any number, rational or irrational, can be reached by following a *Farey path* within this interval. To follow the Farey path, one calculates the *mediant* of the interval $[(p_1 + p_2)/(q_1 + q_2)]$, then one considers the interval to be split into two intervals by this mediant. The path involved making a choice, to choose one of the two subintervals for further splitting with the new mediant. Continually dividing the interval a finite number of times will allow one to find any rational number within the original interval. Infinite divisions are required to find an irrational. Each subdivision can be considered to be a new interval at a different *depth*, both intervals below a given interval are termed *daughters* of the *parent* interval. This thesis defines a depth of zero to be at the interval $\mathcal{I} = [0110]$.

Thus, with reference to the Farey tree, a number is defined by its interval $\mathcal{I}$ and its path $\mathcal{P}$. The path is given by a series of L's and R's, representing a choice of subinterval toward zero and toward infinity respectively. The path is a succession of L's and R's with repeated patterns surrounded with $()^\infty$.

Rationals are converged to when the direction is repeated [e.g. a path ending in $(R)^\infty$] and irrationals are converged to when the direction is alternated forever [e.g. a path ending in $(RL)^\infty$ or $(RRL)^\infty$].

A.6.5 Relationship between the Farey tree technique and the continued fraction representation

The two methods are strongly related. The sum of the continued fraction elements gives the depth on the Farey tree at which the rational occurs, that is,[Mei92]

$$Depth([a_o, a_1, ..., a_i]) = \sum_{j=0}^{i} a_j \ . \tag{A.89}$$

The continued fraction for a daughter on the Farey tree is given by incrementing a_i by 1. As each rational has two equivalent continued fractions,

$$[a_0, a_1, ..., a_i] = [a_0, a_1, ..., a_i - 1, 1] \ . \tag{A.90}$$

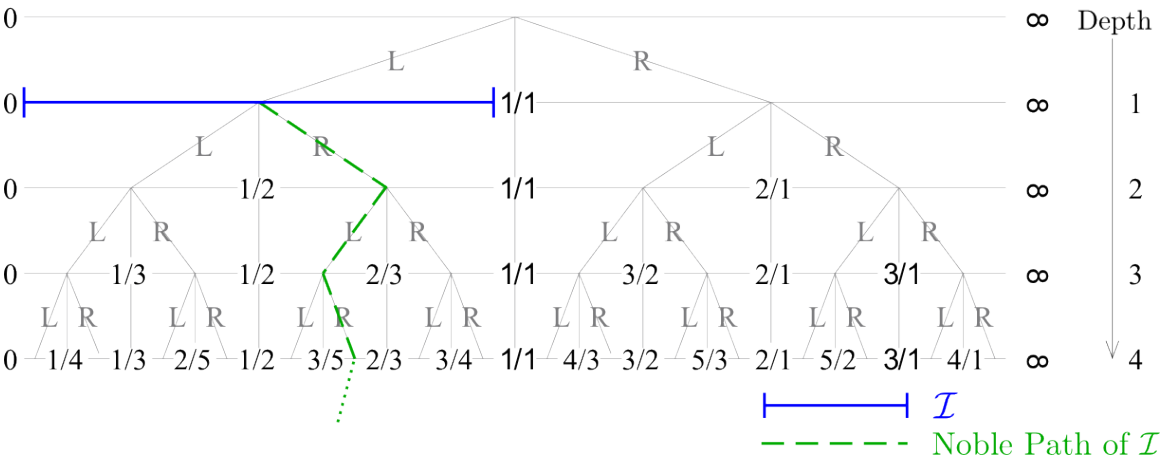

Figure A.2: The Farey tree with a Farey path of the interval [0111]. One initially takes the mediant between 0/1 and 1/1 which is 1/2, to step to the right one takes the mediant between 1/2 and 1/1. This Farey path is the *noble path* because it approaches the noble irrational $\gamma_{[0111]}$.

Adding 1 to the a_ith element gives the two daughters on the Farey tree. In the above equation, $a_i \neq 1$ must be used if the current step in the Farey tree is the same as the last one, and $a_i = 1$ must be used if the current step is in the opposite direction.

A.6.6 Using rationals to approach irrationals

Consider an irrational $\imath = [a_0, a_1, a_2, ...]$. The set of rationals τ_n formed by truncating the series at a_n approach the irrational number and in the limit $n \to \infty$, equal the irrational. The elements in this sequence of rationals are referred to as the *convergents* of $\imath$.

Quantitatively, a measure of irrationality is a measure of the difficulty one has of approaching the irrational number with partial fractions. For example, consider the famous irrational number π. Its continued fraction representation is [Mei92]

$$\pi = [3, 7, 15, 1, 292, 1, 1, 1, 2, ...] \,. \tag{A.91}$$

The approximations to π as a function of its convergents are given in Table A.6.6. One can see that the larger the partial fraction, the smaller the correction. Convergents with large partial fractions must eventually reach its irrational 'faster' than an irrational which has smaller partial fractions in its convergents. By this logic, the irrational whose partial fractions are an infinite string of 1s must be the most irrational, as 1 is the smallest integer. Indeed $[1, 1, 1, 1, ...] = \gamma$, is the golden mean, and is the most irrational number.

Additional Partial Fraction	Convergent.
3	3.00000000
7	3.142857142857143
15	3.141509433962264
1	3.1415929203539825
292	3.1415926530119025
1	3.141592653921421
1	3.1415926534674368

A.6.7 Noble irrationals

All numbers whose continued fraction representation ends in an infinite string of ones $[\cdots, (1)^{\infty}]$ are known as *noble* numbers, and are typically "very" irrational as 1 is the smallest non-trivial integer. Thus a trail of 1's converges slowest. The idea that noble irrationals converge the slowest is related to the idea of the *Diophantine condition*, which identifies irrationals by their "distance" from nearby rationals, specifically,

$$|qw - p| > \frac{C_D}{q^{\epsilon}} \,, \tag{A.92}$$

where $C_D > 0$ and $\epsilon \geq 1$.

The idea of approaching irrationals with a sequence of rationals is built into the concept of a Farey tree. One writes the irrational as an integer and a path. Following the path in the manner described above gives a sequence of rational numbers that approach the irrational of interest.

The phrase "noble" to classify irrationals that are highly irrational and similar to the golden mean is a play on the use of the phrase "noble metals" to classify metals on their similarity to gold (in their resistance to corrosion).

A.6.8 The noble path

As a tail of ones in the continued fraction representation generates a noble irrational, the path down the Farey tree to a noble irrational is $(RL)^{\infty}$, what this thesis refers to as a *noble path*. The sequence of this path is given by a simple equation. Starting from the custom interval $\mathcal{I} = [p_1/q_1, p_2/q_2]$, one takes the mediant $(p_1 + p_2)/(q_1 + q_2)$ then considers, say the right interval R. This involves taking the mediant between the interval $[(p_1 + p_2)/(q_1 + q_2), p_2/q_2]$, which is $(p_1 + 2p_2)/(q_1 + 2q_2)$. Next one must consider the interval to the left $[(p_1 + p_2)/(q_1 + q_2), (p_1 + 2p_2)/(q_1 + 2q_2)]$, and the mediant of this is $[(2p_1 + 3p_2)/(2q_1 + 3q_2)]$. In general, the path (RL) results in a

sequence of rationals τ_n given by

$$\tau_n = \frac{F[n]p_1 + F[n+1]p_2}{F[n]q_1 + F[n+1]q_2} \,, \tag{A.93}$$

where $F[n]$ is the nth value of the Fibonacci sequence $F[n] = F[n-1] + F[n-2]$ where $F[0] = 1$ and $F[1] = 1$. Dividing the fraction in Equation (A.93) by $F[n]$, gives the more common form

$$\tau_n = \frac{p_1 + F[n+1]/F[n]p_2}{q_1 + F[n+1]/F[n]q_2} \,. \tag{A.94}$$

After an infinite number of steps $(RL)^\infty$ down the Farey tree the rationals $\tau_n^{[p_1q_1p_2q_2]}$ will approach an irrational unique to the interval, and so the irrational is written as $\gamma_{[p_1q_1p_2q_2]}$. That is,

$$\lim_{n\to\infty} \tau_n^{[p_1q_1p_2q_2]} = \gamma_{[p_1q_1p_2q_2]} \,. \tag{A.95}$$

The limit of the ratio of Fibonacci terms is a well known result

$$\lim_{n\to\infty} F[n+1]/F[n] = \gamma \,, \tag{A.96}$$

where γ is the golden mean.

Thus the equation

$$\frac{p_1 + \gamma p_2}{q_1 + \gamma q_2} = \gamma_{[p_1q_1p_2q_2]} \,, \tag{A.97}$$

gives the most noble (most irrational) number between the rationals p_1/q_1 and p_2/q_2.

The most noble irrational in the positive real number line results from following the Farey tree from the interval [0110], giving the limit $\gamma_{[0110]} = \gamma$.

Note that if the noble path (LR) for the interval $[p_1/q_1, p_2/q_2]$ is taken instead, one can consider it to be an (RL) path from the interval $[p_1/q_1, (p_1+p_2)/(q_1+q_2)] = \gamma_{[0111]} = 1/\gamma$.

In this thesis, the most noble irrationals are investigated because they tend to persist according to the KAM theorem. As described in Section 3.2.1, the `PJH` code should investigate low rotational transforms to improve accuracy. It is for this reason that $\gamma_{[0111]}$ (the lowest of the two most noble irrationals) is the most investigated irrational in this thesis.

A.6.9 Rationals nearby to irrationals

Each step n down the noble path to an irrational gives rational numbers $\tau_n^{[p_1q_1p_2q_2]}$ that come closer and closer to the noble irrational $\gamma_{[p_1q_1p_2q_2]}$. At each successive step, the rationals alternate from being larger than the irrational, to being smaller. On an R step, $\tau_n^{[p_1q_1p_2q_2]} > \gamma_{[p_1q_1p_2q_2]}$, and on an L step, $\tau_n^{[p_1q_1p_2q_2]} < \gamma_{[p_1q_1p_2q_2]}$.

When computationally investigating an irrational trajectory, it is impossible to calculate something like the tangent map because it requires following the trajectory around its entire lengh (which is infinite). However, Greene in his 1979 paper showed that one can investigate a *sequence* of rationals and infer from this the properties of the irrational of interest. The noble path is a unique, simple and well defined sequence that can be used as a standard from which to select the rationals that will approximate the irrational of interest, and is the class of rational approximates which Greene bases his criterion.[Gre79] For more information on Greene's residue, see Section 3.3.

A.7 Example PJH input file

The following describes the input file required by `PJH`. The systems investigated in this thesis use outputs from the `SPEC` code, so this input file was adapted from the output of `SPEC`.

The structure of the file is:

```
   mpol     ntor     Nper
I  G    p_1     q_1     p_2     q_2     iota
   m        n        Rmn       Zmn        fmn        (line repeats)
```

The first line provides the maximum number of poloidal Fourier terms, the maximum number of toroidal Fourier terms and the periodicity of the torus respectively. The second line contains the linear coefficients of f^- (I and G), followed by the four integers that define the rotational transform of the prescribed field ($\iota = \gamma_{[p_1q_1p_2q_2]} = (p_1 + \gamma p_2)/(q_1 + \gamma q_2)$. The final quantity on this line is the value of ι which is not used by `PJH` as it can be calculated from the previous four integers.

The rest of the input is a list of the Fourier components of R, Z, and f. The order is not important and not every term needs to be included. Included below are the first few lines of an example input, that of the file:
`ftype=flux:d=+000000070:i=1213:m=50:n=25.pj`.

It describes the geometry of the flux surface investigated in section Section 5.5 at deformation $d = 0.0007$:

```
  50    25     1
1.602482782598277E-01  2.170964943090546E+01     1     2     1     3  3.819660112501052E-01
  0     0  0.000000000000000E+00  1.011883293862249E+00  0.000000000000000E+00
```

```
    0     1  1.903682304824032E-03  2.743723715999463E-05 -2.649053788556549E-05
    0     2 -7.215186204071873E-08  4.010105268195271E-07 -4.037489994378693E-07
    0     3 -9.414894633177399E-11  9.019503117908511E-10 -8.929292943761234E-10
    0     4  1.786932821030318E-11 -1.862855860289560E-12  6.876148162324898E-12
    0     5  4.236357807392120E-12  5.970444496832302E-13  3.414712149341478E-12
    0     6  1.518009145671197E-12  8.460986740156065E-13  1.235087065607961E-12
    0     7 -2.292649597167320E-13  5.915493894908175E-13  7.544340300943025E-13
    0     8 -1.188196864976156E-13  2.970334017405310E-13 -7.400373501624922E-15
    0     9 -3.531894977999118E-13  7.273873963657775E-14  1.197434069522337E-13
    0    10 -1.593831782852235E-13 -1.151337091388156E-13  2.670914857066155E-13
    0    11 -8.367145004801490E-14 -1.122133125240327E-13  2.220974156581872E-13
    0    12  8.739927610373481E-14 -1.390714686144284E-13  2.773010866364469E-13
    0    13 -1.350883917311067E-13 -1.594805248828504E-13  1.354471483221640E-13
    0    14 -1.329063074016138E-13 -1.678059793769671E-13  2.450463850439677E-13
    0    15 -6.739912245746812E-14 -9.910774225860136E-14  2.430722413664868E-13
    0    16 -2.327735299827873E-14 -1.391636909994966E-13  2.051999889200389E-13
    0    17 -3.174150136267247E-14 -5.324123255693829E-14  1.677671068103827E-13
    0    18 -4.784418041610107E-14 -6.735578065487449E-14  1.383994315687093E-13
    0    19 -2.447378535118569E-14 -6.383912634804883E-14  1.090205421488613E-13
    0    20 -2.342237267088002E-14 -9.825481339943048E-14  9.833907638461509E-14
    0    21  2.421055735380396E-14 -4.253225195626140E-14  7.328129459926446E-14
    0    22 -1.664755146012630E-14 -4.220994181855950E-14  6.532894935669340E-14
    0    23  1.486197756742576E-14 -4.950148500718326E-14  6.645425704027112E-14
    0    24 -1.173617541706657E-14 -4.388494979998016E-14  3.044285856817655E-14
    0    25 -2.871595621459857E-15 -3.562278815007381E-14  1.764153718771605E-21
    1   -25 -4.135134406290914E-14  7.905676202629663E-14  6.894147311828538E-14
    1   -24  2.279152768746409E-14  5.619171351570669E-14  7.780760717796765E-14
    1   -23 -1.906146009512602E-13  1.948920719878788E-14  9.335245358890085E-14
    1   -22  1.588700383385743E-13  4.483783903158251E-14  9.654596009162614E-14
    1   -21 -3.547326706792123E-13  1.811792163856202E-14  8.954138647462649E-14
    1   -20  2.036588874061538E-13  2.393444814689247E-14  9.669577881902347E-14
    1   -19 -6.211145744716014E-15  3.174606333405774E-14  9.888304241641806E-14
...
```

Bibliography

[Arn89] V. I. Arnol'd. *Mathematical Methods of Classical Mechanics*. Springer, New York, 2nd edition, 1989. Translated by K. Vogtmann and A. Weinstein.

[Bar11] D Barmaz. High-n stability of a pressure discontinuity in a three-dimensional plasma. Master's thesis, Research School of Physics and Engineering, Australian National University, 2011.

[BFKK58] I B Bernstein, E A Frieman, M D Kruskal, and R M Kulsrud. An energy principle for hydromagnetic stability problems. *Proc. R. Soc. Lond. A*, 244:17–40, 1958.

[BFL$^+$86] H L Berk, J P Freidberg, X Llobet, P J Morrison, and J A Tataronis. Existence and calculation of sharp boundary magnetohydrodynamic equilibrium in three-dimensional toroidal geometry. *Phys. Fluids*, 29(10):3281–3290, October 1986.

[BL96] O P Bruno and P Laurence. Existence of three-dimensional toroidal MHD equilibria with nonconstant pressure. *Comm. Pure Appl. Math.*, 49(7):717–764, 1996.

[Boo83] A H Boozer. Evaluation of the structure of ergodic fields. *Phys. Fluids*, 26(5):1288–1291, May 1983.

[Boo04] A H Boozer. Physics of magnetically confined plasmas. *Reviews of Modern Physics*, 76:1071–1141, 2004.

[Bou78] T Bountis. *Nonlinear Models in Dynamics and Statistical Mechanics*. PhD thesis, Physics Dept., University of Rochester, N.Y., 1978.

[Bro04] H W Broer. Kam theory: The legacy of Kolmogorov's 1954 paper. *American Mathematical Society*, 41(4):507–521, Feb 2004.

[DH98] R L Dewar and S R Hudson. Stellarator symmetry. *Physica D*, 112:275–280, 1998.

[DHCS91] W D D'haeseleer, W N G Hitchon, J D Callen, and J L Shohet. *Flux Coordinates and Magnetic Field Structure*. Springer Series in Computational Physics. Springer-Verlag, 1991.

[DHM+08] R L Dewar, M J Hole, M McGann, R Mills, and S R Hudson. Relaxed plasma equilibria and entropy-related plasma self-organization principles. *Entropy*, 10:621–634, 2008.

[DM92] R L Dewar and J D Meiss. Flux-minimizing curves for reversible area-preserving maps. *Physica D*, 57:476–506, April 1992.

[EMB+06] T E Evans, R A Moyer, K H Burrell, M E Fenstermacher, I Joseph, A W Leonard, T H Osborne, G D Porter, M J Schaffer, P B Snyder, P R Thomas, J G Watkins, and W P West. Edge stability and transport control with resonant magnetic perturbations in collisionless tokamak plasmas. *Nature Physics*, 2:419 – 423, 2006.

[ET12] T E Evans and the D-IIID Team. Suppression and mitigation of edge localised modes in (the d-iiid) tokamak with 3D magnetic perturbations. *Plasma and Fusion Research: Regular Articles*, 7:2402046, 2012.

[Eva13] T E Evans. ELM mitigation techniques. *Journal of Nuclear Materials (Supplement: Proceedings of the 20th International Conference on Plasma-Surface Interactions in Controlled Fusion Devices)*, 438:S11–S18, 2013.

[Fre87] J. P. Freidberg. *Ideal Magnetohydrodynamics*. Plenum Press, New York, 1987.

[Gar64] P R Garabedian. *Partial Differential Equations*. John Wiley & sons, 1964.

[GMVF81] J M Greene, R S MacKay, F Vivaldi, and M J Feigenbaum. Universal behaviour in families of area-preserving maps. *Physica D*, 3(3):468–486, 1981.

[Gol01] Christophe Golé. *Symplectic Twist Maps, Global Variational Techniques*, volume 18 of *Advanced series in nonlinear dynamics*. World Scientific, 2001.

[GP81] J M Greene and I C Percival. Hamiltonain maps in the complex plane. *Physica 3D*, 3:530–548, 1981.

[GR58] H Grad and H Rubin. Hydromagnetic equilibria and force-free fields. *2nd Int. Conf. Peac. Uses of Atom. Energy*, 1:190–197, 1958.

[Gra67] H Grad. Toroidal containment of a plasma. *Phys. Fluids*, 10(1):137–154, Jan 1967.

[Gre79] J M Greene. A method for determining a stochastic transition. *J. Math. Phys.*, 20(6):1183–1201, Jun 1979.

[Gre80] J M Greene. KAM surfaces computed from the Henon–Heiles Hamiltonian. *AIP Conference Proceedings*, 57:257–271, 1980.

[HDHM12] S R Hudson, R L Dewar, M J Hole, and M McGann. Nonaxisymmetric, multi-region relaxed magnetohydrodynamic equilibrium solutions. *Plasma Physics and Controlled Fusion*, 54:014005, 2012.

[HHD06] M J Hole, S R Hudson, and R L Dewar. Stepped pressure profile equilibria in cylindrical plasmas via partial Tayor relaxation. *J. Plasma Physics*, 72(6):1167–1171, 2006.

[HHD07] S R Hudson, M J Hole, and R L Dewar. Eigenvalue problems for beltrami fields arising in a 3-D toroidal magnetohydrodynamic equilibrium problem. *Phys. Plasmas*, 14:052505 1–12, May 2007.

[HL86] S P Hirshman and D K Lee. Momcon: A spectral code for obtaining three-dimensional magnetohydrodynamic equilibria. *Comput. Phys. Commun.*, 39:161–172, April 1986.

[HN10] S R Hudson and N Nakajima. Pressure, chaotic magnetic fields and magnetohydrodynamic equilibria. *Physics of Plasmas*, 17:052511, 2010.

[Hud04] S R Hudson. Destruction of invariant surfaces and magnetic coordinates for perturbed magnetic fields. *Phys. Plasmas*, 11:677 –685, 2004.

[Hud08] S R Hudson. Temperature contours and ghost surfaces for chaotic magnetic fields. *Phys. Rev. Lett.*, 100:095001, 2008.

[Hud09] S R Hudson. An expression for the temperature gradient in chaotic fields. *Phys. Plasmas*, 16:010701, 2009.

[HW83] S P Hirshman and J C Whitson. Steepest-descent moment method for three-dimensional magnetohydrodynamic equilibria. *Phys. Fluids*, 26(12):3553–3568, December 1983.

[Jac91] E A Jackson. *Perspectives on nonlinear dynamics. Volume 1.* Cambridge University Press, Cambridge, 1991.

[KK58] M D Kruskal and R M Kulsrud. Equilibrium of a magnetically confined plasma in a toroid. *Phys. Fluids*, 1(4):265–274, Jul 1958.

[KS94] R Kaiser and A Salat. Surface current equilibria from a geometric point of view. *Phys. Plasmas*, 1(2):281–295, Feb 1994.

[KU04] R Kaiser and H Uecker. Relaxed plasma-vacuum states in cylinders. *Q. Jl Mech. Appl. Math.*, 57(1):1–17, Jun 2004.

[LL92] A J Lichtenberg and M A Lieberman. *Regular and Chaotic Dynamics*. Springer-Verlag, 1992.

[Mac86] R MacKay. Transition to chaos for area-preserving maps. In *Lecture Notes in Physics*, volume 247, pages 390–454. Springer Berlin / Heidelberg, 1986.

[Mac92] R S MacKay. Greene's residue criterion. *Nonlinearity*, 5:161–187, Sep 1992.

[Mac93] R Mackay. *Renormalisation in Area Preserving Maps*. World Scientific Publishing, 1993.

[Mei92] J D Meiss. Symplectic maps, variational principles, and transport. *Rev Mod Phys*, 64(3):795–848, 1992.

[MHD09] R Mills, M J Hole, and R L Dewar. Magnetohydrodynamic stability of plasmas with ideal and relaxed regions. *Journal of Plasma Physics*, 75:637–659, 2009.

[MHDv10] M McGann, S R Hudson, R L Dewar, and G von Nessi. Hamilton–Jacobi theory for continuation of magnetic field across a toroidal surface supporting a plasma pressure discontinuity. *Phys Lett A*, 374(33):3308–3314, 2010.

[MM83] R S MacKay and J D Meiss. Linear stability of periodic orbits in Lagrangian systems. *Phys. Lett. A*, 98A(3):92–94, 1983.

[MMS89] R S MacKay, J D Meiss, and J Stark. Converse KAM theory for symplectic twist maps. *Nonlinearity*, 2:555–570, 1989.

[MS92] R S MacKay and J Stark. Locally most robust circles and boundary circles for area-preserving maps. *Nonlinearity*, 5:867–888, Dec 1992.

[MW01] J E Marsden and M West. Discrete mechanics and variational integrators. *Acta Numerica*, 10:357–514, 2001.

[Niv56] I Niven. *Irrational Numbers*. The Mathematical Association of America, ISBN 0-88385-038-9, 1956.

[Par94] E Parker. *Spontaneous Current Sheets in Magnetic Fields*. Oxford University Press, 1994.

[PDJ90] R D Parker, R L Dewar, and J L Johnson. Symmetry breaking bifurcations of a current sheet. *Phys Fluids B*, 2(3):508–515, 1990.

[PR94] A Paul and P H Richter. Application of Greene's method and the MacKay residue criterion to the double pendulum. *Z Phys B*, 93:515–520, August 1994.

[RD82] E Rosengaus and R L Dewar. Renormalized Lie perturbation theory. *J Math Phys*, 23(12):2328–2338, July 1982.

[RS84] P H Richter and H J Scholz. *Chaos in Classical Mechanics: The Double Pendulum*. Springer Berlin Heidelberg, 1984.

[RWB09] M Z Rafat, M S Wheatland, and T R Bedding. Dynamics of a double pendulum with distributed mass. *Am. J. Phys.*, 77:216–223, 2009.

[SK81] S J Shenker and L P Kadanoff. Critical behavior of a KAM Surface: I. empirical results. *J Stat Phys*, 27(4):631–655, July 1981.

[spe] *SPEC Documentation,* http://w3.pppl.gov/~shudson/spec/.

[Tay74] J B Taylor. Relaxation of toroidal plasma and generation of reverse magnetic fields. *Phys. Rev. Lett.*, 33(19):1139–1141, Nov 1974.